UAB
Universitat Autònoma de Barcelona

Holographic Insights into Conformal Transitions and BSM Phenomena

Lindber Ivan Salas Escobar

ADVERTIMENT. L'accés als continguts d'aquesta tesi queda condicionat a l'acceptació de les condicions d'ús establertes per la següent llicència Creative Commons:  https://creativecommons.org/licenses/?lang=ca

ADVERTENCIA. El acceso a los contenidos de esta tesis queda condicionado a la aceptación de las condiciones de uso establecidas por la siguiente licencia Creative Commons:  https://creativecommons.org/licenses/?lang=es

WARNING. The access to the contents of this doctoral thesis it is limited to the acceptance of the use conditions set by the following Creative Commons license:  https://creativecommons.org/licenses/?lang=en

Holographic Insights into Conformal Transitions and BSM Phenomena

A thesis presented for the degree of *Doctor of Physics* by:

Lindber Ivan Salas Escobar

Supervisors: Prof. Dr. Àlex Pomarol Clotet and Prof. Dr. Mariano Quirós Carcelén

July 10, 2025

...

Acknowledgements

Primeramente, me gustaría expresar mi profundo agradecimiento a mis directores de tesis, Àlex y Mariano, por confiar en mí y brindarme la oportunidad de realizar este trabajo. A Àlex, en particular, le agradezco las conversaciones sobre fútbol y política que siguieron a los largos, pero siempre enriquecedores, intercambios sobre física. Aquellos diálogos hicieron que estos años de investigación fueran mucho más amenos y humanos. También agradezco sinceramente a Oriol y Eugenio, quienes colaboraron conmigo a lo largo de estos años y siempre estuvieron dispuestos a compartir su tiempo y conocimiento para hablar de física. Quisiera, además, agradecer a Rafel por su ayuda constante en los últimos años, que me permitió impartir clases en la universidad y llegar a culminar esta tesis. Agradezco también a quien fue más que un profesor, un hermano: Eduardo. Siempre lo recordaré con cariño y estaré eternamente agradecido por haberme ayudado a venir a Barcelona y por todo lo que me enseñó, tanto en la física como en la vida.

Mi gratitud se extiende a IFAE, por ofrecerme un entorno propicio para la realización de este trabajo, y al Ministerio de Educación, a través de la beca Severo Ochoa, por el apoyo financiero. También quiero expresar mi aprecio a todos los compañeros con quienes compartí charlas y momentos gratos en IFAE: a Xavi, el Danni, Víctor y Rudin. En especial, quiero agradecer a todo el equipo administrativo del instituto, por la ayuda brindada incluso antes de mi llegada a Barcelona; muy particularmente a Elisabet, Sara y Marta, por su cercanía y generosidad.

Estos últimos años también trajeron desafíos personales, especialmente en lo referente a mi salud. Agradezco especialmente a mi fisioterapeuta Alba, quien fue y sigue siendo un pilar fundamental en mi rehabilitación. De igual forma, agradezco a mi hermana entrenadoncia Adriana y a sus niñas del fútbol: gracias a ellas, recuperé la confianza para volver a salir de casa y encontré un refugio que me ayudó enormemente a retomar mi vida con normalidad. En este contexto, me siento especialmente agradecido con mi director Àlex, cuyo apoyo constante en esos años difíciles superó ampliamente su rol académico; más que un director, gané un amigo para toda la vida.

Quiero expresar mi más sincero agradecimiento a mi familia. En especial a mi madre Armida, a mi tío Wilber y a mi querido Ciro, que desde Perú me han acompañado siempre con su amor y sus palabras de aliento. Aunque no los tenga cerca físicamente, su presencia ha sido constante y fundamental para encontrar la fuerza necesaria y cumplir con este objetivo. Asimismo, mi gratitud va dirigida a todas las personas que hicieron que mi vida en Barcelona fuera cálida y llena de buenos momentos. Y, muy especialmente a mi entrenadoncia Adriana, a Juanito el profe y a la Joselyn, por estar siempre ahí y por las incontables historias compartidas en esta ciudad. Sus consejos, su apoyo y su compañía han hecho que Barcelona se sienta como un verdadero hogar.

...

Contents

List of publications

This thesis is submitted for its evaluation in partial fulfillment of the requirements for the PhD in Physics at the Universitat Autònoma de Barcelona. It is structured around a collection of three papers, which are listed below. Following the introductory overview in Chapter 1, Chapter 2 presents a comprehensive summary and discussion of the results, while Chapter 3 contains the concluding remarks. The full versions of the three papers are included in Chapter 4. The contents of the papers are structured along two distinct lines of research.

Conformal transition from a holographic perspective

- A. Pomarol, O. Pujolas and L. Salas, *Holographic conformal transition and light scalars*, JHEP **10**, 202 (2019)
- A. Pomarol and L. Salas. *Exploring the conformal transition from above and below*, JHEP **08**, 149 (2024)

Vector-like leptons in warped extra-dimensional models.

- E. Megias, M. Quiros, and L. Salas, $g_\mu - 2$ *from Vector-Like Leptons in Warped Space, JHEP* **05***, 016 (2017)*

Other articles produced during the doctoral period but not included in this thesis are the following:

- E. Megias, M. Quiros and L. Salas, *Lepton flavor universality limits in warped space, Phys. Rev. D* **96***, no. 7, 075030 (2017)*
- *E. Megias, M. Quiros and L. Salas, Lepton-flavor universality violation in* R_K *and* $R_{D^{(*)}}$ *from warped space, JHEP* **1707***, 102 (2017)*

Chapter 1

Introduction

The dynamics of strongly-coupled gauge theories near the edge of the conformal window have become a central topic in high-energy theoretical physics, motivated by both analytical studies and lattice simulations [1–10]. These QCD-like theories with a large number of fermion flavors N_f offer an ideal framework to investigate mechanisms of mass generation, scale separation, and the emergence of light composite states. A particularly intriguing feature is the presence of a light scalar resonance near the transition between the confining and conformal regimes, which may provide insight into fundamental questions such as the origin of the electroweak scale [11] and the nature of strong dynamics beyond the Standard Model [12].

A theoretical mechanism that captures this phenomenon is the conformal transition, in which the theory evolves from an infrared (IR) fixed point to a non-conformal confining phase. A plausible scenario for this behavior is the merging of IR and ultraviolet (UV) fixed points [13], expected to occur as the number of flavors N_f is lowered. In the Veneziano limit, where the ratio $x \equiv N_f/N_c$ (with N_c the number of colors) becomes continuous, the transition takes place at a critical value x_{crit}. For $x > x_{\text{crit}}$, the theory lies inside the conformal window and displays approximate scale invariance, while for $x < x_{\text{crit}}$, it flows to a confining phase with chiral symmetry breaking.

This behavior was captured in a holographic framework in [14], where the conformal transition was modeled via a five-dimensional weakly-coupled theory dual to a four-dimensional strongly-coupled CFT. The central idea was to associate the loss of conformality with a scalar field in the bulk whose mass squared violates the Breitenlohner-Freedman (BF) bound [15, 16]:

$$M_\Phi^2 L^2 < -4, \tag{1.1}$$

which results in a complex scaling dimension of the dual operator. According to the AdS/CFT correspondence, the conformal dimension of a scalar operator $\mathcal{O}_\Phi$ is related to the bulk mass via [17–19]:

$$\text{Dim}[\mathcal{O}_\Phi] = 2 + \sqrt{4 + M_\Phi^2 L^2}. \tag{1.1}$$

This holographic setup correctly reproduces the emergence of a light scalar in the spectrum: the violation of the BF bound induces an instability in the bulk, interpreted as the spontaneous breaking of conformal symmetry.

Such a condition typically arises when the deformation of the CFT is introduced by a nearly marginal operator. In this model, however, the deformation is induced by a double-trace operator $\mathcal{O}_g = |\mathcal{O}_\Phi|^2$, with $\mathcal{O}_\Phi$ representing the fermion bilinear $q\bar{q}$. The scaling dimension of $\mathcal{O}_g$ is not protected and evolves along the renormalization group flow, being approximately $\mathrm{Dim}[\mathcal{O}_g] = 2 \cdot \mathrm{Dim}[\mathcal{O}_\Phi]$. As a result, the beta function associated with the effective potential grows rapidly, and the dilaton mass is no longer naturally suppressed. The dilaton remains the lightest scalar state in the spectrum, but its lightness is not parametric: the theory does not exhibit a truly massless dilaton as would be expected in a genuine spontaneous breaking of scale invariance.

Lattice simulations support this picture, showing the presence of a light scalar state with 0^{++} quantum numbers in theories near the conformal transition, with mass close to that of the pion and lighter than vector mesons [1–8]. However, the model in [14] showed that the dilaton, while the lightest state in the scalar channel, is not sufficiently separated from the rest of the spectrum to account for the light scalar seen in numerical data.

A central goal of the comprehensive holographic analysis in [20] is to determine how physical observables behave as the theory interpolates across the conformal transition. Utilizing holography, the study demonstrates that the meson mass spectrum is largely governed by the interplay between chiral and conformal symmetries and their respective breaking mechanisms. It is found that the spin-1 meson masses and the pion decay constant F_π evolve continuously across the transition. In contrast, the scalar mesons f_0 and a_0 exhibit a discontinuity in their masses, which originates from a logarithmic violation of conformal invariance.

The analysis reveals that the mass of the dilaton interpreted as a scalar glueball in the holographic model also varies smoothly across the transition. This continuity implies that the lightness of the dilaton cannot be solely attributed to spontaneous breaking of conformal symmetry on the confining side. Rather, its persistent lightness on both sides suggests that it should not be identified with the 0^{++} state observed in lattice simulations. This challenges earlier interpretations and supports the view that the light scalar originates from the strong dynamics associated with the fermion bilinear operator $\mathcal{O}_\Phi = q\bar{q}$, whose scaling dimension approaches the unitarity bound near the conformal transition.

Taken together, these analyses indicate that the progression from the earlier holographic construction [14] to the more comprehensive framework in [20] marks a major step forward in our understanding of conformal transitions. While the initial model captured the essential holographic structure and scalar spectrum, the latter analysis clarified that the light scalar is not a pseudo-Goldstone dilaton but rather a mesonic state arising from fermionic dynamics. Together, these studies offer a coherent, holographically-motivated description of the non-perturbative behavior of strongly-coupled gauge theories near conformality.

In a different context, although no direct signals of physics beyond the Standard Model (BSM) have been observed at the LHC to date, persistent deviations in precision observables suggest the presence of new physics. One of the most significant anomalies is the long-standing discrepancy between the experimental measurement and the theoretical prediction of the anomalous magnetic moment (AMM) of the muon [21]. This tension, which has persisted over several decades and across independent measurements,

motivates a detailed theoretical investigation within well-motivated BSM frameworks.

In parallel, the Standard Model exhibits from the naturalness problem, commonly referred to as the hierarchy problem, due to the instability of the electroweak scale under radiative corrections. Among the most compelling classes of theories addressing this issue are supersymmetric models and those based on warped extra dimensions [22], where the electroweak scale is dynamically generated via gravitational warping from a fundamental Planck-scale cutoff.

The framework considered here belongs to the latter class, focusing on five-dimensional warped geometries with two branes, an ultraviolet (UV) and an infrared (IR) brane, and a background strongly deformed with respect to AdS_5 near the IR brane due to the backreaction of a stabilizing scalar field ϕ[1]. This deformation results in a so-called soft-wall geometry with a naked singularity outside the physical interval [23–31]. Within this construction, Standard Model fields propagate in the bulk, and the theory remains consistent with electroweak and flavor precision constraints without invoking custodial symmetries, due to the suppressed couplings between light fermions and Kaluza-Klein (KK) excitations.

In this setting, the anomalous magnetic moment of the muon is analyzed. At tree level, the muon magnetic moment is given by

$$\vec{M}_\mu = g_\mu \frac{e}{2m_\mu} \vec{S}_\mu,$$

with gyromagnetic ratio $g_\mu = 2$. Quantum corrections induce a deviation from this value, which is conveniently parameterized as

$$a_\mu = \frac{g_\mu - 2}{2}. \tag{1.4}$$

The Standard Model yields a highly precise prediction for a_μ, incorporating contributions from QED, electroweak loops, and hadronic vacuum polarization. The most recent estimates [32] exhibit a statistically significant deviation from the experimental measurement [21], quantified as

$$\Delta a_\mu \equiv a_\mu^{\text{exp}} - a_\mu^{\text{SM}} = (2.49 \pm 0.48) \times 10^{-9}. \tag{1.5}$$

Numerous theoretical proposals have been developed to explain this discrepancy by introducing BSM effects, such as additional vector bosons, leptoquarks, or new scalar and fermion degrees of freedom [33–38]. In the context of supersymmetry, viable contributions to Δa_μ can be achieved through specific parameter configurations that enhance loop-level effects [39].

The present analysis is carried out within the class of warped extra-dimensional theories that simultaneously address the hierarchy problem. The soft-wall geometry outlined in [23–31] is adopted, where the localization of fermion wavefunctions in the fifth dimension can be tuned to replicate the flavor structure of the Standard Model. This geometric localization also determines the overlap between fermions and KK modes, which in turn governs their contributions to loop-level observables such as a_μ.

[1]This scalar field ϕ corresponds to the definition given in [42]. It should not be confused with alternative definitions in [14, 20].

It is demonstrated, however, that the minimal realization of this scenario is insufficient to account for the measured value of the muon AMM. Chirality-flipping amplitudes, which are necessary for a nonzero Δa_μ, are suppressed by a factor of $\mathcal{O}(m_\mu/m_{\rm KK})$, leading to loop contributions that fall short by at least an order of magnitude. This observation is consistent with previous studies in Randall-Sundrum-type models [40, 41].

To remedy this deficiency, the model is extended by incorporating a set of vector-like leptons (VLLs) propagating in the bulk [42]. These fields mix with the muon through localized Yukawa interactions and exhibit a high degree of compositeness, enhancing their coupling to gauge KK-modes and facilitating substantial chirality flips. The resulting loop contributions to Δa_μ can saturate the experimental discrepancy while remaining compatible with electroweak precision constraints, including those arising from modifications to the $Z\bar{\mu}\mu$ vertex and oblique parameters.

Chapter 2

Summary and Discussion

In our studies presented in references [14, 20, 42], we have investigated several novel aspects related to two fundamental problems in high-energy theoretical physics: the conformal transition in strongly coupled gauge theories, and the anomalous magnetic moment (AMM) of the muon. In this chapter, we present an in depth summary and discussion of the results obtained in [14, 20, 42]. The summary and discussion are structured along two main lines of research: papers [14] and [20] address the conformal transition from a holographic perspective, while paper [42] focuses on the resolution of the AMM discrepancy via vector-like leptons in warped extra dimensional models.

2.1 Conformal transition from a holographic perspective

We present a comprehensive holographic analysis of the conformal transition in strongly-coupled gauge theories, focusing on scenarios where this transition arises via the merging of infrared (IR) and ultraviolet (UV) fixed points. Such transitions are expected to occur in non-Abelian gauge theories, including QCD, when the number of fermionic flavors N_f is sufficiently large to bring the system close to the conformal window. This work is motivated by recent lattice simulations that report the appearance of a light 0^{++} scalar resonance in proximity to the lower boundary of this window, suggesting non-trivial infrared dynamics associated with the spontaneous or explicit breaking of approximate scale invariance.

To investigate this phenomenon, we construct five-dimensional warped geometries within the AdS/CFT framework that capture the non-perturbative dynamics of nearly conformal four-dimensional gauge theories. In this holographic setup, the conformal transition is modeled through the backreaction of a bulk scalar field, dual to a gauge-invariant operator such as $q\bar{q}$, whose scaling dimension approaches the Breitenlohner-Freedman (BF) bound from above. The scalar profile induces a deformation of the AdS_5 background, signaling the loss of conformality as the dual operator acquires a complex anomalous dimension, in line with the mechanism of fixed-point annihilation.

The spectrum of composite states is computed within this framework, revealing that the lightest scalar mode corresponds to the dilaton (or radion), arising from the fluctuations of the extra-dimensional volume. Although this state is generically lighter than the tower

of vector and axial-vector resonances, it is not parametrically light in the sense of being protected by an exact Goldstone symmetry. An analytic expression for the dilaton mass is derived, showing its sensitivity to the position of the infrared brane and the strength of the explicit scale-breaking deformations, in particular through a nearly marginal double-trace operator.

To elucidate the physical implications of the conformal transition, we systematically analyze the behavior of several observables across the transition point. Particular attention is devoted to the masses of spin-1 mesons, the pion decay constant F_π, and the scalar sector. We find that spin-1 states and F_π vary continuously across the transition, consistent with the analytic continuation of the solutions to the bulk equations of motion on both sides of the critical point. In contrast, scalar meson masses, such as those of the f_0 and a_0, exhibit discontinuities. This non-analytic behavior originates from logarithmic terms in the scalar correlators, whose form changes across the transition and reflects the distinct analytic structure on either side of the lower edge of the conformal window

Importantly, the dilaton mass is also shown to evolve smoothly across the conformal boundary, both from the broken and unbroken sides. This behavior challenges the interpretation of the light 0^{++} scalar observed in lattice simulations as a pseudo-Goldstone dilaton arising from spontaneous breaking of scale invariance alone. Instead, the data suggest that this scalar is more naturally identified as a $q\bar{q}$ meson whose lightness stems from the proximity of the operator dimension to the marginality point $\Delta = 2$, the point at which the dual bulk field becomes marginal and decouples from the strongly coupled sector.

Our holographic results are in qualitative agreement with lattice computations and provide a unifying perspective on the dynamics near the conformal edge. The model captures essential features of walking dynamics and Miransky scaling, while offering a controlled setup in which to explore the interplay between chiral symmetry breaking and conformal symmetry deformation. The utility of the holographic approach lies in its capacity to compute the full spectrum and response functions in a semi-analytic fashion, allowing for predictions that can be confronted with future numerical studies.

2.1.1 Discussion of paper 1: Holographic conformal transition and light scalars

The five-dimensional holographic framework constructed in [14] provides a robust platform to explore the dynamics of conformal symmetry breaking via a fixed-point merging mechanism. This model captures the essential features of the conformal transition through a bulk scalar field Φ, dual to the $q\bar{q}$ operator, whose mass is tuned to approach the Breitenlohner-Freedman (BF) bound. The spontaneous breaking of scale invariance is realized when this bound is violated in the bulk, giving rise to a tachyonic instability that induces a nontrivial vacuum profile for Φ.

A central aspect of the model is the introduction of an IR brane at a dynamically determined position z_{IR}, associated with the radion field. The effective IR dynamics depends sensitively on three key parameters: the dimensionless brane-localized mass $\hat{m}_b^2$; the effective quartic coupling $\hat{\lambda}$, which combines bulk and brane scalar interactions; and the detuning parameter $\delta\hat{\Lambda}$, which quantifies the deviation of the IR brane tension from the AdS value.

The interplay between these parameters determines whether a stable minimum for the radion potential is dynamically generated, which in turn controls whether the system exits the conformal phase. The solutions fall into two regimes: in one limit, the chiral symmetry breaking scale exceeds that of confinement, while in the other, the ordering is reversed. In both cases, the spectrum consistently exhibits a light scalar mode the dilaton whose mass remains suppressed relative to the Kaluza-Klein scale.

The parameter space analyzed in **Figure 3** of [14] illustrates the structure of solutions that lead to radion stabilization. For fixed values of the gravitational coupling $\hat{\kappa}^2$ and the sign of the scalar quartic coupling $\lambda = \pm 1$, only specific, precisely localized regions allow for the spontaneous breaking of scale invariance. These regions are bounded by loci where the radion becomes massless, signaling proximity to the conformal transition point. The most infrared-localized stable solution is obtained in the limit $\hat{m}_b^2 \to -2$ and $\delta\hat{\Lambda} = 0$, where the geometry is closest to conformality. These findings emphasize how sensitive the low-energy physics is to the brane-localized parameters.

Fluctuation analysis around these stabilized solutions confirms that the lightest scalar mode corresponds to the dilaton, and that its mass remains parametrically small as the theory approaches the critical limit. This behavior is robust throughout the allowed range of $\hat{m}_b^2$, and is supported by both analytic approximations and numerical calculations. The spectrum also reveals that the mass separation between singlet and non-singlet scalar modes originates from double-trace deformations, parametrized by λ_2, which become particularly relevant in the large-N_F regime These deformations become particularly relevant in the large-N_F regime because, as the number of flavors N_F increases, they contribute at higher orders in the $1/N_F$ expansion, significantly influencing the spectral structure and enhancing the mass splitting between these scalar modes.

A comparison with non-perturbative lattice QCD results for theories with many fermion flavors further supports the model's predictions. Lattice simulations near the conformal window [1–8] have repeatedly observed the appearance of a light scalar resonance with 0^{++} quantum numbers, significantly lighter than the vector and axial-vector mesons. The holographic construction presented in [14] successfully captures this feature without the need for tuning associated with exact dilaton symmetry.

In particular, **Figure 7** of [14] displays a direct comparison between the predicted holographic spectrum and lattice results, showing that the light scalar emerges as the lowest-lying massive state in the theory. The relative hierarchy between the scalar, vector, and axial-vector states aligns well with the trends found in numerical simulations. This agreement provides substantial validation for the model's assumptions about the nature of the conformal transition and the associated infrared dynamics.

Notably, the emergence of the light scalar does not originate from spontaneous breaking of an exact scale symmetry, but from the influence of a nearly marginal deformation induced by a double-trace operator. Since the dimension of this operator is not protected under renormalization group evolution, the resulting dilaton acquires a small mass, consistent with lattice results that indicate light but massive scalar states near the edge of the conformal window. The presence of such a mode reflects the universal behavior of theories near conformal transitions, rather than a specific tuning of model parameters.

The holographic model presented in [14] provides a concrete, calculable realization of light scalar dynamics in theories with near-conformal behavior. Its predictions are consistent

with lattice observations and demonstrate the power of holographic duals to capture strongly coupled phenomena beyond the reach of perturbative techniques.

2.1.2 Discussion of paper 2: Exploring the conformal transition from above and below

The conformal transition in QCD like theories has been investigated through a five dimensional holographic model that captures the merging of IR and UV fixed points. This framework, first introduced in [14], describes a $\mathrm{SU}(N_F)_L \times \mathrm{SU}(N_F)_R$ gauge theory in AdS_5 space coupled to a complex scalar field Φ, dual to the operator $q\bar{q}$ in the 4D CFT. The breaking of conformal and chiral symmetries is encoded in a nontrivial bulk profile $\phi(z)$, which depends on both the scalar potential and boundary dynamics.

A central element in controlling the transition is the bulk mass of the scalar field, written as

$$M_\Phi^2 = -\frac{4+\epsilon}{L^2}.$$

This parametrization allows one to approach the Breitenlohner-Freedman bound from either side. For $\epsilon < 0$, the system remains in the conformal phase. When $\epsilon > 0$, the BF bound is violated, and the scalar turns on in the bulk, triggering the breaking of conformal symmetry.

The scalar profile $\phi(z)$ admits analytic solutions in both regimes under suitable approximations. For positive ϵ, the solution includes a sinusoidal dependence on the logarithm of the holographic coordinate, while for negative ϵ, it becomes logarithmic. These two forms converge smoothly in the limit $\epsilon \to 0$, ensuring that the profile remains continuous across the conformal transition when the quark mass M_q is nonzero. As a result, physical quantities related to this background such as vector and axial-vector meson masses and the pion decay constant exhibit continuous behavior near the transition.

This is confirmed by the numerical results presented. The ratios m_{a_1}/m_ρ and F_π/m_ρ vary smoothly across the transition and show minimal dependence on the value of M_q, as illustrated in **Figure 2** of [20]. This behavior is further supported by the insensitivity of these quantities to quark mass variation for $\epsilon > 0$, as shown in **Figure 3** of [20].

A particularly relevant prediction of the model is the existence of a light dilaton, identified with the radion of the 5D theory. Its mass is found to be continuous and light on both sides of the transition and remains largely insensitive to M_q. These features indicate that the dilaton's lightness is not related to spontaneous breaking of scale invariance, but instead emerges from the near-critical structure of the model. This is in agreement with the original analysis in [14].

In contrast, scalar mesons such as f_0 and a_0, which originate from the fluctuations of the scalar field, exhibit distinct behavior depending on the sign of ϵ. Their correlators acquire logarithmic corrections from scale invariance breaking, and the scalar mass spectrum reflects this difference. For $\epsilon < 0$, the correlator depends on the UV scale and yields a standard KK spectrum. For $\epsilon > 0$, the logarithmic structure is regulated by an emergent IR scale, leading to discontinuities in the scalar masses, which become heavier across the transition but tend to align with the conformal regime as M_q increases.

This qualitative behavior is consistent with expectations from hyperscaling and is confirmed numerically. The pion, meanwhile, remains massless in the $\epsilon > 0$ regime when $M_q = 0$, and acquires a mass governed by hyperscaling in the conformal phase.

When moving further into the conformal window, by increasing the scalar mass M_Φ^2 from $-4/L^2$ to $-3/L^2$, the operator dimension $\mathrm{Dim}[q\bar{q}]$ increases from 2 to 3. The scalar profile becomes flatter and more UV-dominated, reducing the effective chiral symmetry breaking. This results in a decrease of mass splittings among meson chiral partners, as illustrated by the convergence $m_{a_1} \to m_\rho$, and $m_{a_0}, m_{f_0} \to m_\pi$, which can be observed in **Figure 4** of [20].

The predictions of the model have been compared with lattice simulations of SU(3) QCD for different flavor numbers. For $N_F = 8$, lattice studies [1, 2, 4, 5] suggest the theory lies near the conformal edge, exhibiting a light scalar 0^{++} state. For $N_F = 12$, the behavior is consistent with a conformal phase and hyperscaling [6–8]. The holographic model reproduces key features observed in the lattice data, such as the emergence of a light scalar near the transition and the suppression of chiral mass splittings as N_F increases.

However, a discrepancy arises in the interpretation of the lightest scalar state. In the holographic model, the dilaton remains light throughout, but its glueball nature and independence from M_q differ from lattice observations, which favor a $q\bar{q}$ interpretation. The scalar f_0 meson, in contrast, shows a dependence on M_q that aligns more closely with the lattice data, suggesting it is the physical 0^{++} state observed in simulations.

This tension may reflect limitations of the IR-brane setup used in the model. More refined holographic constructions, such as that of [43], do not predict a light dilaton, reinforcing the idea that its appearance here may be model-dependent. This view is further supported by the comparison shown in **Figure 5** of [20], where the behavior of the dilaton and f_0 as functions of M_q diverge, with only the latter matching lattice trends [44].

2.2 Vector-like leptons in warped extra-dimensional models

The anomalous magnetic moment of the muon, a_μ, has long served as a sensitive probe for physics beyond the Standard Model (BSM). Although its theoretical prediction within the Standard Model framework is highly precise, experimental measurements exhibit a persistent deviation, suggesting the presence of new interactions or particle content. This discrepancy, typically quantified as $\Delta a_\mu \equiv a_\mu^{\mathrm{exp}} - a_\mu^{\mathrm{SM}} = (2.74 \pm 0.76) \times 10^{-9}$, remains one of the most compelling low-energy signals indicative of BSM dynamics. The fact that this deviation appears specifically in the muon sector, and not in its electronic counterpart, implies the existence of flavor non-universal couplings, which puts into question the flavor-blind structure of most Standard Model extensions.

Within this context, extra-dimensional models that incorporate warped geometries provide a natural and robust framework to address both the electroweak hierarchy problem and potential low-energy anomalies such as Δa_μ. A concrete realization of this idea is explored in detail in [42], which considers five-dimensional theories with a warped background strongly deformed relative to the pure AdS_5 geometry near the IR brane. The

deformation is induced by the backreaction of a stabilizing scalar field ϕ, resulting in a soft-wall metric with a naked singularity situated beyond the physical interval. This configuration permits the localization of Standard Model fields along the extra dimension and enables the realization of fermion hierarchies without invoking additional symmetries or flavor structures.

It is shown that the minimal version of this class of models, with Standard Model fermions propagating in the bulk and gauge fields acquiring KK excitations, fails to generate a sufficiently large contribution to a_μ. The structure of chirality-flipping transitions is suppressed by the small muon mass relative to the KK scale, typically yielding corrections that fall short by an order of magnitude. Therefore, an extension of the model is necessary to accommodate the experimental value of the muon's magnetic moment.

In [42], this limitation is addressed by introducing a new sector of vector-like leptons (VLLs), propagating in the bulk of the extra dimension. These VLLs couple to the muon via localized Yukawa interactions and exhibit a high degree of compositeness, with their profiles strongly localized toward the IR brane. This setup increases their interactions with gauge KK-modes and facilitates chirality-changing processes, producing significant loop-level contributions to Δa_μ. The mechanism arises naturally from the geometric configuration and field content of the model.

The model is tested against several experimental and theoretical constraints. Among the most sensitive are electroweak precision observables, including corrections to the $Z\bar{\mu}\mu$ vertex, oblique parameters (S and T), and the requirement of vacuum stability for the Higgs potential. Perturbativity of the Yukawa sector and the preservation of the electroweak minimum further restrict the parameter space. A viable region is identified in which the compositeness parameter satisfies $c \lesssim 0.37$ and the lightest VLL mass exceeds 270 GeV.

This framework also provides distinctive collider signatures. Vector-like leptons can be efficiently produced via Drell-Yan processes at the LHC with $\sqrt{s} = 13$ TeV. Their decay patterns, governed by mixing with muons and couplings to electroweak bosons, offer experimentally accessible probes of the underlying structure responsible for the observed value of Δa_μ.

Warped extra-dimensional models deformed by a soft-wall geometry, when extended to include vector-like leptons, provide a consistent and phenomenologically viable explanation for the muon anomalous magnetic moment, while preserving the geometric resolution of the hierarchy problem and satisfying all current experimental constraints.

2.2.1 Discussion of paper 3: $g_\mu - 2$ from Vector-Like Leptons in Warped Space

The warped extra-dimensional framework considered in this analysis is based on a five-dimensional spacetime where both gauge and matter fields propagate in the bulk. The deviation from AdS_5 geometry near the infrared (IR) brane, induced by the backreaction of a scalar field ϕ, enables the realization of a soft-wall structure that addresses the electroweak hierarchy problem through geometrical suppression mechanisms.

The Higgs field is treated as a bulk scalar with a background profile exponentially localized towards the IR brane. This configuration allows electroweak symmetry breaking to be

triggered by a potential localized at the IR boundary. A dimensionless parameter α governs the strength of this localization and the form of the background solution $h(y)$, determining the mass scale of the theory.

In the fermion sector, chiral zero modes emerge from bulk Dirac fields. Their localization, determined by mass parameters c_f, is essential for reproducing the observed fermion mass hierarchy and for controlling the overlaps with KK modes. For the muon, the localization is selected to balance electroweak precision constraints, in particular the $Z\bar{\mu}\mu$ coupling, and to enhance interaction with the new vector-like leptons (VLLs) introduced in the model.

One of the key contributions of the original study [42] is the inclusion of bulk-propagating VLLs, which play a central role in addressing the anomalous magnetic moment of the muon. These new fermionic states satisfy boundary conditions that produce massive Dirac spinors in four dimensions. Their strong IR localization implies a high degree of compositeness in the dual 4D theory, enhancing their couplings to KK gauge bosons and enabling sizable chirality-flipping contributions in the loop-level corrections to a_μ.

The structure of these interactions is constrained by electroweak precision data, which requires small mixing between VLLs and the physical muon. For analytical feasibility, approximate unitary matrices $U_{L,R}$ are used, along with the simplifying condition $c_L = c_R \equiv c$, reducing the number of free parameters while maintaining the phenomenological consistency of the model.

Various experimental and theoretical constraints restrict the viable parameter space. Among the most rigorous are the oblique parameters S and T, which arise from VLL contributions to gauge boson self-energies and impose upper bounds on the parameters a and c. These translate into a lower limit for the VLL mass, $M_{\widetilde{\mathcal{L}}} \gtrsim 230$ GeV. Additional restrictions come from the modification of the Higgs diphoton decay width $\Gamma(H \to \gamma\gamma)$, where loop contributions from VLLs must remain within LHC bounds, excluding scenarios with strong couplings or very light masses.

Theoretical considerations, particularly electroweak vacuum stability, impose further constraints. VLLs influence the renormalization group evolution of the Higgs quartic coupling λ, potentially driving it negative at lower scales. For moderate VLL masses (e.g., $M \sim 500$ GeV), this effect becomes significant, leading to bounds such as $c \lesssim 0.37$ and $a \lesssim 0.36$, consistent with those from oblique parameters and precision data.

Collider phenomenology provides complementary information. VLLs can be pair-produced through Drell-Yan processes at the LHC, with cross-sections determined by their mass and couplings. LEP2 imposes a lower limit $M_{\widetilde{\mathcal{L}}} > 101.2$ GeV, while LHC searches at $\sqrt{s} = 8$ TeV exclude masses below 168 GeV at 95% CL. Current and future runs at $\sqrt{s} = 13$ TeV are expected to probe the region up to $M_{\widetilde{\mathcal{L}}} \sim 500$ GeV, where production remains significant.

Taken together, the constraints from precision observables, Higgs physics, vacuum stability, and direct collider searches significantly reduce the acceptable parameter space. Nevertheless, a viable region remains in which the anomalous magnetic moment of the muon can be accommodated, provided the VLLs exhibit sufficient compositeness ($c \lesssim 0.37$) and possess masses above approximately 270 GeV.

Chapter 3

Conclusions

As in the previous chapter of summary and discussion, the conclusions are structured along two main lines of research: papers [14] and [20] address the conformal transition from a holographic perspective, while paper [42] focuses on resolving the AMM discrepancy via vector-like leptons in warped extra-dimensional models.

3.1 Conclusion of conformal transition from a holographic perspective

We have presented a comprehensive holographic study of the conformal transition in strongly coupled gauge theories, focusing on the transition arising from the merging of IR and UV fixed points. Extending the initial results of [14] and further developed in [20], we constructed a five-dimensional model that captures the key dynamics near the lower edge of the conformal window in large-N_c QCD-like theories.

The analysis confirm that the presence of a light scalar state commonly identified with a dilaton naturally emerges near the conformal boundary. While initially suggested to be associated with the spontaneous breaking of scale invariance, our extended analysis reveals that its lightness is, instead, a consequence of the proximity of the dimension of the operator $O_\Phi \sim q\bar{q}$ to the unitarity bound $\mathrm{Dim}[O_\Phi] = 2$. As the conformal edge is approached, the scalar operator decouples from the IR dynamics, resulting in a parametrically suppressed mass independently of the sign of the parameter ϵ controlling the RG flow.

We demonstrated, both analytically and numerically, that the scalar profile $\phi(z)$, as well as physical quantities such as the dilaton mass, F_π, and the vector and axial-vector meson spectra, exhibit smooth behavior across the conformal transition. The continuity of these quantities, especially the dilaton mass, indicates that the conformal transition does not induce discontinuous signatures in the low-energy observables, in contrast with earlier expectations. Moreover, the hyperscaling relation $m_i \propto M_q^{1/(4-\mathrm{Dim}[O_\Phi])}$ is preserved for both $\epsilon > 0$ (outside the conformal window) and $\epsilon < 0$ (inside the conformal window), demonstrating that the scaling behavior of hadronic masses with respect to the quark mass remains valid across the transition. This is explicitly confirmed in **Figure 3** of [20], where the mass ratios (e.g. F_π/m_ρ, m_{a_1}/m_ρ) remain constant as M_q is varied in the $\epsilon > 0$

phase, matching the analytic expectation from the $\epsilon < 0$ regime and further emphasizing the universality of the spectrum near criticality.

The proposed holographic model successfully reproduces the pattern observed in recent lattice simulations, including the appearance of a light scalar in the non-conformal regime. However, the continuity of the dilaton mass across the conformal boundary challenges the interpretation of this state as a true dilaton arising from spontaneous scale breaking. Rather, our results support the identification of the light 0^{++} state with a scalar meson associated to the operator $\bar{q}q$, whose scaling dimension approaches its minimal allowed value near the conformal edge. As it nears this bound, the operator effectively decouples from the infrared dynamics of the CFT, and the associated scalar meson becomes light, not due to spontaneous breaking of scale invariance, but because of its proximity to the unitarity limit where a scalar naturally tends toward masslessness.

This analysis clarifies the predictive power of holographic methods in exploring nonperturbative dynamics near conformal transitions and provides a coherent picture for the nature of light scalar states in near-conformal gauge theories. Future investigations may extend this analysis to explore finite temperature effects, baryonic states, and potential implications for composite Higgs models and early-universe cosmology.

3.2 Conclusion of vector-like leptons in warped extra-dimensional models

The analysis presented in [42] explores the phenomenological implications of a warped extra-dimensional model formulated to provide a theoretical resolution to the persistent deviation observed in the muon anomalous magnetic moment a_μ. Within this framework, vector-like leptons (VLLs) propagate in the bulk and mix with the muon via localized Yukawa interactions. The model is formulated in a background geometry deviating from pure AdS_5 near the IR brane due to the presence of a scalar field, which induces a soft-wall structure.

One of the central results is that the anomalous magnetic moment of the muon can be explained through chirality-flipping contributions mediated by VLLs that are significantly localized toward the IR brane, corresponding to a high degree of compositeness. These effects are consistent with current electroweak precision constraints, particularly the severe bounds from the $Z\bar{\mu}\mu$ coupling.

The allowed parameter space, determined by the overlap of all theoretical and experimental constraints including those from oblique parameters, Higgs diphoton decay width, vacuum stability, and collider searches, is significantly constrained. However, a viable region remains, primarily where the localization parameter satisfies $c \lesssim 0.37$ and VLL masses exceed approximately 270 GeV.

Importantly, **Figure 15** in [42] provides a comprehensive visualization of the allowed parameter space after incorporating all theoretical and experimental constraints. This contour plot in the (c, a) plane displays iso-curves of the VLL mass $M_{\tilde{\mathcal{L}}}$ (in solid blue) and the effective Yukawa coupling $\sqrt{k}\, Y_{LR}$ (in dashed black), while also highlighting exclusion regions arising from electroweak precision observables (gray), vacuum stability (red), and Yukawa perturbativity bounds (brown). These results encapsulate the combined effect

of all constraints and delineate the viable region where the model remains consistent with the observed value of Δa_μ. Specifically, the overlap between the regions compatible with the muon anomalous magnetic moment and the electroweak observables confirms the necessity of partially composite VLLs in the mass range $M_{\widetilde{\mathcal{L}}} \sim 300$ to $800\,\mathrm{GeV}$, for $0.2 \lesssim a \lesssim 0.5$ and $c \lesssim 0.37$.

In conclusion, this work demonstrates that warped extra-dimensional models incorporating bulk VLLs remain viable candidates for explaining the muon $g-2$ anomaly while simultaneously satisfying a set of precision observables and collider bounds.

Bibliography

[1] Y. Aoki et al., *Light flavor-singlet scalars and walking signals in Nf = 8 QCD on the lattice*, *Phys. Rev. D* **96** (2017) 014508 [arXiv:1610.07011].

[2] Y. Aoki et al., *Light composite scalar in eight-flavor QCD on the lattice*, *Phys. Rev. D* **89** (2014) 111502 [arXiv:1403.5000].

[3] R. C. Brower, A. Hasenfratz, C. Rebbi, E. Weinberg and O. Witzel, *Composite Higgs model at a conformal fixed point*, Phys. Rev. D **93** (2016) no.7, 075028. [arXiv:1512.02576 [hep-ph]].

[4] T. Appelquist et al., *Strongly interacting dynamics and the search for new physics at the LHC*, *Phys. Rev. D* **93** (2016) 114514 [arXiv:1601.04027].

[5] T. Appelquist et al., *Nonperturbative investigations of SU(3) gauge theory with eight dynamical flavors*, *Phys. Rev. D* **99** (2019) 014509 [arXiv:1807.08411].

[6] Z. Fodor et al., *Twelve massless flavors and three colors below the conformal window*, *Phys. Lett. B* **703** (2011) 348 [arXiv:1104.3124].

[7] Y. Aoki et al., "Lattice study of conformality in twelve-flavor QCD," *Phys. Rev. D* **86** (2012) 054506 [arXiv:1207.3060].

[8] Y. Aoki et al., *Light composite scalar in twelve-flavor QCD on the lattice*, *Phys. Rev. Lett.* **111** (2013) 162001 [arXiv:1305.6006].

[9] T. DeGrand, *Lattice tests of beyond Standard Model dynamics*, Rev. Mod. Phys. 88, 015001 (2016)[arXiv:1510.05018 [hep-ph]].

[10] B. Lucini and M. Panero, *Introductory lectures to large-N QCD phenomenology and lattice results*, Prog. Part. Nucl. Phys. 75,1-40(2014)[arXiv:1309.3638 [hep-th]].

[11] W. A. Bardeen, *On naturalness in the standard model*, FERMILAB-CONF-95-391-T.

[12] F. Sannino, *Conformal Dynamics for TeV Physics and Cosmology*, Acta Phys. Polon. B 40, 3533 (2009) [arXiv:0911.0931 [hep-ph]].

[13] D. B. Kaplan, J. W. Lee, D. T. Son and M. A. Stephanov, *Conformality Lost*, Phys. Rev. D **80**, 125005 (2009) doi:10.1103/PhysRevD.80.125005 [arXiv:0905.4752 [hep-th]].

[14] A. Pomarol, O. Pujolàs and L. Salas, *Holographic conformal transition and light scalars*, *JHEP* **10** (2019) 202 [arXiv:1905.02653].

[15] P. Breitenlohner and D. Z. Freedman, *Positive energy in anti-de Sitter backgrounds and gauged extended supergravity*, Phys. Lett. B 115 (1982) 197.

[16] P. Breitenlohner and D. Z. Freedman, *Stability in gauged extended supergravity*, Annals Phys. 144 (1982) 249.

[17] J. M. Maldacena, *The large N limit of superconformal field theories and supergravity*, Adv. Theor. Math. Phys. **2** (1998) 231 [arXiv:hep-th/9711200].

[18] S. S. Gubser, I. R. Klebanov and A. M. Polyakov, *Gauge theory correlators from non-critical string theory*, Phys. Lett. B **428** (1998) 105 [arXiv:hep-th/9802109].

[19] E. Witten, *Anti-de Sitter space and holography*, Adv. Theor. Math. Phys. **2** (1998) 253 [arXiv:hep-th/9802150].

[20] A. Pomarol and L. Salas, *Exploring the conformal transition from above and below*, *JHEP* **08** (2024) 149 [arXiv:2312.08332].

[21] G. W. Bennett *et al.* [Muon g-2 Collaboration], *Final Report of the Muon E821 Anomalous Magnetic Moment Measurement at BNL*, Phys. Rev. D **73**, 072003 (2006) [arXiv:hep-ex/0602035 [hep-ex]].

[22] L. Randall and R. Sundrum, *A Large mass hierarchy from a small extra dimension*, Phys. Rev. Lett. **83**, 3370 (1999) [arXiv:hep-ph/9905221 [hep-ph]].

[23] J. A. Cabrer, G. von Gersdorff and M. Quiros, *Soft-Wall Stabilization*, New J. Phys. **12**, 075012 (2010) [arXiv:0907.5361 [hep-ph]].

[24] J. A. Cabrer, G. von Gersdorff and M. Quiros, *Warped Electroweak Breaking Without Custodial Symmetry*, Phys. Lett. B **697**, 208 (2011) [arXiv:1011.2205 [hep-ph]].

[25] J. A. Cabrer, G. von Gersdorff and M. Quiros, *Suppressing Electroweak Precision Observables in 5D Warped Models*, JHEP **05**, 083 (2011) [arXiv:1103.1388 [hep-ph]].

[26] J. A. Cabrer, G. von Gersdorff and M. Quiros, *Improving Naturalness in Warped Models with a Heavy Bulk Higgs Boson*, Phys. Rev. D **84**, 035024 (2011) [arXiv:1104.3149 [hep-ph]].

[27] J. A. Cabrer, G. von Gersdorff and M. Quiros, *Warped 5D Standard Model Consistent with EWPT*, Fortsch. Phys. **59**, 1135 (2011) [arXiv:1104.5253 [hep-ph]].

[28] A. Carmona, E. Ponton and J. Santiago, *Phenomenology of Non-Custodial Warped Models*, JHEP **10**, 137 (2011) [arXiv:1107.1500 [hep-ph]].

[29] J. de Blas, A. Delgado, B. Ostdiek and A. de la Puente, *LHC Signals of Non-Custodial Warped 5D Models*, Phys. Rev. D **86**, 015028 (2012) [arXiv:1206.0699 [hep-ph]].

[30] M. Quiros, *Higgs Bosons in Extra Dimensions*, Mod. Phys. Lett. A **30**, 1540012 (2015) [arXiv:1311.2824 [hep-ph]].

[31] E. Megias, O. Pujolas and M. Quiros, *On dilatons and the LHC diphoton excess*, JHEP **05**, 137 (2016) [arXiv:1512.06106 [hep-ph]].

[32] S. Navas *et al.* [Particle Data Group], Phys. Rev. D **110**, no.3, 030001 (2024)

[33] A. Freitas, J. Lykken, S. Kell and S. Westhoff, *Testing the Muon g-2 Anomaly at the LHC*, JHEP **05**, 145 (2014) [arXiv:1402.7065 [hep-ph]].

[34] W. Altmannshofer, M. Carena and A. Crivellin, $L_\mu - L_\tau$ *theory of Higgs flavor violation and* $(g-2)_\mu$, Phys. Rev. D **94**, 095026 (2016) [arXiv:1604.08221 [hep-ph]].

[35] B. Batell, N. Lange, D. McKeen, M. Pospelov and A. Ritz, *Muon anomalous magnetic moment through the leptonic Higgs portal*, Phys. Rev. D **95**, 075003 (2017) [arXiv:1606.04943 [hep-ph]].

[36] W. Altmannshofer, C. Y. Chen, P. S. Bhupal Dev and A. Soni, *Lepton flavor violating* Z' *explanation of the muon anomalous magnetic moment*, Phys. Lett. B **762**, 389 (2016) [arXiv:1607.06832 [hep-ph]].

[37] C. Biggio, M. Bordone, L. Di Luzio and G. Ridolfi, *Massive vectors and loop observables: the g-2 case*, JHEP **10**, 002 (2016) [arXiv:1607.07621 [hep-ph]].

[38] E. Coluccio Leskow, G. D'Ambrosio, A. Crivellin and D. Müller, *(g-2)$_\mu$, lepton flavor violation and Z decays with leptoquarks: Correlations and future prospects*, Phys. Rev. D **95**, 055018 (2017) [arXiv:1612.06858 [hep-ph]].

[39] D. Stockinger, *The Muon Magnetic Moment and Supersymmetry*, J. Phys. G **34**, R45 (2007) [arXiv:hep-ph/0609168 [hep-ph]].

[40] M. Beneke, P. Dey and J. Rohrwild, *The muon anomalous magnetic moment in the Randall-Sundrum model*, JHEP **08**, 010 (2013) [arXiv:1209.5897 [hep-ph]].

[41] P. Moch and J. Rohrwild, *(g-2)$_\mu$ in the custodially protected RS model*, J. Phys. G **41**, 105005 (2014) [arXiv:1405.5385 [hep-ph]].

[42] E. Megias, M. Quiros and L. Salas, $g_\mu - 2$ *from Vector-like leptons in warped space*, JHEP **05**, 016 (2017) [arXiv:1701.05072 [hep-ph]].

[43] M. Järvinen, *Massive holographic QCD in the Veneziano limit*, *JHEP* **07** (2015) 033 [arXiv:1501.07272].

[44] T. Appelquist et al. [LSD Collaboration], *Hidden conformal symmetry from the lattice*, *Phys. Rev. D* **108** (2023) L091505 [arXiv:2305.03665].

Chapter 4

Papers

This chapter includes the three published papers [14, 20, 42] that serve as the scientific basis for the main results and conclusions of this thesis, compiled in compendium form.

4.1 Paper 1: Holographic conformal transition and light scalars

Published for SISSA by Springer

Received: *June 24, 2019*
Revised: *September 19, 2019*
Accepted: *October 8, 2019*
Published: *October 18, 2019*

Holographic conformal transition and light scalars

Alex Pomarol,[a,b] **Oriol Pujolas**[a] **and Lindber Salas**[a]

[a] *IFAE and BIST, Universitat Autònoma de Barcelona, 08193 Bellaterra, Barcelona*
[b] *Departament de Física, Universitat Autònoma de Barcelona, 08193 Bellaterra, Barcelona*

E-mail: alex.pomarol@uab.cat, oriol.pujolas@gmail.com, lsalas@ifae.es

Abstract: We present an holographic approach to strongly-coupled theories close to the conformal to non-conformal transition, trying to understand the presence of light scalars as recent lattice simulations seem to suggest. We find that the dilaton is always the lightest resonance, although not parametrically lighter than the others. We provide a simple analytic formula for the dilaton mass that allows us to understand this behavior. The pattern of the meson mass spectrum, as we get close to the conformal transition, is found to be quite similar to that in lattice simulations. We provide further predictions from holography that can be checked in the future. These five-dimensional models can also implement new solutions to the hierarchy problem, having implications for searches at the LHC and cosmology.

Keywords: Beyond Standard Model, Conformal Field Theory, Large Extra Dimensions, Technicolor and Composite Models

ArXiv ePrint: 1905.02653

Open Access, © The Authors.
Article funded by SCOAP[3].

https://doi.org/10.1007/JHEP10(2019)202

JHEP10(2019)202

Contents

JHEP10(2019)202

1 Introduction

Theories close to being conformally invariant are of utmost interest as they can generate large hierarchies of scales that can be useful in particle physics and cosmology. This motivates the understanding of how theories behave at the critical point at which, by varying the parameters of the theory, we pass from a conformal regime to a non-conformal one.

This is especially interesting in strongly-coupled theories as they can give rise to non-trivial dynamics. An example is QCD where by increasing the number of flavors N_F, the theory is expected to become conformally invariant at some critical value $N_F = N_F^{\rm crit}$. It is unclear where this exactly happens, but lattice simulations suggest that this could be around $N_F^{\rm crit} \sim 10$ for $N_c = 3$ where N_c is the number of colors. For $N_F \geq N_F^{\rm crit}$,

QCD becomes a conformal field theory (CFT) till reaching $N_F = \frac{11}{2}N_c$, at which the theory reaches the Banks-Zaks fixed point, becoming IR free for $N_F > \frac{11}{2}N_c$. The region $N_F^{\rm crit} \leq N_F \leq \frac{11}{2}N_c$ is called the conformal window.

Recent lattice simulations suggest that, contrary to real QCD, theories close to the conformal transition have as the lightest resonance a 0^{++} state (apart, of course, from the Goldstone bosons, the pions) [1–5]. It is unclear what is the origin of the lightness of this state. Some arguments suggest that this could be a dilaton, the Goldstone associated to the spontaneous breaking of scale invariance. If this is the case, it would be interesting to know whether in the large-N_c limit, where $N_F^{\rm crit}/N_c \equiv x_{\rm crit}$ becomes a continuous parameter, the dilaton mass tends to zero as we approach the critical point from below $N_F/N_c \to x_{\rm crit}$.

In this article we would like to analyze the physics of conformal transitions using holography. We will follow ref. [6] that argued that the exit of the conformal window of large-N_c QCD occurs when the IR fixed point disappears by merging with a UV fixed point. Close to the conformal edge the theory contains a marginal operator $\mathcal{O}_g$ whose dimension gets a small imaginary part when conformal invariance is lost (see next section for details). Assuming that this is the case, the AdS/CFT correspondence [7–9] can provide a simple realization of this idea as a complex operator dimension matches to a scalar having a mass below the Breitenlohner-Freedman (BF) bound $M_\Phi^2 = -4/L^2$. When this happens, the scalar becomes tachyonic and gets a non-zero profile that results into a departure from the Anti-de-Sitter (AdS) geometry [6].

The presence of a marginal operator $\mathcal{O}_g$ in the model could suggest the presence of a light dilaton, along the lines of refs. [10–14]. The argument goes as follows. The dilaton potential can be written as

$$V_{\rm eff}(\phi_d) = \lambda_{\rm eff}(\phi_d)\,\phi_d^4\,, \tag{1.1}$$

such that, when a minimum exists, leads to a dilaton mass given by

$$\frac{m_{\phi_d}^2}{\langle\phi_d\rangle^2} = \beta_{\lambda_{\rm eff}}(4+\beta'_{\lambda_{\rm eff}})\,, \tag{1.2}$$

where $\beta_{\lambda_{\rm eff}} = d\lambda_{\rm eff}/d\ln\phi_d$ and $\beta'_{\lambda_{\rm eff}} = d\beta_{\lambda_{\rm eff}}/d\lambda_{\rm eff}$. A nonzero $\beta_{\lambda_{\rm eff}}$ arises only from an explicit breaking of scale invariance. When this latter comes only from[1] $g\,\mathcal{O}_g \in \mathcal{L}$, we expect $\beta_{\lambda_{\rm eff}} \propto \beta_g$, and eq. (1.2) predicts $m_{\phi_d}^2 \propto \beta_g$. Therefore, a dilaton can be parametrically light if the dimension of $\mathcal{O}_g$ is given by $4+\delta$ with $\delta \ll 1$ (i.e., $\beta_g \ll 1$) being a controllable small parameter till the end of the RG-flow. The holographic implementation of this is the Goldberger-Wise mechanism [15], where the operator $\mathcal{O}_g$ matches to an almost massless scalar in 5D (protected by a shift symmetry) [10–14]. Nevertheless, we will see that this is not the case at the conformal transition, as the marginal operator $\mathcal{O}_g$ corresponds to a double-trace operator whose dimension is not protected along the RG-flow. Having the explicit breaking of conformal invariance arising from an almost marginal operator however will have as a consequence that the dilaton is light, although not parametrically light.

We will be working with a simple weakly-coupled AdS_5 theory, with the extra-dimension cut off by an IR-brane, that will contain the basic ingredients to describe the

[1] We remark that g is a coupling of the theory not necessarily related with the gauge coupling.

JHEP10(2019)202

conformal transition. We will calculate the mass spectrum of resonances and show that the lightest resonance is the dilaton (the radion of the compact extra-dimension). We will present a simple analytical formula for the mass of the dilaton that will allow to understand its lightness as a function of the change of the tachyon as we move the IR-brane. This will show that either at small or large positions of the IR-brane, the dilaton is always parametrically light. In between these two regions, we will see that the dilaton mass does not have "room" to grow and as a consequence the dilaton is always kept light.

We will compare our results with lattice simulations, showing good agreement in the pattern of masses when the conformal critical point is approached. Furthermore, we will provide further predictions to be checked in the future by lattice simulations.

The 5D model presented here could also be useful to generate small scales and explain, for example, the difference between the electroweak scale and the Planck scale. Moreover, the presence of a light scalar can have an important impact in the searches for new resonances at the LHC as predicted in composite Higgs models.

There have been previous approaches using holography to understand the conformal transition and the existence of a light dilaton [16–29]. We find however that these studies were not exhaustive nor conclusive. Our goal is not only to provide evidence for a relatively light dilaton, but also to explain the reasons behind this.

The article is organized as follows. In section 2 we introduce the idea of leaving the conformal window by fixed-point merging and remark its implications. In section 3 we present the five-dimensional model and its relation with the large N_c and N_F expansion. We also discuss the tachyon solution and the stabilization of the radion. Next we present the predictions for the resonance mass spectrum, presenting an analytical formula for the case when the dilaton is light, as well as discussing the other scalar and vector resonance masses. In section 4 we compare the mass spectrum calculated within our model with that obtained from lattice simulations, and in section 5 we discuss how these models could also be useful for explaining the smallness of the electroweak scale. Conclusions are given in section 6. We also present two appendices. In appendix A we give the coupled system of equations of motion for the scalar and gravitational sectors, and derive the approximate analytical formula for the dilaton mass. In appendix B we present the 4D effective theory of a tachyon and dilaton valid when they are the lightest states.

2 Conformal transition by fixed-point merging

There are several ways to lose an IR fixed point as we move the parameters of the theory. Either the fixed point goes to zero, to infinity or it merges with a UV fixed point. Following ref. [6] we will consider conformal transitions characterized by the third case, the merging of the IR fixed point with a UV fixed point, as depicted in figure 1. In this case, the beta function can be written as

$$\beta_g \simeq -\epsilon - (g - g_*)^2 \,, \tag{2.1}$$

where g is a coupling of the theory (not necessarily related to the gauge coupling in gauge theories), and ϵ depends on the parameters of the theory, e.g., N_F. The IR and UV fixed

JHEP10(2019)202

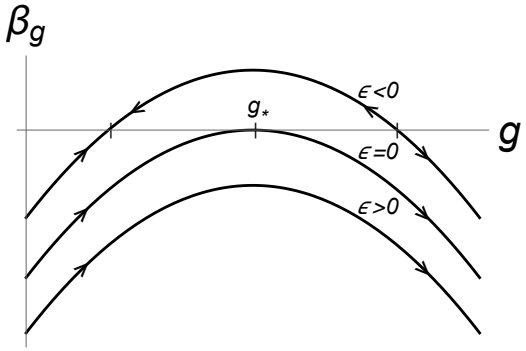

Figure 1. Beta function of the coupling g for different values of ϵ. For $\epsilon = 0$, the IR and UV fixed points merge at g_*.

point are respectively at

$$g = g_* \mp \sqrt{-\epsilon}\,. \tag{2.2}$$

As we vary ϵ from negative to positive values, we have the merging of the IR and UV fixed points at $\epsilon = 0$, while for $\epsilon > 0$ the theory abandons conformality, i.e., the IR fixed point is at complex coupling.

As argued in ref. [30], for ϵ negative and close to zero, the operator $\mathcal{O}_g$ with coupling g must have dimension

$$\mathrm{Dim}[\mathcal{O}_g] = 4 + \frac{d\beta_g}{dg} \simeq 4 + 2\sqrt{-\epsilon}\,, \tag{2.3}$$

and can be considered to be responsible for the RG flow towards the IR fixed point. For $\epsilon = 0$ we have that $\mathcal{O}_g$ becomes marginal, and develops a complex dimension for $\epsilon > 0$, signaling the end of conformality.

The above properties of this conformal transition have a straightforward holographic interpretation using the correspondence (or duality) between strongly-coupled CFT_4 (in the large N_c and large 't Hooft coupling) and weakly-coupled five-dimensional Anti-de-Sitter theories (AdS_5) [7–9]. Operators in the CFT_4 ($\mathcal{O}$) correspond to scalars in the AdS_5 (Φ) where dimensions and masses are related via the AdS/CFT relation [7–9]:

$$\mathrm{Dim}[\mathcal{O}] = 2 + \sqrt{4 + M_\Phi^2 L^2}\,. \tag{2.4}$$

Eq. (2.4) tells us that in order to have a dual of a CFT operator with complex dimension, the AdS_5 must have a scalar slightly below the BF-bound, $M_\Phi^2 = -(4+\epsilon)/L^2$. Eq. (2.4) also tells us that this operator of complex dimension ($\mathcal{O}_*$) has, in the limit $\epsilon \to 0$, dimension 2 instead of 4. Therefore the natural identification for the $\mathcal{O}_g$ operator discussed above is $\mathcal{O}_g = |\mathcal{O}_*|^2$, since in the large N_c this implies $\mathrm{Dim}[\mathcal{O}_g] = 2\mathrm{Dim}[\mathcal{O}_*]$ and that gives us eq. (2.3). In other words, $\mathcal{O}_g$ must be a double-trace operator.[2]

The existence of $\mathcal{O}_*$ in the conformal transition is only an implication from large-N_c theories, and could be not true in general. In QCD, as argued in ref. [6], $\mathcal{O}_*$ is expected to be

[2]It has been proven in refs. [30, 31] that this is always the case for theories in the large-N_c limit.

JHEP10(2019)202

the $q\bar{q}$ operator whose dimension will go from ~ 3 when entering the conformal window (at the Banks-Zaks fixed point) to 2 when leaving it at the other side when it becomes complex.

When the theory is close but outside the conformal window (i.e. $0 < \epsilon \ll 1$), one can calculate the RG flow "time" required to cross the region where $g \sim g_*$ and $|\beta_g| \ll 1$. This gives us the IR-scale $\Lambda_{\rm IR}$ at which the theory is expected to confine as g becomes large. From eq. (2.1) one gets

$$\Lambda_{\rm IR} \sim e^{-\pi/\sqrt{\epsilon}} \Lambda_{\rm UV}\,, \tag{2.5}$$

where $\Lambda_{\rm UV}$ is roughly the scale at which $g \lesssim g_*$. Eq. (2.5) is usually referred as *walking* or *Miransky* scaling.

3 A five-dimensional model for the conformal transition

We want to study the conformal transition described above using holography. For this reason we will consider the simplest but at the same time most generic five-dimensional model containing the basic ingredients needed to describe the conformal transition via fixed-point merging. Our purpose is to generically understand the mass spectrum at the conformal transition and the presence or not of light scalars.

Let us recapitulate the basic ingredients of the theory in the 4D side. This is a strongly-coupled deformed CFT with a scalar operator, $q_L^i \bar{q}_R^j$ $(i,j = 1,\ldots,N_F)$ for concreteness, whose dimension is $2 + \sqrt{-\epsilon}$ with $0 < \epsilon \ll 1$. This means that the scalar $q_L^i \bar{q}_R^j$ gets a vacuum expectation value (VEV), signaling the loss of conformality. The global symmetry of this theory is $\mathrm{SU}(N_F)_L \otimes \mathrm{SU}(N_F)_R \otimes \mathrm{U}(1)_B$ that is broken by the VEV of the scalar $\langle q_L^i \bar{q}_R^j \rangle \propto \mathbb{1}$ down to the diagonal subgroup $\mathrm{SU}(N_F)_L \otimes \mathrm{SU}(N_F)_R \to \mathrm{SU}(N_F)_V$.[3]

The corresponding holographic model will consist in a $\mathrm{SU}(N_F)_L \otimes \mathrm{SU}(N_F)_R \otimes \mathrm{U}(1)_B$ gauge theory in 5D with a complex scalar Φ transforming as a $(\mathbf{N_F},\overline{\mathbf{N}}_\mathbf{F})_\mathbf{0}$. This scalar plays the role of the $q\bar{q}$ operator whose VEV is responsible for the breaking of the conformal and gauge symmetry, and therefore its mass will be related to the dimension of the $q\bar{q}$ operator. We also impose parity, defined as the interchange $L \leftrightarrow R$. The action is given by

$$S_5 = \int d^4x \int dz\, \sqrt{g}\, M_5 \left[\frac{1}{\kappa^2}\left(\mathcal{R} + \Lambda_5\right) + \mathcal{L}_5\right]\,, \tag{3.1}$$

where, up to dimension-four operators,[4] the most general Lagrangian is given by

$$\mathcal{L}_5 = -\frac{1}{4}\,\mathrm{Tr}\left[L_{MN}L^{MN} + R_{MN}R^{MN}\right] - \frac{1}{4}B_{MN}B^{MN} + \frac{1}{2}\,\mathrm{Tr}\,|D_M\Phi|^2 - V_\Phi(\Phi)\,, \tag{3.2}$$

with L_{MN}, R_{MN} and B_{MN} being the field-strength of the $\mathrm{SU}(N_F)_L$, $\mathrm{SU}(N_F)_R$ and $\mathrm{U}(1)_B$ gauge bosons respectively, and the indices run over the five dimensions, $M = \{\mu, 5\}$. We parametrize the fields as $\Phi = \Phi_s + T_a\Phi_a$ with $\mathrm{Tr}[T_aT_b] = \delta_{ab}$. The fields Φ_s and Φ_a will

[3] The $\mathrm{U}(1)_A$ is anomalous and will not be considered here.

[4] Following the Effective Field Theory (EFT) approach, higher-dimensional operators are supposed to be suppressed by the cutoff scale of the model ($\Lambda_{\rm cutoff}$) estimated to be the scale at which the 5D theory becomes strongly coupled (i.e., when loops are as important as tree-level contributions), that is $\Lambda_{\rm cutoff} \sim 24\pi^3 M_5$ [32] — see also section 3.1.

JHEP10(2019)202

respectively transform as singlet and adjoint under the $\mathrm{SU}(N_F)_V$. The covariant derivative is defined as

$$D_M\Phi = \partial_M\Phi + ig_5 L_M\Phi - ig_5\Phi R_M\,, \tag{3.3}$$

and the potential is given by[5]

$$V_\Phi(\Phi) = \frac{1}{2}M_\Phi^2\,\mathrm{Tr}\,|\Phi|^2 + \frac{1}{4}\lambda_1\,\mathrm{Tr}\,|\Phi|^4 + \frac{1}{4}\lambda_2(\mathrm{Tr}\,|\Phi|^2)^2\,. \tag{3.4}$$

The 5D metric in conformal coordinates is defined as

$$ds^2 = a(z)^2\big(\eta_{\mu\nu}dx^\mu dx^\nu - dz^2\big)\,, \tag{3.5}$$

where $\eta_{\mu\nu} = \mathrm{diag}(1,-1,-1,-1)$ and $a(z)$ is the warp factor. Before the scalar Φ turns on, the presence of Λ_5 leads to an AdS_5 geometry:

$$a(z) = \frac{L}{z}\,, \tag{3.6}$$

where $L^2 = 12/\Lambda_5$ is the squared AdS curvature radius.

As explained above, our important ingredient here is to consider that the conformal breaking arises when $\mathrm{Dim}[q\bar{q}]$ becomes imaginary. In AdS this corresponds from eq. (2.4) to take the 5D mass of Φ below the BF bound. For this purpose, we will consider

$$M_\Phi^2 = -\frac{4+\epsilon}{L^2}\,. \tag{3.7}$$

When $\epsilon > 0$ the mass of Φ is below the BF bound and Φ turns on in the 5D bulk, breaking the conformal and chiral symmetry $\mathrm{SU}(N_F)_L \otimes \mathrm{SU}(N_F)_R \to \mathrm{SU}(N_F)_V$. Φ will grow as $\sim z^2$, as expected from a dimension-two perturbation in the dual 4D theory. When the energy-momentum tensor induced by the nonzero Φ profile gets of order of the inverse 5D Newton constant, κ^2, the backreaction on the metric will be important, starting to depart then from AdS, and signaling the breaking of the conformal symmetry. This simple model, however, does not lead to a mass gap for all bulk fields, as the extra dimension is not ending at any z. In fact, as we will see, the tachyon Φ would stabilize at the minimum of the potential eq. (3.4) and the metric would become again AdS. As we know that in strongly-coupled models outside the conformal window, like QCD, all resonances are heavy, we need to implement the same in our holographic version. The simplest way is to cut off the 5D space by an IR-brane at some point $z = z_{\mathrm{IR}}$ to be determined dynamically.

The presence of the IR-brane add extra parameters to the theory as Φ might also have a potential on the IR-boundary. We will limit ourselves to up to quadratic terms in Φ:

$$\mathcal{L}_{\mathrm{IR}} = -a^4\tilde{V}_b(\Phi)\big|_{z_{\mathrm{IR}}}\,, \qquad \tilde{V}_b(\Phi) = \frac{\Lambda_4}{\kappa^2} + \frac{1}{2}m_b^2\,\mathrm{Tr}\,|\Phi|^2\,, \tag{3.8}$$

and study their impact on the properties of the model. We could also add to eq. (3.8) quartic terms but these are not expected to change significantly our predictions, since they

[5] We notice that one can absorb one coupling into M_5, as we will do later.

JHEP10(2019)202

are suppressed by $1/(M_5 L)$ with respect to the bulk terms.[6] As it is usual in AdS/CFT, we will be regularizing the UV-divergencies by placing a UV-boundary at $z = z_{\rm UV}$ and taking the limit $z_{\rm UV} \to 0$ at the end of the calculation of physical quantities.

In this 5D model the two phases are determined, as in the strongly-coupled model described in section 2, by the ϵ parameter:

- For $\epsilon < 0$, we have $\Phi = 0$ and $z_{\rm IR} = \infty$: AdS_5 (CFT_4) phase.
- For $\epsilon > 0$, we have $\Phi \neq 0$ and $z_{\rm IR} \neq \infty$: non-AdS_5 (non-CFT_4) phase.

3.1 The large N_c and N_F power counting

By the AdS/CFT correspondence, the 5D scalar and gauge bosons are associated to the meson operators $\bar{q}q$ and $\bar{q}\gamma_\mu q$ respectively. Therefore 5D couplings from single-trace operators must scale in this sector as $1/N_c$. This can be implemented by assuming

$$\frac{1}{M_5 L} \sim \frac{16\pi^2}{N_c}\,, \quad \lambda_1 \sim g_5 \sim N_c^0\,. \tag{3.9}$$

On the other hand, double-trace operators are suppressed with respect to single-trace ones:

$$\lambda_2 \sim \frac{1}{N_c}\,. \tag{3.10}$$

For this reason these latter terms were neglected in previous holographic approaches to QCD [33–35]. Nevertheless, in some physical quantities the parameter λ_2 is accompanied by a factor N_F, as we will see explicitly below (e.g. eq. (3.14)), and then its effect is not suppressed for large values of N_F. Therefore it is important to keep double-trace operators in eq. (3.2) when comparing our results to strongly-coupled theories in the large N_c and N_F limit. In particular, λ_2 will be responsible for generating a mass splitting in the scalar sector between the singlet (Φ_s) and the adjoint states (Φ_a), as observed in lattice results with large N_F [1–5].

Using the scaling eq. (3.9), one realizes that in the limit $N_F \sim N_c$, 5D models are in danger of not providing reliable calculations by the usual perturbative expansion. Indeed, in this limit loops of vector or scalar resonances in the adjoint of $\mathrm{SU}(N_F)_V$ contribute as $\frac{1}{16\pi^2}\frac{N_F}{M_5 L} \sim \frac{N_F}{N_c} \sim 1$, meaning that loops could be as important as tree-level contributions. The N_F enhancement of these corrections is due to the large number of fields (for example,Φ_a consists of $N_F^2 - 1$ fields). Still, by extending the results to $N_F/N_c \sim 1$, one hopes to capture well the qualitative dynamics.

A case that is more under control arises if one can restrict only to the flavor-singlet sector of the theory [36], which is justified when the other sectors are heavier. In this case the N_F dependence enters only into the couplings of the flavor-singlet sector, which can be treated perturbatively (loops are always small since the number of fields is not large) even in the strict Veneziano limit where N_F is of order or even larger than N_c. In fact, ref. [36]

[6] Even though the same is true for the two terms in eq. (3.8), these are respectively quartically and quadratically UV sensitive so they can be sizable.

JHEP10(2019)202

provides an example of a weakly-coupled closed string dual description of the flavor-singlet sector of a gauge theory in the Veneziano limit.

From the AdS/CFT dictionary, we are also able to relate the gravitational sector of the 5D theory with the glueball sector of the 4D CFT, and derive the scaling of the 5D Newton constant with the number of colors: $\kappa^2/(M_5 L^3) \sim 16\pi^2/N_c^2$ that using eq. (3.9) implies

$$\frac{\kappa^2}{L^2} \sim \frac{1}{N_c}\,. \tag{3.11}$$

From the above we can estimate the mixing between the flavor-singlet meson sector and the glueball sector (dual respectively to the scalar and gravitational sectors in 5D) to go as

$$\hat{\kappa}^2 \equiv \frac{\kappa^2 N_F}{L^2} \sim \frac{N_F}{N_c}\,, \tag{3.12}$$

that becomes order one for $N_F \sim N_c$. Therefore, contrary to previous holographic models, the impact of the gravitational sector in the singlet scalar sector cannot be neglected in this case.

3.2 The tachyon solution

The non-zero profile for Φ will be taken to be along the $\phi = |\Phi_s|$ direction, whose 5D Lagrangian is given by

$$\mathcal{L}_\phi = N_F \left[\frac{1}{2}(\partial_M \phi)^2 - V(\phi)\right] + g_5^2 \phi^2 \,\mathrm{Tr}\, A_M^2\,, \tag{3.13}$$

where

$$V(\phi) = \frac{1}{2} M_\Phi^2 \phi^2 + \frac{1}{4}\lambda\phi^4\,, \qquad \lambda \equiv \lambda_1 + N_F \lambda_2\,, \tag{3.14}$$

being $A_M = (L_M - R_M)/\sqrt{2}$ the axial-vector gauge bosons that will get masses from their coupling to ϕ. The IR-brane potential can be written as

$$\mathcal{L}_{\rm IR} = -a^4 N_F V_b(\phi)\big|_{z_{\rm IR}}, \qquad V_b(\phi) = \frac{\Lambda_4}{\hat{\kappa}^2 L^2} + \frac{1}{2} m_b^2 \phi^2\,. \tag{3.15}$$

Notice that the presence of a factor N_F in front the Lagrangian means that the couplings of ϕ are suppressed by an extra $1/N_F$ with respect to those in the non-singlet sector, as expected in strongly-coupled theories in the large $N_c \sim N_F$ limit. The equation of motion (EOM) for ϕ from eq. (3.13) must be solved including the metric back-reaction that via the Einstein equations (see appendix A) determines the warp factor:

$$-\frac{\dot{a}}{a^2} = \sqrt{\frac{1}{L^2} + \frac{\hat{\kappa}^2 L^2}{12}\left(\frac{\dot{\phi}^2}{2a^2} - V(\phi)\right)}\,, \tag{3.16}$$

where from now on we will be using the dot notation: $\dot{\phi} \equiv \partial_z \phi$. It is important to notice that by the field redefinition $\phi \to \phi/\sqrt{|\lambda|}$ we could factorize $|\lambda|$ in front of the first term of eq. (3.13) and make the EOM that determines the solution for ϕ independent of $|\lambda|$ (only sensitive to its sign). This redefinition introduces $|\lambda|$ in the interactions of ϕ with

JHEP10(2019)202

the gauge and gravitational fields (second term of eq. (3.13) and eq. (3.16) respectively). Nevertheless, this can be reabsorbed respectively in g_5^2 and $\hat{\kappa}^2$, making the solutions and full mass spectrum of the model insensitive to $|\lambda|$. Therefore, with no loss of generality, we will consider $\lambda = \pm 1$.

We are interested to study the model close to the conformal transition. Therefore we will work in the limit $\epsilon \to 0$. The solution for ϕ then only depends on $z_{\rm IR}$, $\hat{\kappa}^2$ and m_b^2 (and the sign of λ). At the UV-boundary we will impose $\phi = 0$, otherwise we would be breaking the chiral symmetry from UV-physics (as adding an explicit mass term to the quarks in the dual theory).[7] On the other hand, at the IR-brane we must impose the boundary condition determined by the model:

$$\left(\frac{M_5}{a}\dot{\phi} + V_b'\right)\Big|_{z_{\rm IR}} = 0\,, \tag{3.17}$$

where we defined $V_b' \equiv \partial_\phi V_b$. For the metric we must impose the junction condition [37]:

$$\left(-\frac{6M_5}{\hat{\kappa}^2 L^2}\frac{\dot{a}}{a^2} + V_b\right)\Big|_{z_{\rm IR}} = 0\,. \tag{3.18}$$

3.2.1 Region $\hat{m}_b^2 > -2$

We will start looking for solutions of the tachyon for $\hat{m}_b^2 > -2$, where we define

$$\hat{m}_b^2 \equiv \frac{m_b^2 L}{M_5}\,. \tag{3.19}$$

In this case non-trivial solutions from eq. (3.13) fulfilling eq. (3.17) are only found if the IR-brane is beyond some critical value, $z_{\rm IR} > z_{\rm IR}^c$. It is easy to find $z_{\rm IR}^c$, as this corresponds to the critical value at which we pass from having all Kaluza-Klein (KK) states of ϕ with positive squared masses to having 4D tachyons in the theory. Therefore at $z_{\rm IR} = z_{\rm IR}^c$ there must be a 4D massless mode, $\phi_t(x)$. The wave-function of this massless mode must satisfy the linearized bulk EOM with $p^2 = 0$. We obtain [16, 17]

$$\phi(x,z) = \frac{\phi_t(x)}{N}\, z^2 \sin\left(\sqrt{\epsilon}\ln\frac{z}{z_{\rm UV}}\right)\,, \tag{3.20}$$

with N a normalization constant, and where the IR-boundary condition eq. (3.17) at $z_{\rm IR} = z_{\rm IR}^c$ leads to

$$\tan\left(\sqrt{\epsilon}\ln\frac{z_{\rm IR}^c}{z_{\rm UV}}\right) = -\frac{\sqrt{\epsilon}}{2+\hat{m}_b^2} \quad \Rightarrow \quad \sqrt{\epsilon}\ln\frac{z_{\rm IR}^c}{z_{\rm UV}} \simeq n\pi\,, \quad n = 1, 2, \ldots\,. \tag{3.21}$$

Notice that to have non-trivial solutions, the limit $\epsilon \to 0$ must be taken with $z_{\rm UV} \to 0$, such that the angle in eq. (3.20) is kept fixed. The presence of n solutions in eq. (3.21) is a well-known feature of these configurations, and it is associated to the existence of Efimov states. We will be considering $n = 1$, that will give us the global minimum, being the other possibilities just local minima. Eq. (3.21) reproduces eq. (2.5) for $\Lambda_{\rm IR} \sim 1/z_{\rm IR}^c$ and

[7] Imposing a different boundary condition, such as $z\dot{\phi}|_{z_{\rm UV}} \propto \phi|_{z_{\rm UV}}$, would lead to the same predictions in the limit $\epsilon \to 0$ ($z_{\rm UV} \to 0$).

JHEP10(2019)202

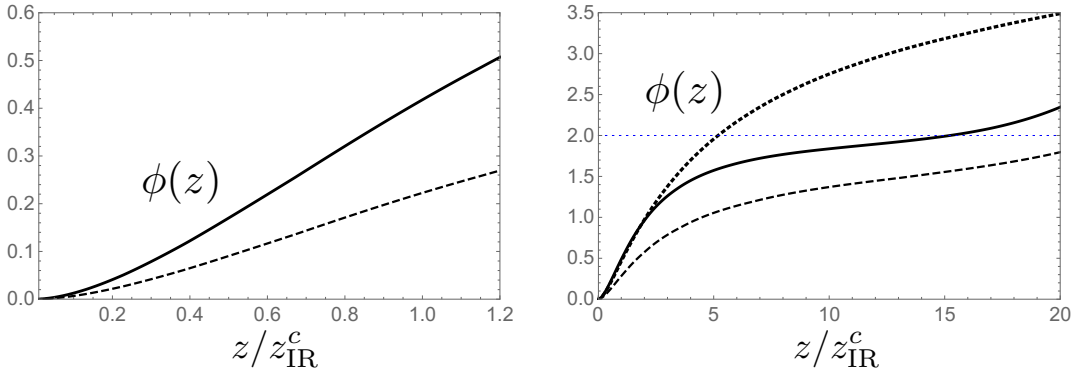

Figure 2. 5D tachyon solutions (in units of $1/L$) for $\hat{m}_b^2 = -1$. LEFT: limit I with $z_{\rm IR} = 1.2\, z_{\rm IR}^c$. RIGHT: limit II with $z_{\rm IR} = 20\, z_{\rm IR}^c$. We have taken $\lambda = 1$, and $\hat{\kappa}^2 = 1$ (4) for the solid (dashed) line, and $\lambda = -1$, $\hat{\kappa}^2 = 4$ for the dotted line.

$\Lambda_{\rm UV} \sim 1/z_{\rm UV}$. The origin of the logarithm in eq. (3.20), that will play an important role, can be more easily understood by looking at the strongly-coupled dual theory; this has an explicit breaking of the conformal symmetry due to the double-trace marginal operator $\mathcal{O}_g = |\mathcal{O}_*|^2$ that leads to a log-running of the couplings [38].

Depending on the position of the IR-brane with respect to $z_{\rm IR}^c$, we can distinguish two limiting cases that will help to understand the physics of the model. These are illustrated in figure 2 and corresponds to

I) $z_{\rm IR} \approx z_{\rm IR}^c$. In this case $\phi L \ll 1$ for all z, meaning that the scale of confinement $\sim 1/z_{\rm IR}$ is larger than the scale of chiral breaking that is of order $\sim L\phi(z_{\rm IR})/z_{\rm IR}$.

II) $z_{\rm IR} \gg z_{\rm IR}^c$. In this case ϕL reaches $O(1)$ values at some $z = z_\chi \ll z_{\rm IR}$, and then the scale of chiral breaking $\sim 1/z_\chi$ is larger than the scale of confinement $\sim 1/z_{\rm IR}$.

These two cases should be considered as formal limits, since in most of the parameter space of the model we will find that the IR-brane sits at $z_{\rm IR} \sim$ few $\times\, z_{\rm IR}^c$, i.e., between limits I and II, implying that naturally the scale of chiral breaking is similar to the scale of confinement.

Let us start considering the limit I, where $z_{\rm IR}$ is assumed to be just slightly above $z_{\rm IR}^c$. In this case the 4D mode $\phi_t(x)$ gets a small negative mass-squared, becoming a 4D tachyon. We find this mass is given by

$$m_t^2 \simeq -\frac{\beta}{z_{\rm IR}^2} \ln \frac{z_{\rm IR}}{z_{\rm IR}^c}\,, \quad \text{where} \quad \beta = \frac{4(\hat{m}_b^2+2)^2}{\hat{m}_b^4 + 6\hat{m}_b^2 + 10}\,. \tag{3.22}$$

Eq. (3.22) is only valid for $|m_t^2| \ll 1/z_{\rm IR}^2$ that, obviously, requires a tuning in the parameter space: either $\ln z_{\rm IR}/z_{\rm IR}^c \ll 1$ (that we will see later cannot be achieved by the radion minimization) or $\beta \ll 1$ that requires $\hat{m}_b^2 \to -2$. To find a stable configuration this 4D tachyon must have a positive quartic self-interaction, $\lambda_t > 0$, and this can arise either from λ or the feedback from gravity. We find

$$\lambda_t = \lambda\, c_\lambda(\hat{m}_b^2) + \hat{\kappa}^2 c_\kappa(\hat{m}_b^2)\,, \tag{3.23}$$

JHEP10(2019)202

where $c_{\lambda,\kappa}$ are smooth and positive functions of $\hat{m}_b^2$ as derived in appendix B.1. The 4D tachyon VEV is then given by

$$\langle \phi_t \rangle = \frac{1}{z_{\rm IR}} \sqrt{\frac{\beta}{\lambda_t} \ln \frac{z_{\rm IR}}{z_{\rm IR}^c}} \,. \tag{3.24}$$

Therefore, in the limit I the z-profile of ϕ is given by eq. (3.20) with eq. (3.24) and $N = L z_{\rm IR} \epsilon/\beta$, as we follow the normalization of ϕ_t of appendix B.1. This solution is shown in the left plot of figure 2 for $\lambda = 1$ and $\hat{\kappa}^2 = 1, 4$. In the limit $\hat{\kappa}^2 \gg 1$, we see from eqs. (3.20)–(3.24) that $\hat{\kappa}^2 \phi^2 L^2$ stays constant and small. This means that the metric remains always close to AdS_5.

Let us now move to the limiting case II. First, let us neglect the feedback from the metric ($\hat{\kappa}^2 \ll 1$). As the IR-brane is now placed far away from $z_{\rm IR}^c$, the tachyon profile grows $\propto z^2$ till the quartic term of the potential becomes relevant. Solutions only exist if $\lambda > 0$, such that $\phi(z)$ settles at the minimum of the 5D potential $V(\phi)$ where it takes the constant value $\phi(z) \simeq \sqrt{M_\Phi^2/\lambda} = 2/(L\lambda)$ (see right plot of figure 2).[8] This means, in the dual interpretation, that the CFT flows at around $1/z_{\rm IR}^c$ towards another CFT in which the global symmetry has been reduced to $\mathrm{U}(N_F)_V$ with Φ_s and Φ_a respectively transforming in the singlet and adjoint representation. In this new CFT, scale invariance is broken at a much lower scale $1/z_{\rm IR}$. Let us now consider the feedback of the metric. For large $\hat{\kappa}^2$ the gravitational feedback becomes important before ϕ reaches the $V(\phi)$ minimum, making ϕ to enter into a "slow-roll" condition (see appendix A for details) delaying the position z at which ϕ gets its maximum $\sim 2/(L\lambda)$. In this case $\lambda < 0$ is also possible as the slow-roll condition keeps $\phi(z)$ slowly growing till reaching the IR-brane (see right plot of figure 2). The metric evolves from AdS_5 at $z \approx z_{\rm IR}^c$ to another approximately AdS_5 space at $z \gg z_{\rm IR}^c$.

3.2.2 Region $\hat{m}_b^2 < -2$

In this region we have that $2 + \hat{m}_b^2$ is negative, and from the left-hand side of eq. (3.21), the smallest $z_{\rm IR}^c$ is determined by

$$\ln \frac{z_{\rm IR}^c}{z_{\rm UV}} \simeq -\frac{1}{2 + \hat{m}_b^2} \,, \tag{3.25}$$

that does not depend on ϵ. This means that non-trivial solutions for ϕ exist even if $\epsilon < 0$. These solutions however are supported by the IR-brane and for $z_{\rm IR} \to \infty$ we have $\phi \to 0$. Therefore as soon as the IR-brane is not stabilized for $\epsilon < 0$ (i.e., $z_{\rm IR} \to \infty$), we can also consider this region of the parameter space for studying the conformal transition.

In this case the solution for ϕ, as we vary $z_{\rm IR}$, behaves in the following way. For $z_{\rm IR}^c < z_{\rm IR} < z_{\rm IR}^{c\prime}$, where $z_{\rm IR}^{c\prime}$ is determined by $\ln(z_{\rm IR}^{c\prime}/z_{\rm UV}) \sim \pi/\sqrt{\epsilon}$, we find that ϕ takes a nonzero value with a profile localized towards the IR-brane, $\phi \sim (z/z_{\rm IR})^2$, as we said. The origin of this nonzero profile is that the IR-brane mass $\hat{m}_b^2$, and not the 5D mass, is exceedingly negative. $\phi(z_{\rm IR})$ is mostly constant in this region and it does not help to

[8] To satisfy the boundary condition at the IR-brane, ϕ must depart from $2/(L\lambda)$ when approaching the IR-boundary, as can be appreciated in figure 2.

JHEP10(2019)202

stabilize the IR-brane. On the other hand, for $z_{\rm IR} > z^{c\prime}_{\rm IR}$, the profile of ϕ grows to become similar to the limit II discussed before (see right-hand side of figure 2), indicating that ϕ behaves as a genuine 5D tachyon. This latter behavior only occurs if the 5D mass is below the BF bound and can lead to a stable IR-brane.

3.3 Radion/dilaton stabilization

Since the position of the IR-brane $z_{\rm IR}$ is associated to a dynamical field, the radion (not necessary a mass eigenstate), its value must be determined dynamically. The extremization condition for $z_{\rm IR}$ is exactly the junction condition eq. (3.18) after putting on-shell all other fields. This can be written, using eq. (3.16) and eq. (3.17), as

$$\left(\frac{6M_5}{\hat{\kappa}^2 L^2} \sqrt{\frac{1}{L^2} + \frac{\hat{\kappa}^2 L^2}{12}\left(\frac{V_b'^{\,2}}{2M_5^2} - V(\phi)\right)} + V_b \right)\Bigg|_{z_{\rm IR}} = 0\,. \tag{3.26}$$

For our particular case, this reduces to a quadratic equation for $\phi(z_{\rm IR})$:

$$\frac{4}{L^2}\left(\delta\hat{\Lambda} - \frac{\delta\hat{\Lambda}^2}{12}\right) + \hat{\kappa}^2 L^2 \left[\frac{1}{2}\bar{m}^2\phi^2(z_{\rm IR}) - \frac{\bar{\lambda}}{4}\phi^4(z_{\rm IR})\right] = 0\,, \tag{3.27}$$

where have introduced $\bar{m}^2 \equiv [(\hat{m}_b^2+2)^2 - 2\delta\hat{\Lambda}\,\hat{m}_b^2/3]/L^2$, $\bar{\lambda} \equiv \lambda + \hat{\kappa}^2\hat{m}_b^4/3$, and

$$\delta\hat{\Lambda} \equiv \frac{L}{M_5}\Lambda_4 + 6\,, \tag{3.28}$$

that is a measure of the detuning of the IR-brane tension away from the AdS_5 value. Their values are bounded to be in the region

$$0 \leq \delta\hat{\Lambda} \leq 6\,. \tag{3.29}$$

The lower bound arises from demanding that for $\epsilon < 0$, the IR-brane is driven to $z_{\rm IR} \to \infty$, such that the theory is in the AdS_5 (CFT_4) phase. From appendix B, in particular eq. (B.4), we see that $\delta\hat{\Lambda}$ is related to the self-coupling of the dilaton and $\delta\hat{\Lambda} \geq 0$ comes from requiring a positive dilaton self-coupling. On the other hand, the upper limit in eq. (3.29) is a more basic (geometrical) requirement: to possibly solve the junction condition even for dynamical solutions that start away from the minimum. If $\delta\hat{\Lambda} > 6$, the IR-brane tension Λ_4 is positive and it is easy to see that there would be no solutions where the IR-brane acts as an IR boundary (i.e., a cutoff of the AdS_5 space at $z = z_{\rm IR}$). Therefore these regions must be discarded.

By playing with the parameters of the model, $\lambda = \pm 1$, $\hat{\kappa}^2$, $\hat{m}_b^2$ and $\delta\hat{\Lambda}$, we can find regions where $z_{\rm IR}$ is stabilized thanks to the presence of the 5D tachyon. These are shown in figure 3 in the plane $\hat{m}_b^2 - \delta\hat{\Lambda}$ for $\hat{\kappa}^2 = 4$ and $\lambda = 1$ (left plot), and $\lambda = -1$ (right plot). These regions are bounded from the left and the right at which, as it will be discussed later, the radion is massless. At the left boundary one obtains the lowest value of (a stabilized) $z_{\rm IR}$. For $\hat{m}_b^2 > -2$, this lowest value of the IR-brane position is achieved when $\delta\hat{\Lambda} = 0$; for $\hat{m}_b^2 \to -2$ we obtain the smallest $z_{\rm IR}/z^c_{\rm IR}$ that is given by $z_{\rm IR} = e^{1/2} z^c_{\rm IR}$, as can be

JHEP10(2019)202

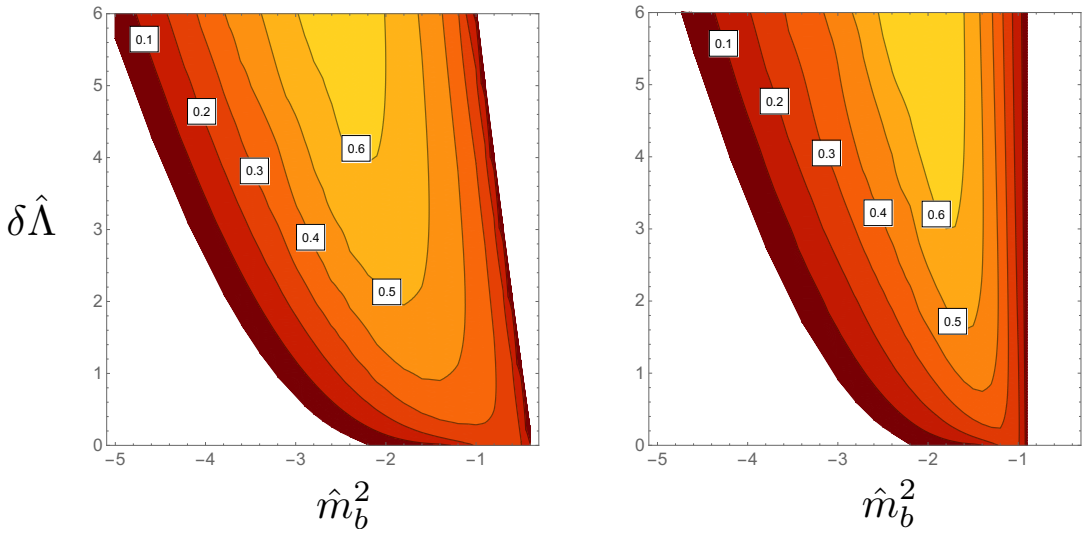

Figure 3. Region of the parameter space that leads to a stable IR-brane for $\hat{\kappa}^2 = 4$ and $\lambda = 1$ (left) and $\lambda = -1$ (right). We also provide the value of the lightest scalar mass, m_{S_1}/m_ρ.

analytically found by looking at the 4D effective theory (see appendix B). On the other hand, as we get close to the boundary on the right of the regions in figure 3, we have $z_{\rm IR} \to \infty$ (limit II). In most of the colored regions however we have that $z_{\rm IR} \sim z_\chi$. In other words, the model naturally predicts the scale of chiral symmetry breaking to be around the scale of confinement.

If the radion is the lightest 4D mode in the theory, we can use eq. (3.26) to obtain its effective potential. The radion corresponds in the dual 4D CFT to the dilaton, ϕ_d, whose VEV determines the scales of the model. For this reason ϕ_d at the minimum is related with the warp factor evaluated at $z = z_{\rm IR}$. Nevertheless, outside the minimum eq. (3.26) the relation of $z_{\rm IR}$ with ϕ_d is a more complicated function, $z_{\rm IR} = f(\phi_d)$, especially in the basis where ϕ_d is canonically normalized. Going off-shell requires not equating the l.h.s. of eq. (3.26) to zero, and identifying this with the first derivative of the dilaton effective potential:

$$\frac{dV_{\rm eff}(\phi_d)}{d\phi_d} = \frac{\phi_d^3}{n(\phi_d)} \left(\sqrt{1 + \frac{\hat{\kappa}^2 L^4}{12} \left(\frac{V_b'^{\,2}}{2M_5^2} - V(\phi) \right)} + \frac{\hat{\kappa}^2 L^3}{6M_5} V_b \right) \Bigg|_{z_{\rm IR} = f(\phi_d)} , \tag{3.30}$$

where $n(\phi_d) > 0$ is in general a complicated function of ϕ_d (that cannot be zero, otherwise we will have an extra minimum beyond eq. (3.26)) that we do not need to specify here. By integrating eq. (3.30) over ϕ_d, one can obtain the dilaton effective potential $V_{\rm eff}(\phi_d)$. For the simple case in which the backreaction is neglected and the space is just AdS_5, we have $z_{\rm IR} \propto 1/\phi_d$ and $n(\phi_d)$ is just a constant. For this case we show the effective potential (up to an overall constant) in figure 4. We can see that the potential has a minimum at $z_{\rm IR} \simeq 2 - 3\, z_{\rm IR}^c$ and goes to a constant value at large $z_{\rm IR}$, where ϕ becomes constant as it approaches the minimum of its 5D potential. For a better understanding of the dilaton effective potential, we can analytically calculate the effective potential of the 4D tachyon

JHEP10(2019)202

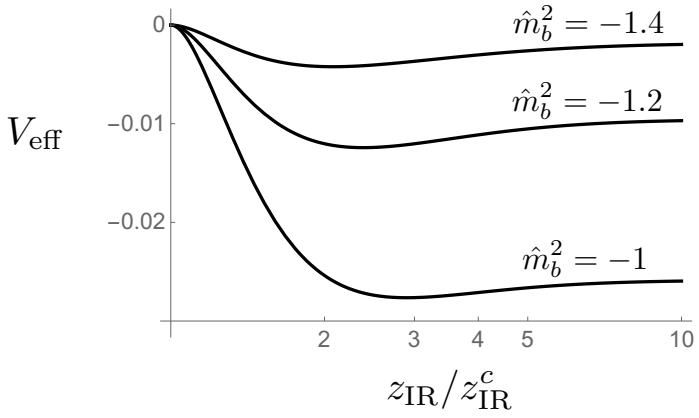

Figure 4. Dilaton effective potential for $\lambda = 1$, $\hat{\kappa}^2 = 0$, $\delta\hat{\Lambda} = 0$ and different values of $\hat{m}_b^2$.

and dilaton in the limit $z_{\rm IR}/z_{\rm IR}^c \approx 1$. This is done in appendix B. This shows that the origin of the existence of a minimum in $V_{\rm eff}(\phi_d)$ can be tracked back to the log-dependence in eq. (3.22).

3.4 Excitations around the 5D tachyon

The main interest of the article is to know whether close to the conformal transition there is a light dilaton, as often claimed in the literature. Therefore we will start considering the flavor-singlet 0^{++} spectrum of the theory, to analyze later other sectors.

3.4.1 The singlet scalar sector and light dilaton

The flavor-singlet 0^{++} spectrum is composed by the radion (the only scalar in the gravitational sector) and the excitations of Φ_s around the background $\phi(z)$. Since the mixing of the dilaton with Φ_s is in principle sizable for $N_F \sim N_c$ ($\hat{\kappa}^2 \sim 1$), we must consider the coupled EOM between the scalar sector and the gravitational sector. The equations for the mass spectrum are given in appendix A.2 and must be solved numerically.

For the lightest mode S_1 the results are presented in figure 3 for $\lambda = \pm 1$. We have normalized the S_1 mass to the one of the lightest vector resonance, m_ρ, being this latter the lightest state in real QCD and holographic versions [33–35]. Figure 3 shows that the 0^{++} state is always lighter than the vector in all regions of the parameter space. At the boundary of the regions at which IR-brane stabilization is achieved, the dilaton is massless, but its mass is roughly below half of the ρ mass in most of the interior region. We have checked that for larger $\hat{\kappa}^2$, the value of m_{S_1} increases but not significantly.

To understand why the dilaton mass is small, it is convenient to show how its mass varies as a function of $z_{\rm IR}$ for different values of $\hat{m}_b^2$. This corresponds to moving in vertical lines in the plane of figure 3 from the bottom to the top, trading the parameter $\delta\hat{\Lambda}$ for $z_{\rm IR}$ by means of eq. (3.27). We remark however that we will present results for a wide region of $z_{\rm IR}$, going beyond the allowed region eq. (3.29). This will help us to understand the origin of the smallness of m_{S_1}/m_ρ. The result is shown in figure 5 for different values of

JHEP10(2019)202

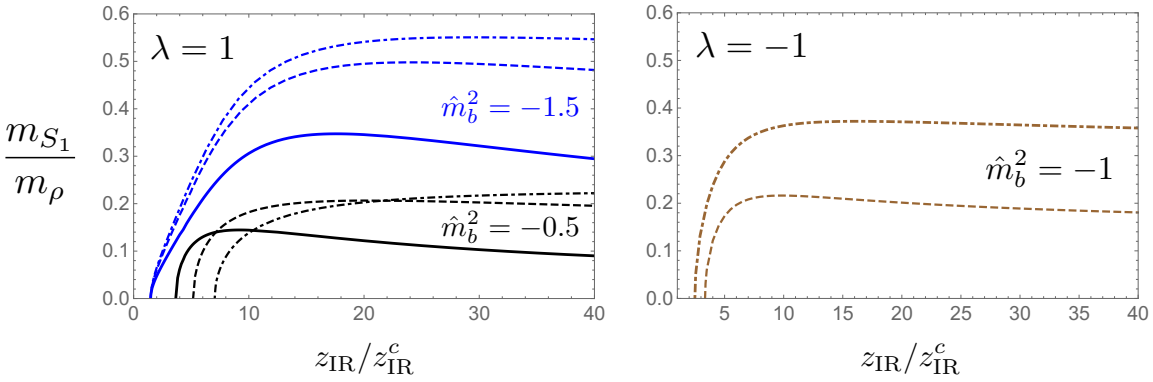

Figure 5. Masses of the lightest singlet scalar S_1 normalized to the vector mass. We have taken $\hat{\kappa}^2 = 1$ (solid line), $\hat{\kappa}^2 = 4$ (dashed line) and $\hat{\kappa}^2 = 10$ (dot-dashed line). LEFT: $\lambda = 1$ and $\hat{m}_b^2 = -1.5$ (-0.5) for the upper blue (lower black) lines. RIGHT: $\lambda = -1$ and $\hat{m}_b^2 = -1$.

$\hat{m}_b^2 > -2$. We see that the dilaton mass starts at zero at $z_{\rm IR} \simeq z_{\rm IR}^c$, grows for intermediate $z_{\rm IR}/z_{\rm IR}^c$, and tends again to zero for $z_{\rm IR}/z_{\rm IR}^c \to \infty$.

We can understand this behaviour analytically. Assuming that S_1 is the radion/dilaton, we can analytically obtain its mass by taking the derivative of eq. (3.30) evaluated at the minimum eq. (3.26). We obtain

$$m_{\phi_d}^2 \simeq 4\hat{\kappa}^2 a(z_{\rm IR}) L^2 \left[\frac{a^2}{24\dot{a}}\left(\frac{V_b' V_b''}{M_5^2} - V'\right) - \frac{V_b'}{6M_5}\right]_{z_{\rm IR}} \partial_{z_{\rm IR}}\phi(z_{\rm IR})\,, \tag{3.31}$$

where we have used that at the minimum $\phi_d^3 \partial_{\phi_d} f(\phi_d)/n(\phi_d) \simeq -4a(z_{\rm IR})/L$ derived in appendix A. In our particular case eq. (3.31) reduces, after normalizing to the vector mass eq. (3.39), to

$$\frac{m_{\phi_d}^2}{m_\rho^2} \simeq P(\phi(z_{\rm IR}))\, Q(\phi(z_{\rm IR}))\, \beta_\phi(z_{\rm IR})\,, \tag{3.32}$$

where we have defined the dimensionless functions

$$P(\phi(z_{\rm IR})) \equiv \frac{\hat{\kappa}^2\phi^2(z_{\rm IR})}{6m_\rho^2} \simeq \frac{8\hat{\kappa}^2 L^2 \phi^2(z_{\rm IR})}{27\pi^2\, \dot{A}_{\rm IR}^2\big|_{\hat{m}_b^2=0}}\,, \tag{3.33}$$

$$Q(\phi(z_{\rm IR})) \equiv \frac{1}{\dot{A}_{\rm IR}}\left[\lambda\phi^2(z_{\rm IR})L^2 - (\hat{m}_b^2+2)^2 - 4\hat{m}_b^2(\dot{A}_{\rm IR}-1)\right]\,, \tag{3.34}$$

$$\beta_\phi(z_{\rm IR}) \equiv \frac{L}{a(z_{\rm IR})}\frac{\partial_{z_{\rm IR}}\phi(z_{\rm IR})}{\phi(z_{\rm IR})}\,, \tag{3.35}$$

with

$$\dot{A}_{\rm IR} \equiv -\frac{\dot{a}L}{a^2}\bigg|_{z_{\rm IR}} = \sqrt{1 + \frac{\hat{\kappa}^2 L^2\phi^2}{24}\left(4 + \hat{m}_b^4 - \frac{\lambda L^2}{2}\phi^2\right)}_{z_{\rm IR}}\,, \qquad \dot{A}_{\rm IR} \geq 1\,, \tag{3.36}$$

JHEP10(2019)202

where we have used eq. (3.16). From eq. (3.32) we can infer different regimes at which the dilaton can be light:

- The prefactor $P(\phi(z_{\rm IR}))$ is suppressed for $\hat{\kappa}^2\phi^2(z_{\rm IR}) \ll 1/L^2$. Therefore in the limit I the dilaton is always light, even when formally we take $\hat{\kappa}^2 \gg 1$ (see discussion after eq. (3.24)). Also for large values of $L\phi$, possible in the limit II with $\lambda < 0$, we have $P \to 1/(L\phi)^2$, and consequently the dilaton mass is suppressed.

- The function $Q(\phi(z_{\rm IR}))$ determines the sign of $m^2_{\phi_d}$. In the limit I we have $\phi L \to 0$ and $\dot{A}_{\rm IR} \to 1$, and then Q becomes negative. This means that the dilaton effective potential has actually no minimum, as we already pointed out in section 3.3. As we increase $z_{\rm IR}/z^c_{\rm IR}$, Q increases till becoming zero, corresponding to the points seen in figure 5 with $m_{\phi_d} = 0$. One can check that they are inflection points of the dilaton potential.

- The function β_ϕ is the main responsible for natural light dilatons in Goldberger-Wise models [10–14]. Since moving simultaneously the UV and IR boundaries does not change physical quantities, we can deduce

$$\partial_{z_{\rm IR}}\phi(z_{\rm IR}) = -\frac{a(z_{\rm IR})}{a(z_{\rm UV})}\partial_{z_{\rm UV}}\phi(z_{\rm IR})\,, \tag{3.37}$$

  showing that β_ϕ is in fact sensitive to the dependence of the tachyon ϕ with variations of the UV boundary, and therefore to the explicit breaking of conformal invariance (that arises due to the presence of the UV cutoff). For this reason β_ϕ is directly related with the beta function $\beta_{\lambda_{\rm eff}}$ of the dilaton effective coupling of eq. (1.1). β_ϕ explains why the dilaton mass always goes to zero for large $z_{\rm IR}/z^c_{\rm IR}$. Indeed, as we approach the limit II for $\lambda > 0$, the 5D tachyon goes to the minimum of its potential where it becomes constant. We then expect $\beta_\phi \ll 1$. Also in the limit II for $\lambda < 0$ the slow-roll conditions are achieved and β_ϕ tends to zero. Unfortunately, these regions of a parametrically light dilaton are very small in the full parameter space of the model, see figure 3, since stabilizing the IR-brane at large $z_{\rm IR}/z^c_{\rm IR}$ requires an adjustment of the parameters of the model. In the limit I we can derive from eq. (3.20) and eq. (3.24) that $\beta_\phi \sim 1/(2\ln(z_{\rm IR}/z^c_{\rm IR}))$, and using the eq. (B.5) we get $\beta_\phi \sim \beta$ that is nonzero but smallish in the regions considered.[9]

The situation is similar in regions with $\hat{m}_b^2 < -2$ (see figure 3 or figure 8). The only main difference is that the dilaton mass goes to zero for small values of $z_{\rm IR}/z^{c\prime}_{\rm IR}$, not due to $Q \to 0$, but because $\phi(z_{\rm IR})$ tends to a constant value as explained in section 3.2.2, and therefore $\beta_\phi \to 0$.

We conclude that the dilaton mass is parametrically smaller than m_ρ at small and large $z_{\rm IR}$ (respectively corresponding to the left and right boundaries of the regions of figure 3). At small $z_{\rm IR}$, the reason is either the existence of an inflection point in the dilaton potential

[9] Notice that $\partial_{z_{\rm IR}}\phi(z_{\rm IR}) \neq \partial_z\phi|_{z_{\rm IR}}$, and then β_ϕ does not measure the growth of the tachyon (that is power-law $\sim z^2$), but its variation as we move the IR-brane (or UV-boundary) that it is much milder (logarithmic).

JHEP10(2019)202

(for the case $\hat{m}_b^2 > -2$) or that $\phi(z_{\rm IR})$ becomes frozen and $\beta_\phi \to 0$ (for the case $\hat{m}_b^2 < -2$). Also at small 5D tachyon values its log-dependence on $z_{\rm IR}$ gives a smallish β_ϕ and therefore a smallish dilaton mass. At large $z_{\rm IR}$ (limit II) the geometry approaches again AdS_5 (the dual model flows towards another approximate CFT_4) where scale invariance is partially recovered and therefore the dilaton mass must go to zero. "Trapped" between these two limits, the dilaton mass cannot grow much in the intermediate region and then remains always the lightest resonance (although not parametrically lighter than the others).

Finally, we would also like to discuss the mass of the second lightest singlet scalar, S_2. This is also obtained numerically (see appendix A.2), and the result is shown in figure 6 for certain representative values of the parameter space. This scalar S_2 is mostly the excitation around the profile $\phi(z)$ (up to a small mixing with the radion), a Higgs-like state. For this reason when $z_{\rm IR} \to z_{\rm IR}^c$, we expect $m_{S_2}^2 \to \lambda_t \phi_t^2 \to 0$, as appreciated in figure 6.

3.4.2 Non-singlet scalars, vector and axial-vector excitations

For the scalars in the adjoint under the $SU(N_F)_V$ symmetry, Φ_a, the EOM is given by

$$[\partial_\mu^2 - a^{-3}\partial_z a^3 \partial_z + a^2 M_\Phi^2 + a^2(3\lambda - 2N_F\lambda_2)\phi^2(z)]\Phi_a = 0\,. \tag{3.38}$$

As we already mentioned, there are two important difference with respect the singlet scalar case. First, the scalars in the adjoint do not mix with the radion/dilaton. Second, the quartic coupling in eq. (3.38) is different from the singlet case due to the presence of λ_2. This implies that the adjoint scalar masses are expected to be different from the singlet scalar masses, with the magnitude of the mass splitting being sensitive to $\hat{\kappa}^2$ and λ_2.

We are also interested in the vector $V_M = (L_M + R_M)/\sqrt{2}$ and axial-vector $A_M = (L_M - R_M)/\sqrt{2}$ spectrum [33–35]. The vector spectrum is only indirectly sensitive to the tachyon through its impact to the metric. Therefore, since flavor-singlet resonances (the ω in QCD) and adjoint resonances (the ρ in QCD) feel the same metric and have the same boundary conditions, they get equal masses. This is an important prediction of the 5D model.[10]

It is useful to have an approximate analytic value for m_ρ, since we are using this mass to normalize the other resonance masses. This is possible in the limit in which the 5D space is approximately AdS, that corresponds to limits I and II, as we explained in section 3.2. In AdS_5 we have $m_\rho \sim -(3\pi/4)(\dot{a}/a)$. We find that a reasonably good approximation for $\dot{a}/a$ in the limit of small and large $z_{\rm IR}$ is given by eq. (3.16) neglecting the derivative terms and taking ϕ at $z = z_{\rm IR}$.[11] We then have:

$$m_\rho \simeq \frac{3\pi}{4}\frac{a(z_{\rm IR})}{L}\,\dot{A}_{\rm IR}\Big|_{\hat{m}_b^2=0}\,. \tag{3.39}$$

We have checked that this value is within $\lesssim 20\%$ the exact mass of ρ for the regions of the parameter space studied in this article.

[10] Of course, mass splittings could be generated at the loop level or from higher-dimensional operators in eq. (3.2), but these are expected to be suppressed.

[11] We put to zero the derivative terms to avoid the drastic change of ϕ near the IR boundary -see footnote 8.

JHEP10(2019)202

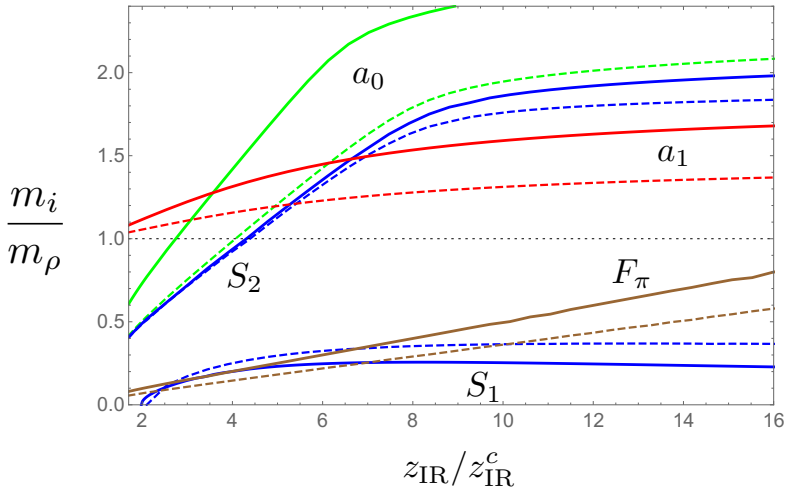

Figure 6. Masses of the two lightest singlet scalars, S_1 and S_2, lightest adjoint scalar (a_0), lightest axial-vector (a_1) and F_π, normalized to the vector mass for $\hat{m}_b^2 = -1$, $\lambda = 1$, $\lambda_2 = -2$, $g_5^2 = 1$ and $\hat{\kappa}^2 = 1$ (4) for the solid (dashed) line.

The axial-vector spectrum depends directly on the ϕ profile via eq. (3.13), being this responsible for the mass splitting from the vector spectrum. Another important quantity is the Goldstone decay constant F_π, that is the order parameter of the chiral breaking. This can be calculated via holography from the axial-vector two-point correlator at zero momentum [33–35]:

$$F_\pi = \Pi_A(0) = -\frac{M_5 L}{2 z_{\rm UV}} \left.\frac{\partial_z A(z)}{A(z)}\right|_{z_{\rm UV}} , \tag{3.40}$$

where $A(z)$ is the 5D solution of the axial-vector with Dirichlet UV-boundary condition.

The results (with no approximations) are shown in figure 6 for some representative values of the parameter space. Following the notation in QCD, we denote with a_0 and a_1 the adjoint scalar and axial-vector respectively. Since F_π is the only quantity that depends on M_5 (N_c in the dual theory), we have fixed its value using eq. (4.4) with $N_c = 3$. For $z_{\rm IR} \approx z^c_{\rm IR}$ (limit I) where the chiral breaking is small, we see that indeed F_π and $(m_\rho - m_{a_1})/m_\rho$ are small. As we increase $z_{\rm IR}$, we move towards limit II where the breaking of the chiral symmetry is larger, as can be appreciated by the growth of F_π and $S_2 - a_0$ and $\rho - a_1$ mass splittings. On the other hand, the mass of a_0 strongly depends on λ_2, and we have chosen a negative value, $\lambda_2 = -2$, that makes the mass splitting with the singlet sector positive, as lattice simulations (see later) seem to suggest. Similarly to the singlet scalars, we also have that m_{a_0} goes to zero as $z_{\rm IR} \to z^c_{\rm IR}$, since the tachyon value goes to zero in this limit and we recover the chiral symmetry.

Let us briefly comment on what happens for other values of the parameters of the model. The effect of $\hat{\kappa}^2$ in the mass spectrum is clear from figure 6 where we show the spectrum for two different values of $\hat{\kappa}^2$. The main effect is that as we increase $\hat{\kappa}^2$, the profile of ϕ becomes flatter and smaller, as appreciated in figure 2, giving a smaller breaking of the chiral symmetry. The spectrum is mildly sensitive to the values of $\hat{m}_b^2$, unless we take

JHEP10(2019)202

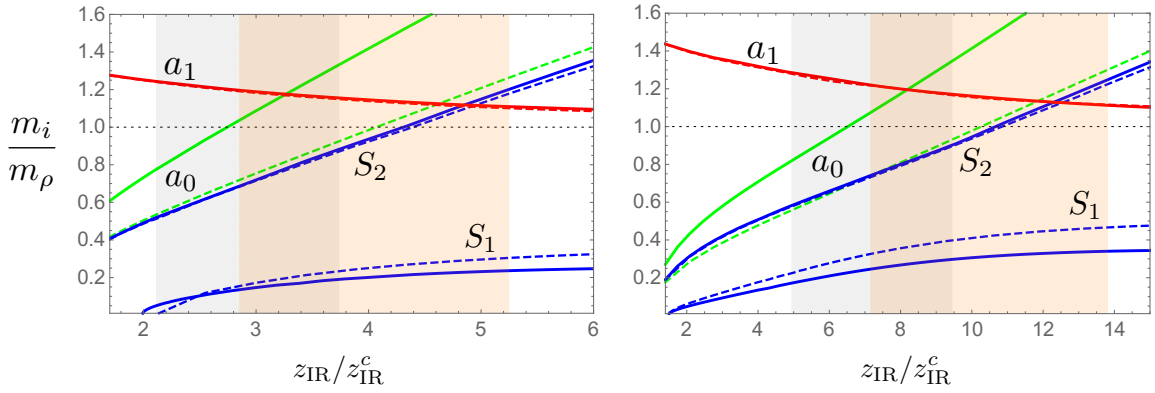

Figure 7. Masses of the two lightest singlet scalars, S_1 and S_2, lightest adjoint scalar (a_0), lightest axial-vector (a_1) normalized to the lightest vector mass (m_ρ) for constant $F_\pi \sim m_\rho/7$ as a function of $z_{\rm IR}/z^c_{\rm IR}$ for $\lambda = 1$. We have taken $\hat{\kappa}^2 = 1$ (4) for solid (dashed) lines. The left grey (right orange) band corresponds to the region $0.5 < g_5^2 < 2$ for $\hat{\kappa}^2 = 1$ (4). LEFT: $\hat{m}_b^2 = -1$. RIGHT: $\hat{m}_b^2 = -1.5$.

$\hat{m}_b^2 < -2$ that we will discuss later (figure 8). Finally, g_5^2 only affects F_π and m_{a_1} that will increase as g_5^2 increases.

It is more instructive, also in part to compare later our results with lattice simulations, to analyze the spectrum at constant F_π. For this purpose, we adjust g_5^2 to fulfill, for the different values of $z_{\rm IR}/z^c_{\rm IR}$ (or equivalently $\delta\hat{\Lambda}$), the relation $F_\pi \simeq m_\rho/7$ as in QCD. The results are given in figure 7 for $\hat{m}_b^2 = -1$ (left) and $\hat{m}_b^2 = -1.5$ (right). We have kept g_5^2 in the interval $0.5 < g_5^2 < 2$ and this has limited the possible values of $z_{\rm IR}/z^c_{\rm IR}$ to the blue and orange bands for $\hat{\kappa}^2 = 1$ and 4 respectively.[12] The main conclusions from figure 7 are the following. The lightest resonance is always the scalar S_1, a dilaton-like state. The S_2, the Higgs-like state, is also smaller or around m_ρ, and can only be larger if we take large values of $z_{\rm IR}/z^c_{\rm IR}$ (that implies small values of g_5^2 in order to keep $F_\pi \sim m_\rho/7$). The ratio m_{a_1}/m_ρ is closer to 1 than in real QCD where $m_{a_1}/m_\rho \sim 1.6$ or previous holographic QCD versions [33–35]. The mass of a_0 is also smaller than in real QCD. As we will see in the following, these properties are also found in lattice QCD for large N_F.

The situation is only slightly modified in the region $\hat{m}_b^2 < -2$. In figure 8 we show the mass spectrum for $\hat{m}_b^2 = -3$. The main differences with respect figure 7 is in the scalar mass spectrum where we appreciate that at smaller values of $z_{\rm IR}/z^{c\prime}_{\rm IR}$, where here $z^{c\prime}_{\rm IR} \equiv e^{\pi/\sqrt{\epsilon}} z_{\rm UV}$, the a_0 and S_2 masses do not go to zero. The reason is the following. As explained in section 3.2.2, for $\hat{m}_b^2 < -2$ the profile of ϕ is always non-zero (unless $z_{\rm IR} < z^c_{\rm IR} \sim z_{\rm UV}$). This implies that we do not recover the chiral symmetry in the region of interest, $z_{\rm IR} \sim z^{c\prime}_{\rm IR}$, and the S_2 and a_0 masses never approach zero. Nevertheless, their masses are predicted to be around the ρ mass.

The main lesson that we have learned on the mass spectrum of S_2, a_0 and a_1 is that they seem to tend to be lighter in models close to the conformal transition (as compared to real QCD that is far from the conformal critical point). What is the reason for that?

[12] The constraint $\delta\hat{\Lambda} \leq 0$ has not been imposed. If we impose it, we obtain $z_{\rm IR}/z^c_{\rm IR} \geq 3.06$ (3.37) for $\hat{\kappa}^2 = 1$ (4) in the left plot of figure 7, and $z_{\rm IR}/z^c_{\rm IR} \geq 1.88$ (1.9) for the right plot.

JHEP10(2019)202

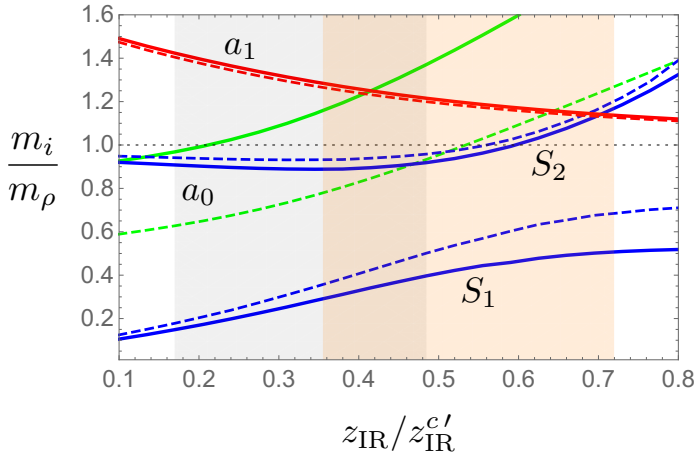

Figure 8. As in figure 7 but for $\hat{m}_b^2 = -3$.

As it is well-known, the dimension of a scalar operator has a minimal value determined by its unitarity bound, in this case $\text{Dim}[\mathcal{O}_*] = 1$, a limit at which the scalar decouples from the CFT [40]. Therefore it is expected that, as a scalar operator approaches this decoupling limit, the mass of the lightest resonance associated to it becomes smaller. By using the AdS/CFT correspondence this means, via eq. (2.4), that the lightest Φ resonance is expected to be lighter the more we approach the BF-bound. We can also understand this "geometrically". The wave-function of the lightest scalar grows as $z^{2+\sqrt{4+M_\Phi^2 L^2}}$, that implies that the wave-function becomes flatter and spread more into the AdS_5 space as we approach the BF-bound $M_\Phi^2 L^2 \to -4$. In this limit, then, the scalar excitation becomes less sensitive to the IR and therefore its mass is expected to be smaller (see also [41]).[13]

The fact that the profile of ϕ becomes flatter as we approach the BF-bound also explains the smaller mass splitting between a_1 and ρ than in real QCD. Indeed, if we keep F_π constant, the flatter the ϕ profile, the smaller $\phi(z_{\rm IR})$. Since the a_1 wave-function is peaked towards the IR-brane, it is mostly sensitive to the value of $\phi(z_{\rm IR})$. Therefore, as the 5D mass of ϕ gets closer to the BF-bound, we expect m_{a_1} to be less sensitive to chiral breaking. For the same reason we understand m_{a_1} becoming smaller as we increase $z_{\rm IR}$ (see figure 7), as ϕ becomes flatter for larger $z_{\rm IR}$.

4 Comparison with lattice QCD in the large N_F

Lattice results for $N_c = 3$ QCD with $N_F = 8$ have been reported in refs. [1–5]. At such large value of N_F, it is believed that QCD is close to the conformal transition, expected to

[13] We could make the wave-function even flatter by quantizing differently the scalar following ref. [39] (valid for $-4 < (M_\Phi L)^2 < -3$). In this case we have $\text{Dim}[\mathcal{O}_*] = 2 - \sqrt{4 + M_\Phi^2 L^2}$ that means that the scalar is the dual of an operator of dimension between 1 and 2. We will get in this case the wave-function $z^{2-\sqrt{4+M_\Phi^2 L^2}}$, reaching the full decoupling from the IR (from the CFT) at $M_\Phi^2 = -3/L^2$ when the mode becomes non-normalizable. Nevertheless the scalar becomes UV sensitive and it is not expected to survive in the spectrum.

JHEP10(2019)202

occur around $N_F \sim 9$. It was found [1–5]

$$\frac{F_\pi}{m_\rho} \simeq 0.14\,, \quad \frac{m_{f_0}}{m_\rho} \simeq 0.5\,, \quad \frac{m_{a_0}}{m_\rho} \simeq 1\,, \quad \frac{m_{a_1}}{m_\rho} \simeq 1.4\,, \tag{4.1}$$

where f_0 is the lightest flavor-singlet 0^{++} state (S_1 in our notation).[14] It is instructive to compare them with real QCD that is supposed to be far from the conformal edge. We have [42]

$$\frac{F_\pi}{m_\rho} \simeq 0.13\,, \quad \frac{m_{f_0}}{m_\rho} \simeq 1.3\,, \quad \frac{m_{a_0}}{m_\rho} \simeq 1.3\,, \quad \frac{m_{a_1}}{m_\rho} \simeq 1.6\,. \tag{4.2}$$

We see that close to the conformal transition, we spectrum of eq. (4.1) shows, as compared to real QCD eq. (4.2), lighter f_0 and a_0 scalars, and a smaller mass splitting between the ρ and a_1 resonance. Surprisingly, the ratio of F_π/m_ρ is quite similar to real QCD, showing that this quantity is quite independent of N_F.

Let us compare our results to the values of eq. (4.1). In order to reduce the number of parameters, we can match the predictions of our model at the UV with those of QCD with N_F flavors. In particular, the two-point vector-vector correlator at large momentum p^2 is given in our model by [34, 35]

$$\Pi_V(p^2) \simeq -\frac{M_5 L}{2g_5^2} p^2 \ln(p^2 z_{\rm UV}^2)\,, \tag{4.3}$$

that matching to that of QCD with N_F flavors gives

$$\frac{M_5 L}{g_5^2} = \frac{N_c}{12\pi^2}\,. \tag{4.4}$$

Using eq. (4.4) our predictions for the mass spectrum were presented in figures 7 and 8 for $F_\pi = m_\rho/7$. We see that our predictions on the spectrum of resonances follow quite close the pattern eq. (4.1). We have m_{a_1}/m_ρ closer to one than in QCD, with the scalars a_0 and S_1 being lighter than the ρ in most of the parameter space. Indeed, in the region $1.2 < m_{a_1}/m_\rho < 1.4$, we find $m_{a_0}/m_\rho \lesssim 1$ and $m_{S_1}/m_\rho \lesssim 0.3$.

There are other important predictions arising from our holographic model that would be interesting to check in future lattice simulations. For example, as we already mentioned, the mass splittings between the adjoint and singlet vectors is zero at leading order, and can only arise from loop effects or higher-dimensional operators that are suppressed. Also the second singlet scalar S_2 (a Higgs-like scalar) seems to be lighter than the ρ in the region where $1.2 < m_{a_1}/m_\rho < 1.4$. Finding this second resonance so light would be a clear indication that the lightest scalar S_1 is a dilaton and not a Higgs-like state. Other properties of the scalars, such as decay constants or couplings, that can also be calculated in these holographic models, are left for future work.

[14] Lattice results are presented for nonzero quark masses. We will assume here that the pattern eq. (4.1) does not drastically change in the limit $M_q \to 0$.

JHEP10(2019)202

5 Models for the hierarchy problem

The model described here open new possibilities for generating small scales. Since the IR-brane is naturally stabilized at $z_{\rm IR} \sim O(z^c_{\rm IR})$, we have a way to generate exponentially small scales. Indeed, from eq. (3.21) we have

$$\frac{1}{z_{\rm IR}} \sim \frac{1}{z^c_{\rm IR}} = e^{-\pi/\sqrt{\epsilon}} \frac{1}{z_{\rm UV}} \ll \frac{1}{z_{\rm UV}} \,. \tag{5.1}$$

The presence of a scalar with a mass just below the BF bound can also be achieved dynamically. If the mass of Φ is z-dependent, for example, $M^2_\Phi L^2 = -4 - \mathcal{E}(z)$, where $\mathcal{E}(z)$ slowly varies from negative to positive values as z increases, the mass of Φ will cross the BF bound at the position $z = z'_{\rm UV}$ at which $\mathcal{E}(z'_{\rm UV}) = 0$. For example, we can consider $\mathcal{E}(z) = \epsilon \ln(z/z'_{\rm UV})$ with $\epsilon \ll 1$ (for other cases, see [43]). This z-dependent mass for Φ can be easily achieved by promoting $\mathcal{E}(z)$ to a scalar R with a 5D potential $V = -\sqrt{\epsilon} R(1 + |\Phi|^2/L^2)$. This scalar gets a profile $R(z) = \sqrt{\epsilon} \ln(z/z_{\rm UV})$, giving a contribution to the mass of Φ proportional to $\epsilon \ln(z/z_{\rm UV})$.

For $M^2_\Phi L^2 = -4 - \mathcal{E}(z)$ with $\mathcal{E}(z) = \epsilon \ln(z/z'_{\rm UV})$, the wave-function of the massless mode is not anymore eq. (3.20) but

$$\phi(z) = \frac{\phi_t(x)}{N} z^2 \sqrt{\ln(z/z_{\rm UV})}\, J_{1/3}\left(\frac{2}{3}\sqrt{\epsilon} \ln^{3/2} \frac{z}{z_{\rm UV}}\right) , \tag{5.2}$$

where $J_{1/3}$ is a Bessel-function of order $1/3$, and the IR-boundary condition eq. (3.17) at $z_{\rm IR} = z^c_{\rm IR}$ leads now in the limit $\epsilon \to 0$ to

$$\frac{2}{3}\sqrt{\epsilon} \ln^{3/2} \frac{z^c_{\rm IR}}{z_{\rm UV}} \simeq \left(n - \frac{1}{12}\right)\pi \,, \quad n = 1, 2, \dots \,, \tag{5.3}$$

corresponding to the zeros of the Bessel function. The situation is quite similar to the case of constant $\mathcal{E}(z)$ discussed above; the only important difference worth to mention is that in the limiting case II with $\lambda > 0$, the maximal value of ϕ is not constant, as M^2_Φ evolves logarithmically. The theory has evolved into a deformed CFT.

We leave the implications of these scenarios for the electroweak scale for future work. We only point out several interesting features. First, the lightness of the dilaton can have important implications for the LHC [44–46]. Also the fact that the mass of a_1 is closer to the mass of ρ implies smaller values for the S-parameter (this was also pointed out in ref. [47] for $M^2_\Phi \to -4/L^2$ from above), favored by precision experimental data. Furthermore, having the operator that drives symmetry breaking a dimension close to 2 helps to pass flavor constraints [48]. Also it was shown in ref. [49] that these models can lead to a long period of supercooling in the early universe with implications in Dark Matter and axion cosmological abundances.

JHEP10(2019)202

6 Conclusions

We have used holography to study strongly-coupled theories close to the conformal transition, that is the transition from the non-conformal regime to the conformal one. This transition is expected to happen in gauge theories (such as QCD) as the number of fermions N_F increases. Recent lattice results [1–5] have shown that as we get closer to the conformal transition, the lightest resonance is a 0^{++} state, claimed to be a dilaton.

We have followed the idea of ref. [6] that suggested that conformality is lost when the IR fixed point merges with a UV fixed point, as shown in figure 1. Holography tells that this must occur by an operator $\mathcal{O}_*$ (probably $q\bar{q}$ in QCD) whose dimension is equal to two that gets a small imaginary part when leaving the conformal regime. In the gravitational dual models this is driven by a scalar whose mass goes below the BF bound and becomes tachyonic.

We have presented a very simple extra-dimensional model with the essential ingredients to study the conformal transition and calculate the mass spectrum. The model consists of a five-dimensional gravitational sector with a scalar and gauge bosons associated to the global $\mathrm{SU}(N_F)_L \otimes \mathrm{SU}(N_F)_R \otimes \mathrm{U}(1)_B$. We have allowed for the most general Lagrangian following the 5D EFT rules, and explained the connection between the 5D couplings and the large N_c and N_F expansion. To model confinement we cut off the space by an IR-brane that we showed to be stabilized by the presence of the tachyon.

We have calculated the mass spectrum of this 5D model, showing that indeed the dilaton corresponds to the lightest resonance. To understand this property, we have derived a simple formula for the dilaton mass, eq. (3.32). This shows that the mass of the dilaton crucially depends on $\beta_\phi(z_{\mathrm{IR}})$ given in eq. (3.35) that is sensitive to the variation of $\phi(z_{\mathrm{IR}})$ as we move the UV boundary (therefore sensitive to the explicit breaking of the conformal symmetry). Either for small or large values of z_{IR}, we have shown that $\beta_\phi(z_{\mathrm{IR}}) \to 0$ and therefore the dilaton mass tends to zero. For small z_{IR} this is due to either the existence of an inflection point in the dilaton potential (for $\hat{m}_b^2 > -2$), or that $\phi(z_{\mathrm{IR}})$ becomes constant (for $\hat{m}_b^2 < -2$). Also for small $\phi(z)$, where we can perform analytical calculations, we find a mild log-dependence of $\phi(z_{\mathrm{IR}})$ with z_{IR} (and therefore a smallish $\beta_\phi(z_{\mathrm{IR}})$) that can be traced back to the explicit breaking of the conformal symmetry due to the double-trace marginal operator $\mathcal{O}_g = |\mathcal{O}_*|^2$. For large z_{IR}, also $\beta_\phi(z_{\mathrm{IR}}) \to 0$ as the tachyon either goes to the minimum of its potential and becomes constant or enter into a "slow-roll" condition, meaning that the geometry approaches again AdS_5. In between these two limiting cases, the dilaton can become heavier but its mass cannot grow enough to overcome m_ρ. Therefore the dilaton is found to be lighter than the rest of the resonances, although it is never parametrically lighter in most of the area of the allowed parameter space, as shown in figure 3.

We have compared our predictions with lattice results for QCD with a large N_F (eq. (4.1)) and showed that our model predicts quite similar resonance mass pattern: the lightest state is the singlet 0^{++}, with the adjoint scalar a_0 mass close to m_ρ and lighter than in real QCD. We have also shown than the mass splitting between the vector (ρ) and axial-vector (a_1) is smaller close to the conformal transition. We have given a geometric explanation for these properties. Furthermore, the 5D model proposed here also provides

JHEP10(2019)202

extra predictions that lattice could check in the future. For example, we find that the second 0^{++} state, S_2, is mostly a Higgs-like state ($q\bar{q}$ state) with a mass around m_ρ, similarly as a_0. The 5D model also predicts that the masses of the flavor singlet and adjoint vector resonances are similar (as it happens also in real QCD).

There are several interesting calculations that are left for the future. For example, it is also possible to calculate decay constants and couplings of the resonances along the lines of refs. [34, 35]. One could also easily add explicit quark masses to the model to see the impact on the spectrum, or study the model at the conformal edge but inside the conformal window. It could also be interesting to understand what are the holographic versions of the complex CFT described in ref. [30]. Finally, as discussed above, this type of models can provide a new approach to the hierarchy problem with a clear impact on LHC phenomenology as the 0^{++} resonance is expected to be the lightest one. All these issues clearly deserve more attention.

Acknowledgments

We would like to thank Eugenio Megias, Giuliano Panico and Mariano Quiros. AP was supported by the Catalan ICREA Academia Program. LS was supported by a Beca Predoctoral Severo Ochoa del Ministerio de Economía y Competitividad (SVP-2014-068850). This work was also partly supported by the grants FPA2017-88915-P, 2017-SGR-1069 and SEV-2016-0588.

A Scalar and gravity coupled equations of motion

In this appendix we present the equations of motion (EOM) of the scalar and gravitational sector, that we use in this article in order to derive the background and mass spectrum of the model. For this purpose it is useful to work with proper coordinates, as the metric-scalar system of EOM simplifies. Once the results are obtained, we have rewritten them in conformal coordinates eq. (3.5) to be presented in the main text. Conformal coordinates allow a better interpretation of the results as $1/z$ determines the natural mass scale at the position z.

A.1 Scalar-metric system

In proper coordinates $\{x^\mu, y\}$ the background metric can be written as

$$ds^2 = e^{-2A(y)}\eta_{\mu\nu}dx^\mu dx^\nu - dy^2\,, \tag{A.1}$$

where $\eta_{\mu\nu} = \text{diag}(1,-1,-1,-1)$, $0 \leq y \leq y_{\text{IR}}$ with the IR-brane localized at $y = y_{\text{IR}}$, and we have conveniently rewritten the warp factor as $a = e^{-A}$. The 5D EOM for the metric-scalar system, that follow from the action in eq. (3.1) in these coordinates, are

JHEP10(2019)202

given by

$$\ddot{\phi} = 4\dot{A}\dot{\phi} + V' \,, \tag{A.2}$$

$$\dot{A} = \sqrt{\frac{1}{L^2} + \frac{\hat{\kappa}^2 L^2}{12}\Big(\frac{\dot{\phi}^2}{2} - V(\phi)\Big)} \,, \tag{A.3}$$

$$\ddot{A} = \frac{\hat{\kappa}^2 L^2}{6}\dot{\phi}^2 \,, \tag{A.4}$$

where in this appendix $\dot{\phi} \equiv \partial_y \phi$, $\dot{A} \equiv \partial_y A$. At the IR-brane we must impose the IR-boundary conditions:

$$\Big(M_5 \dot{\phi} + V_b'(\phi)\Big)\Big|_{y_{\rm IR}} = 0 \,, \tag{A.5}$$

$$\left(\frac{6M_5}{\hat{\kappa}^2 L^2}\dot{A} + V_b(\phi)\right)\Big|_{y_{\rm IR}} = 0 \,, \tag{A.6}$$

where the second equation is the junction condition that determines the value $y_{\rm IR}$ where the IR-brane is dynamically stabilized. Plugging eq. (A.3) into eq. (A.2) gives a differential equation involving only ϕ that can be easily solved. Afterwards, we can solve eq. (A.3) to obtain the metric warp factor $A(y)$. We can go to conformal coordinates by using $dy/dz = e^{-A(y)}$.

Working with proper coordinates, the slow-roll conditions are, in analogy with inflation, given by

$$\frac{\dot{H}}{H^2} \ll 1 \quad \text{and} \quad \frac{1}{H}\frac{\partial_y\left[\frac{\dot{H}}{H^2}\right]}{\left[\frac{\dot{H}}{H^2}\right]} \ll 1 \,, \tag{A.7}$$

where $H = \dot{A}$. Using eq. (A.2)–eq. (A.4), the slow-roll conditions eq. (A.7) can be written in the following equivalent form:

$$\frac{(V')^2}{(V - \frac{12}{\hat{\kappa}^2 L^4})^2} \ll \hat{\kappa}^2 L^2 \quad \text{and} \quad \frac{V''}{V - \frac{12}{\hat{\kappa}^2 L^4}} \ll \hat{\kappa}^2 L^2 \,. \tag{A.8}$$

Since we work with polynomial potentials, the two slow-roll conditions eq. (A.8) reduce to one condition when the feedback of the metric becomes important ($V \gg \frac{12}{\hat{\kappa}^2 L^4}$). This is given by

$$\hat{\kappa}^2 \phi^2 \gg 1/L^2 \,. \tag{A.9}$$

A.2 Singlet scalar-dilaton system

If the dilaton is not a priori assumed to be light, we must solve exactly the eigenmasses of the scalar sector considering the mixing between the singlet scalar Φ_s and the dilaton, which is of order one for $N_F \sim N_c$. This is done conveniently in a diagonal gauge where the brane is straight, corresponding to a constant value of the extra coordinate $y_{\rm IR}$ =const. In this gauge, the EOM reduces to eq. (3.17) of ref. [37], that we can write as

$$\mathcal{D}\psi_n = \frac{3m_n^2}{\hat{\kappa}^2 \dot{\phi}^2 L^2} e^{2A}\psi_n \quad \text{with} \quad \mathcal{D} \equiv 1 - \partial_y\left[\frac{3e^{2A}}{\hat{\kappa}^2 \dot{\phi}^2 L^2}\partial_y[e^{-2A}]\right] \,, \tag{A.10}$$

JHEP10(2019)202

with the IR-boundary condition:

$$m_n^2 \psi_n\Big|_{y_{\rm IR}} = \left(V_b'' + \frac{\ddot{\phi}}{\dot{\phi}}\right) \partial_y[e^{-2A}\psi_n]\Big|_{y_{\rm IR}} . \tag{A.11}$$

A.2.1 Light dilaton limit

When the dilaton becomes the lightest mode of the scalar sector, we can analytically derive its mass, as given in eq. (3.31). Here we present the details to obtain this mass.

The physical meaning of the dilaton field is the IR scale that appears dynamically in the theory. In the 5D model, this is incarnated geometrically by the location of the IR-brane which is indeed dynamical. The picture is more transparent by allowing the IR position to be x^μ-dependent, i.e., that it is a 4D field. This is equivalent to using a gauge where the IR-brane location is not straight, but rather defined by the surface $y = y_{\rm IR}(x^\mu)$. On the other hand, the variable that transforms under a scale dilatation of the x^μ coordinates is not the proper coordinate y itself but the warp factor $a(y)$. Therefore it is natural to identify the dilaton field with the warp factor evaluated at the IR-brane location,

$$\hat{\phi}_d = \frac{1}{L} e^{-A(y_{\rm IR})} . \tag{A.12}$$

This variable is also convenient because it is easy to extract the normalization of both the potential and of the kinetic terms in terms of it. For instance, with this definition the brane tension term (proportional to $\sqrt{-g^{IR}}$ with $g^{IR}_{\mu\nu}$ the induced metric on the brane) is simply a quartic coupling, $\hat{\phi}_d^4$. Below we will see that this variable is actually not canonically normalized in general, although its kinetic term can be easily found. From the normalization of both kinetic and potential terms then a formula for the mass will follow.

Let us start by the potential term. We can redo the argument around eq. (3.30) in terms of $\hat{\phi}_d$, that allows to reconstruct quite directly the derivative of the off-shell effective potential, $dV_{\rm eff}/d\hat{\phi}_d$, which must be proportional to $\hat{\phi}_d^3$ and to the junction condition. The overall normalization constant can be fixed by requiring that in the $\hat{\kappa}^2 \to 0$ limit the effective potential reduces to $V_{\rm eff} = (M_5\, L) \int_{bulk}(V + \dot{\phi}^2/2) + V_b$, with ϕ solving the EOM and depending parametrically on $y_{\rm IR}$. This leads to

$$\frac{dV_{\rm eff}(\hat{\phi}_d)}{d\hat{\phi}_d} = 24\, \frac{M_5}{\kappa^2}\, (L\,\hat{\phi}_d)^3 \left(\sqrt{1 + \frac{\hat{\kappa}^2 L^4}{12}\Big(\frac{V_b'^{\,2}}{2M_5^2} - V\Big)} + \frac{\hat{\kappa}^2 L^3}{6M_5}\, V_b\right)\Bigg|_{y_{\rm IR}} , \tag{A.13}$$

that differs from eq. (3.30) by an overall multiplicative constant; this does not matter much however for the mass eq. (3.31) as long as we factor out the same constant in the kinetic term.

Next, the normalization of the dilaton kinetic term. Another advantage of using a non-straight gauge is that all the kinetic term contributions arise only from localized terms on the IR-brane itself. This is welcome because the dilaton is an IR mode and its properties should arise from the IR only. Moreover, it is also convenient because it allows to identify these kinetic term contributions in the 'probe' limit, where we ignore how the brane bending sources the 5D metric. Following [50], one quickly sees that the radion/dilaton kinetic term

JHEP10(2019)202

arises from two sources. First, the brane tension (potential) term, via the determinant of the induced metric on the brane,

$$\sqrt{-g^{IR}} = a^4(y_{\rm IR})\sqrt{1-\frac{(\partial y_{\rm IR})^2}{a^2(y_{\rm IR})}}\,, \tag{A.14}$$

where $(\partial y_{\rm IR})^2 = \eta^{\mu\nu}\partial_\mu y_{\rm IR}\,\partial_\nu y_{\rm IR}$. Second, the Gibbons-Hawking, proportional to the extrinsic curvature at the $y = y_{\rm IR}(x^\mu)$ surface, generates additional terms. The relevant ones (contributing to the quadratic kinetic part) are proportional to the derivative of the warp factor at the brane location.

At this point we must make a slight detour, to be more precise on how several quantities depend on $y_{\rm IR}$, that is, on the dilaton. The key point is that the bulk scalar ϕ is coupled to the IR-brane (because the IR potential $V_b(\phi)$ acts effectively like a scalar charge). For this reason, the profile of ϕ (and therefore of the metric) in the bulk actually depends on the IR-brane location even when we allow the brane location to be off shell. To make this dependence manifest, we can write that the field profile is a function of both the bulk coordinate and the IR-brane location, $\phi = \phi(y, y_{\rm IR})$.[15] This is indeed implied by eq. (3.20) and eq. (3.24) in the main text. In this notation, the field evaluated on the IR-brane is $\phi(y_{\rm IR}, y_{\rm IR})$, and the derivative with respect to $y_{\rm IR}$ originates from the two arguments. The boundary condition specifies $\partial_y\phi(y, y_{\rm IR})|_{y=y_{\rm IR}}$, but the 'full' derivative $\partial_{y_{\rm IR}}\phi(y_{\rm IR}, y_{\rm IR})$ is left unspecified and it is nontrivial in a nonlinear theory. As we will see shortly this full derivative is the one that controls the dilaton mass (it is the one that appears in eq. (3.31)).

The same qualifications apply also for the metric. After all, the 'Friedman' eq. (A.3) forces $\partial_y a$ to be an algebraic function of $\phi(y, y_{\rm IR})$ and $\partial_y\phi(y, y_{\rm IR})$, so the warp factor profile too depends parametrically on $y_{\rm IR}$, that is, we must write $a = a(y, y_{\rm IR})$. Now, the extrinsic curvature is related to $\partial_y a(y, y_{\rm IR})|_{y=y_{\rm IR}}$. The dilaton variable $\hat{\phi}_d$ defined in eq. (A.12) stands for $a(y_{\rm IR}, y_{\rm IR})$, and its derivative with respect to $y_{\rm IR}$, $\partial_{y_{\rm IR}} a(y_{\rm IR})$ is not the same as $\partial_y a(y, y_{\rm IR})|_{y=y_{\rm IR}}$. To make the distinction clear in the following we will keep this notation and show explicitly the difference. Form eq. (A.3) we have

$$-\ln a(y_{\rm IR}, y_{\rm IR}) = A(y_{\rm IR}, y_{\rm IR}) = \int_{y_{\rm UV}}^{y_{\rm IR}} d\bar{y}\sqrt{\frac{1}{L^2} + \frac{\hat{\kappa}^2 L^2}{12}\left(\frac{\dot{\phi}^2(\bar{y}, y_{\rm IR})}{2} - V(\phi(\bar{y}, y_{\rm IR}))\right)}\,, \tag{A.15}$$

that differentiating with respect to $y_{\rm IR}$ leads to

$$\partial_{y_{\rm IR}} A(y_{\rm IR}, y_{\rm IR}) = \dot{A}(y_{\rm IR}, y_{\rm IR}) + \frac{\hat{\kappa}^2 L^3}{24}\int_{y_{\rm UV}}^{y_{\rm IR}} d\bar{y}\frac{\dot{\phi}\,\partial_{y_{\rm IR}}\dot{\phi} - V'(\phi)\,\partial_{y_{\rm IR}}\phi}{\sqrt{1 + \frac{\hat{\kappa}^2 L^4}{12}(\dot{\phi}^2/2 - V(\phi))}}\,, \tag{A.16}$$

where $\dot{A}(y_{\rm IR}, y_{\rm IR}) \equiv (\partial_y \ln a(y, y_{\rm IR}))\big|_{y=y_{\rm IR}}$ and the rest of the notation should be clear. This shows that both at small and large $\hat{\kappa}^2$, the difference between $\dot{A}$ and $\partial_{y_{\rm IR}} A$ is small.

[15] We could also include the dependence on the UV brane location, $y_{\rm UV}$, however we will omit it here to avoid clutter. The symmetries of the background ensure that $\phi = \phi(y - y_{\rm UV}, y_{\rm IR} - y_{\rm UV})$. This makes manifest that the field evaluated at the IR brane, $\phi(y_{\rm IR} - y_{\rm UV}, y_{\rm IR} - y_{\rm UV})$, is sensitive to $y_{\rm UV}$.

JHEP10(2019)202

Numerically, in our solutions we finds it to be less than 5%. (The same cannot be said about the two types of derivatives acting on ϕ.)

Returning to the kinetic term: after collecting all terms and using the EOM of the background, one arrives at [50]

$$3\frac{M_5}{\kappa^2}\,\dot{A}(y_{\rm IR})\,a^2(y_{\rm IR})\,(\partial_\mu y_{\rm IR})^2\,. \tag{A.17}$$

With the definition eq. (A.12) that implies $\partial_\mu\hat{\phi}_d = -\partial_{y_{\rm IR}}\ln a(y_{\rm IR})\;\hat{\phi}_d\;\partial_\mu y_{\rm IR}$, this gives

$$\frac{3M_5\,L^2}{\kappa^2}\,\frac{\dot{A}(y_{\rm IR})}{[\partial_{y_{\rm IR}}A(y_{\rm IR})]^2}\,(\partial_\mu\hat{\phi}_d)^2\,. \tag{A.18}$$

As discussed above, one can set $\dot{A}(y_{\rm IR})\simeq\partial_{y_{\rm IR}}A(y_{\rm IR})$ to a good approximation, therefore the kinetic term is to a good accuracy

$$\frac{3M_5\,L^2}{\kappa^2}\,\frac{(\partial_\mu\hat{\phi}_d)^2}{\partial_{y_{\rm IR}}A(y_{\rm IR})}\,. \tag{A.19}$$

On the other hand, differentiating eq. (A.13) we get

$$\frac{d^2V_{\rm eff}(\hat{\phi}_d)}{d\hat{\phi}_d^2} = -N_F\,L^4\,M_5\,\hat{\phi}_d^2\left[\frac{1}{\dot{A}}\left(\frac{V_b'\,V_b''}{M_5^2}-V'\right)+\frac{4}{M_5}\,V_b'\right]\,\frac{\partial_{y_{\rm IR}}\phi(y_{\rm IR})}{\partial_{y_{\rm IR}}A(y_{\rm IR})}\,, \tag{A.20}$$

by using the chain rule and eq. (A.12). Taking everything together, and the approximate expression eq. (A.19) we find that the physical dilaton mass is given by

$$m_{\phi_d}^2 \simeq -\frac{\hat{\kappa}^2L^4}{6}\,\hat{\phi}_d^2\left[\frac{1}{\dot{A}}\left(\frac{V_b'\,V_b''}{M_5^2}-V'\right)+\frac{4}{M_5}\,V_b'\right]\,\partial_{y_{\rm IR}}\phi(y_{\rm IR})\,, \tag{A.21}$$

where everything is evaluated at the minimum, which coincides with eq. (3.31) after the change of coordinates $dy = a(z)dz$. As a further cross-check, let us note that this expression agrees with eq. (2.25) of [51]. This was obtained starting directly from eq. (A.10) and obtaining an expression for the lowest KK mass under the assumption that it is light. The formula of [51] has two distinct limits corresponding to whether or not the light dilaton is incarnated by the IR-brane position. It is easy to check that in the limit where the dilaton is the displacement of the IR-brane, eq. (A.21) agrees with eq. (2.25) of [51].

Finally, we remark that using the EOM of the background we can rewrite eq. (A.17) as

$$-\frac{1}{2}\,V_b\big(\phi(y_{\rm IR})\big)\;a^2(y_{\rm IR})\;(\partial_\mu y_{\rm IR})^2\,. \tag{A.22}$$

One immediately realizes an important implication: the positivity of the kinetic energy restricts $V_b(\phi(y_{\rm IR}))<0$. This is equivalent to restricting the effective tension on the IR-brane to be negative — as it should be in order that it gives an end to the geometry at $y_{\rm IR}$. If we demand that this constraint is satisfied by all the solutions, including the one with $\phi(z)=0$ (for $\epsilon<0$), then this translates into a constraint on the IR-brane tension 'detuning parameter',

$$\delta\hat{\Lambda} < 6\,. \tag{A.23}$$

This reproduces the upper bound in (3.29), i.e., that the brane on the IR (on the 'interior') side of the geometry has negative tension.

JHEP10(2019)202

B A tale of two scalars: the 4D effective potential of a tachyon and a dilaton

When both 4D tachyon and dilaton masses are smaller than $1/z_{\rm IR}$, we can easily understand the physics of the system by just looking at the 4D effective theory for these two modes. This is possible when working close to the critical point, $z_{\rm IR} \approx z_{\rm IR}^c$ (limiting case I of section 3.2), where we can obtain the masses and quartic couplings of the model as a perturbation of the model around $z_{\rm IR} = z_{\rm IR}^c$. We find

$$\frac{1}{M_5 L N_F} V_{\rm eff}(\phi_t, \phi_d) = \frac{1}{2}\hat{m}^2(\phi_d)\phi_t^2\phi_d^2 + \frac{1}{4}\lambda_t\phi_t^4 + \frac{1}{4}\lambda_d\phi_d^4\,, \tag{B.1}$$

where $\phi_d = 1/z_{\rm IR}$ is the dilaton and ϕ_t the 4D tachyon. We are working here with non-canonically normalized fields:

$$\frac{1}{M_5 L N_F}\,\mathcal{L}_{\rm kin} = \frac{1}{2}(\partial_\mu\phi_t)^2 + \frac{3}{\hat{\kappa}^2}(\partial_\mu\phi_d)^2\,. \tag{B.2}$$

Eq. (B.1) can only give a non-trivial minimum for $\phi_d \leq \mu_c \equiv 1/z_{\rm IR}^c$ such that $\hat{m}^2(\phi_d)$ is negative. In this regime, this is given by

$$\hat{m}^2(\phi_d) = \beta\ln(\phi_d/\mu_c)\,, \tag{B.3}$$

where β is given in eq. (3.22). Recall that eq. (B.1) is only valid for $\hat{m}^2(\phi_d) \ll 1$ that requires either $|\ln\phi_d/\mu_c| \ll 1$ or $\beta \ll 1$ ($\hat{m}_b^2 \to -2$). The tachyon quartic λ_t has a mild dependence on $\hat{m}_b^2$ and is derived below (section B.1), while the dilaton quartic is given by the detuning of the IR-brane tension:

$$\lambda_d = 4\frac{\delta\hat{\Lambda}}{\hat{\kappa}^2}\,. \tag{B.4}$$

The presence of the tachyon leads to a non-trivial potential for the dilaton with a minimum at

$$\ln\frac{\langle\phi_d\rangle}{\mu_c} = -\frac{1}{4}\left[1+\sqrt{1+16\lambda_t\lambda_d/\beta^2}\right]\,. \tag{B.5}$$

We see that the largest value of the dilaton is given by $\ln\langle\phi_d\rangle/\mu_c \leq -1/4$ that implies that the IR-brane can never be stabilized very close to the critical point $z_{\rm IR}^c$ where the tachyon mass is small. At the closest value $\ln\langle\phi_d\rangle/\mu_c = -1/4$, one finds that the minimum is an inflection point where the minimum coincides with a maximum (and one can check that the dilaton mass is zero at this point). Nevertheless, demanding that the quartic couplings are positive, to guarantee that for $\epsilon < 0$ the theory is conformal ($\phi_d \to 0$), one obtains $\ln\langle\phi_d\rangle/\mu_c \leq -1/2$.

We can also find the masses of the dilaton and tachyon by calculating the eigenvalues of the matrix of second derivatives at the minimum eq. (B.5) after canonically normalizing the fields. These give rather complicated functions of λ_t, λ_d and β. For $\beta^2/(\lambda_d\lambda_t) \ll 1$ they reduce to

$$m_{\phi_d}^2 \simeq \frac{2\beta\,\hat{\kappa}^2}{\hat{\kappa}^2 + 6\sqrt{\lambda_t/\lambda_d}}\,\langle\phi_d\rangle^2\,, \qquad m_{\phi_t}^2 \simeq \lambda_d\left(\frac{\hat{\kappa}^2}{6} + \sqrt{\lambda_t/\lambda_d}\right)\,\langle\phi_d\rangle^2\,, \tag{B.6}$$

JHEP10(2019)202

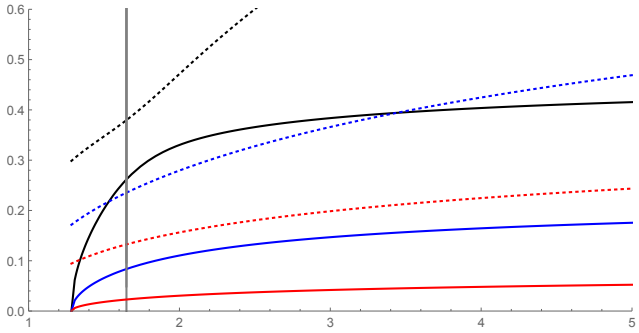

Figure 9. Masses of the two scalars, that play the role of S_1 and S_2, as a function of $\mu_c/\langle\phi_d\rangle$ and normalized to $(3\pi/4)\,\langle\phi_d\rangle$. We have taken $\lambda = 1$, $\hat{\kappa}^2 = 6$ and $\hat{m}_b^2 = -0.5, -1.5, -1.75$ for the black, blue and red lines respectively. The solid (dashed) line indicate the lightest (heaviest) mode. The quartic coupling λ_d varies along the horizontal axis according to eq. (B.5). The vertical line marks where $\lambda_d = 0$, having $\lambda_d > 0$ in the region to the right of it.

while for $\beta^2/(\lambda_d\lambda_t) \gg 1$ these are

$$m_{\phi_d}^2 \simeq \frac{\hat{\kappa}^2}{6}\,\frac{\beta^2}{2\lambda_t}\,\langle\phi_d\rangle^2\,, \qquad m_{\phi_t}^2 \simeq \beta\,\langle\phi_d\rangle^2\,. \tag{B.7}$$

With an abuse of notation, we have identified the lightest of the two modes as the dilaton, even though the eigenmodes corresponding to eq. (B.7) can have a sizeable mixing in the $\phi_d - \phi_t$ basis. We show the full dependence on the parameters in figure 9, where we keep λ_t and β fixed and vary λ_d for various values of $\hat{m}_b^2$ (that is, of λ_t and β). One clearly sees several features:

i) the solutions 'start' at $\ln(\mu_c/\langle\phi_d\rangle) = 1/4$ where the dilaton is massless, corresponding to the inflection point. This requires however $\lambda_d < 0$ that we already said is inapplicable.

ii) the dilaton mass is suppressed by one power of β for $\lambda_t\lambda_d \sim O(1)$ (eq. (B.6)). In our model β can be small only near $\hat{m}_b^2 = -2$. In that case the suppression reads $m_{\phi_d}^2 \sim (\hat{m}_b^2 + 2)^2$. Keep in mind, however, that $\hat{m}_b^2 = -2$ is not protected by any symmetry, so this is not representative of the full allowed parameter space.

iii) the shapes of the lines resemble qualitatively those of figure 5. Nevertheless, the agreement between this and the 5D model is only expected for small $\hat{m}^2(\phi_d)$, since this measures how large is the tachyon VEV. A similar analysis can be done with more general choices of $\hat{m}^2(\phi_d)$ and the same qualitative behavior is observed quite generically as long as $\hat{m}^2(\phi_d)$ changes sign and has a moderate dependence on ϕ_d. Interestingly enough, it suffices to take that $\hat{m}^2(\phi_d)$ goes to a constant as $\phi_d \to 0$, in order to obtain a dilaton mass with a rising-decreasing shape as in figure 5

When the dilaton is lighter than the tachyon, for example for $\beta \ll 1$, we can alternatively integrate out the tachyon from eq. (B.1) and obtain eq. (1.1) with

$$\lambda_{\rm eff}(\phi_d) = \frac{\lambda_d}{4} - \frac{\beta^2}{4\lambda_t}\ln^2(\phi_d/\mu_c)\,, \tag{B.8}$$

JHEP10(2019)202

that tells us that the explicit breaking of scale invariance is logarithmic, as expected from the dual theory due to the presence of the double-trace marginal operator $\mathcal{O}_g$. Eq. (1.1) with eq. (B.8) leads to eq. (B.5) and to the dilaton mass of eq. (B.6). As expected the dilaton mass is proportional to

$$\beta_{\lambda_{\rm eff}}(\langle\phi_d\rangle) = -\frac{\beta^2}{2\lambda_t}\ln(\langle\phi_d\rangle/\mu_c) \sim \beta\,, \tag{B.9}$$

where in the last equality we have used eq. (B.5) with $\beta \ll 1$.

B.1 Effective quartic coupling for the tachyon

The quartic self-coupling for the 4D tachyon can be obtained readily by plugging into the 5D potential quartic term the normalized profile of the 5D tachyon field near the condensation point and performing the integral over z. In the limit $\epsilon \to 0$, $z_{\rm UV}/z^c_{\rm IR} \to 0$ with $\sqrt{\epsilon}\,\ln(z_{\rm UV}/z^c_{\rm IR})$ finite, one obtains

$$\lambda_t = \left(\frac{3}{8} + \frac{9+2\hat{m}_b^2}{2(10+6\hat{m}_b^2+\hat{m}_b^4)^2}\right)\lambda\,. \tag{B.10}$$

Even without any quartic self-coupling λ, the tachyon field experiences a stabilizing effect from its coupling to the metric. This is manifest in the background equation eq. (A.2), because the 'friction' term which depends on ϕ itself, see eq. (A.3). More explicitly, the metric can be integrated out by using eq. (A.3) to obtain a closed equation for ϕ

$$\ddot{\phi} = 4\sqrt{\frac{1}{L^2} + \frac{\hat{\kappa}^2L^2}{12}\left(\frac{\dot{\phi}^2}{2} - V(\phi)\right)}\,\dot{\phi} + V'(\phi)\,.$$

At leading order in $\hat{\kappa}^2$, one identifies a cubic term in the equation of motion

$$\frac{\hat{\kappa}^2L^3}{6}\left(\frac{\dot{\phi}^2}{2} - V(\phi)\right)\,\dot{\phi}\,.$$

This suggests identifying the effective quartic coupling from the 5D integral of ϕ times the previous expression with the normalized tachyon profile. This gives

$$\Delta\lambda_t = \hat{\kappa}^2\,\frac{128+128\hat{m}_b^2+60\hat{m}_b^4+12\hat{m}_b^6+\hat{m}_b^8}{6(10+6\hat{m}_b^2+\hat{m}_b^4)^2}\,. \tag{B.11}$$

The expressions in eq. (B.10) and eq. (B.11) define the functions $c_{\lambda,\kappa}$ introduced in eq. (3.23).

JHEP10(2019)202

Open Access. This article is distributed under the terms of the Creative Commons Attribution License (CC-BY 4.0), which permits any use, distribution and reproduction in any medium, provided the original author(s) and source are credited.

References

[1] LatKMI collaboration, *Light flavor-singlet scalars and walking signals in $N_f = 8$ QCD on the lattice*, *Phys. Rev.* **D 96** (2017) 014508 [arXiv:1610.07011] [INSPIRE].

[2] LatKMI collaboration, *Light composite scalar in eight-flavor QCD on the lattice*, *Phys. Rev.* **D 89** (2014) 111502 [arXiv:1403.5000] [INSPIRE].

[3] R.C. Brower, A. Hasenfratz, C. Rebbi, E. Weinberg and O. Witzel, *Composite Higgs model at a conformal fixed point*, *Phys. Rev.* **D 93** (2016) 075028 [arXiv:1512.02576] [INSPIRE].

[4] T. Appelquist et al., *Strongly interacting dynamics and the search for new physics at the LHC*, *Phys. Rev.* **D 93** (2016) 114514 [arXiv:1601.04027] [INSPIRE].

[5] Lattice Strong Dynamics collaboration, *Nonperturbative investigations of* SU(3) *gauge theory with eight dynamical flavors*, *Phys. Rev.* **D 99** (2019) 014509 [arXiv:1807.08411] [INSPIRE].

[6] D.B. Kaplan, J.-W. Lee, D.T. Son and M.A. Stephanov, *Conformality Lost*, *Phys. Rev.* **D 80** (2009) 125005 [arXiv:0905.4752] [INSPIRE].

[7] J.M. Maldacena, *The Large N limit of superconformal field theories and supergravity*, *Int. J. Theor. Phys.* **38** (1999) 1113 [hep-th/9711200] [INSPIRE].

[8] S.S. Gubser, I.R. Klebanov and A.M. Polyakov, *Gauge theory correlators from noncritical string theory*, *Phys. Lett.* **B 428** (1998) 105 [hep-th/9802109] [INSPIRE].

[9] E. Witten, *Anti-de Sitter space and holography*, *Adv. Theor. Math. Phys.* **2** (1998) 253 [hep-th/9802150] [INSPIRE].

[10] R. Contino, A. Pomarol and R. Rattazzi, unpublished work (2010).

[11] R. Rattazzi, *The naturally light dilation*, talk at *Planck 2010. From the Planck Scale to the ElectroWeak Scale*, CERN, 31 May–4 June 2010.

[12] B. Bellazzini, C. Csáki, J. Hubisz, J. Serra and J. Terning, *A Naturally Light Dilaton and a Small Cosmological Constant*, *Eur. Phys. J.* **C 74** (2014) 2790 [arXiv:1305.3919] [INSPIRE].

[13] F. Coradeschi, P. Lodone, D. Pappadopulo, R. Rattazzi and L. Vitale, *A naturally light dilaton*, *JHEP* **11** (2013) 057 [arXiv:1306.4601] [INSPIRE].

[14] E. Megias and O. Pujolàs, *Naturally light dilatons from nearly marginal deformations*, *JHEP* **08** (2014) 081 [arXiv:1401.4998] [INSPIRE].

[15] W.D. Goldberger and M.B. Wise, *Modulus stabilization with bulk fields*, *Phys. Rev. Lett.* **83** (1999) 4922 [hep-ph/9907447] [INSPIRE].

[16] D. Kutasov, J. Lin and A. Parnachev, *Conformal Phase Transitions at Weak and Strong Coupling*, *Nucl. Phys.* **B 858** (2012) 155 [arXiv:1107.2324] [INSPIRE].

[17] D. Kutasov, J. Lin and A. Parnachev, *Holographic Walking from Tachyon DBI*, *Nucl. Phys.* **B 863** (2012) 361 [arXiv:1201.4123] [INSPIRE].

[18] L. Vecchi, *The Conformal Window of deformed CFT's in the planar limit*, *Phys. Rev.* **D 82** (2010) 045013 [arXiv:1004.2063] [INSPIRE].

JHEP10(2019)202

[19] D. Elander and M. Piai, *Light scalars from a compact fifth dimension*, *JHEP* **01** (2011) 026 [arXiv:1010.1964] [INSPIRE].

[20] S.P. Kumar, D. Mateos, A. Paredes and M. Piai, *Towards holographic walking from $N = 4$ super Yang-Mills*, *JHEP* **05** (2011) 008 [arXiv:1012.4678] [INSPIRE].

[21] M. Jarvinen and E. Kiritsis, *Holographic Models for QCD in the Veneziano Limit*, *JHEP* **03** (2012) 002 [arXiv:1112.1261] [INSPIRE].

[22] N. Evans and K. Tuominen, *Holographic modelling of a light technidilaton*, *Phys. Rev.* **D 87** (2013) 086003 [arXiv:1302.4553] [INSPIRE].

[23] J. Erdmenger, N. Evans and M. Scott, *Meson spectra of asymptotically free gauge theories from holography*, *Phys. Rev.* **D 91** (2015) 085004 [arXiv:1412.3165] [INSPIRE].

[24] M. Jarvinen, *Massive holographic QCD in the Veneziano limit*, *JHEP* **07** (2015) 033 [arXiv:1501.07272] [INSPIRE].

[25] D. Elander, R. Lawrance and M. Piai, *Hyperscaling violation and Electroweak Symmetry Breaking*, *Nucl. Phys.* **B 897** (2015) 583 [arXiv:1504.07949] [INSPIRE].

[26] N. Evans, P. Jones and M. Scott, *Soft walls in dynamic AdS/QCD and the technidilaton*, *Phys. Rev.* **D 92** (2015) 106003 [arXiv:1508.06540] [INSPIRE].

[27] D. Arean, I. Iatrakis, M. Jarvinen and E. Kiritsis, *CP-odd sector and θ dynamics in holographic QCD*, *Phys. Rev.* **D 96** (2017) 026001 [arXiv:1609.08922] [INSPIRE].

[28] K. Bitaghsir Fadafan, W. Clemens and N. Evans, *Holographic Gauged NJLS Model: the Conformal Window and Ideal Walking*, *Phys. Rev.* **D 98** (2018) 066015 [arXiv:1807.04548] [INSPIRE].

[29] D. Elander, M. Piai and J. Roughley, *Holographic glueballs from the circle reduction of Romans supergravity*, *JHEP* **02** (2019) 101 [arXiv:1811.01010] [INSPIRE].

[30] V. Gorbenko, S. Rychkov and B. Zan, *Walking, Weak first-order transitions and Complex CFTs*, *JHEP* **10** (2018) 108 [arXiv:1807.11512] [INSPIRE].

[31] E. Pomoni and L. Rastelli, *Large N Field Theory and AdS Tachyons*, *JHEP* **04** (2009) 020 [arXiv:0805.2261] [INSPIRE].

[32] E. Ponton, *TASI 2011: Four Lectures on TeV Scale Extra Dimensions*, in *The Dark Secrets of the Terascale: Proceedings, TASI 2011*, Boulder, Colorado, U.S.A., June 6–July 11, 2011, pp. 283–374 (2013) [DOI:10.1142/9789814390163_0007] [arXiv:1207.3827] [INSPIRE].

[33] J. Erlich, E. Katz, D.T. Son and M.A. Stephanov, *QCD and a holographic model of hadrons*, *Phys. Rev. Lett.* **95** (2005) 261602 [hep-ph/0501128] [INSPIRE].

[34] L. Da Rold and A. Pomarol, *Chiral symmetry breaking from five dimensional spaces*, *Nucl. Phys.* **B 721** (2005) 79 [hep-ph/0501218] [INSPIRE].

[35] L. Da Rold and A. Pomarol, *The Scalar and pseudoscalar sector in a five-dimensional approach to chiral symmetry breaking*, *JHEP* **01** (2006) 157 [hep-ph/0510268] [INSPIRE].

[36] A. Gadde, E. Pomoni and L. Rastelli, *The Veneziano Limit of $N = 2$ Superconformal QCD: Towards the String Dual of $N = 2$ SU(N_c) SYM with $N_f = 2N_c$*, arXiv:0912.4918 [INSPIRE].

[37] C. Csáki, M.L. Graesser and G.D. Kribs, *Radion dynamics and electroweak physics*, *Phys. Rev.* **D 63** (2001) 065002 [hep-th/0008151] [INSPIRE].

JHEP10(2019)202

[38] E. Witten, *Multitrace operators, boundary conditions and AdS/CFT correspondence*, hep-th/0112258 [INSPIRE].

[39] I.R. Klebanov and E. Witten, *AdS/CFT correspondence and symmetry breaking*, *Nucl. Phys.* **B 556** (1999) 89 [hep-th/9905104] [INSPIRE].

[40] B. Grinstein, K.A. Intriligator and I.Z. Rothstein, *Comments on Unparticles*, *Phys. Lett.* **B 662** (2008) 367 [arXiv:0801.1140] [INSPIRE].

[41] L. Vecchi, *A Natural Hierarchy and a low New Physics scale from a Bulk Higgs*, *JHEP* **11** (2011) 102 [arXiv:1012.3742] [INSPIRE].

[42] Particle Data Group collaboration, *Review of Particle Physics*, *Chin. Phys.* **C 40** (2016) 100001 [INSPIRE].

[43] C. Eröncel, J. Hubisz and G. Rigo, *Self-Organized Higgs Criticality*, *JHEP* **03** (2019) 046 [arXiv:1804.00004] [INSPIRE].

[44] S. Fichet, G. von Gersdorff, E. Pontón and R. Rosenfeld, *The Excitation of the Global Symmetry-Breaking Vacuum in Composite Higgs Models*, *JHEP* **09** (2016) 158 [arXiv:1607.03125] [INSPIRE].

[45] S. Fichet, G. von Gersdorff, E. Pontón and R. Rosenfeld, *The Global Higgs as a Signal for Compositeness at the LHC*, *JHEP* **01** (2017) 012 [arXiv:1608.01995] [INSPIRE].

[46] D. Buarque Franzosi, G. Cacciapaglia and A. Deandrea, *Sigma-assisted natural composite Higgs*, arXiv:1809.09146 [INSPIRE].

[47] D.K. Hong and H.-U. Yee, *Holographic estimate of oblique corrections for technicolor*, *Phys. Rev.* **D 74** (2006) 015011 [hep-ph/0602177] [INSPIRE].

[48] G. Panico and A. Pomarol, *Flavor hierarchies from dynamical scales*, *JHEP* **07** (2016) 097 [arXiv:1603.06609] [INSPIRE].

[49] P. Baratella, A. Pomarol and F. Rompineve, *The Supercooled Universe*, *JHEP* **03** (2019) 100 [arXiv:1812.06996] [INSPIRE].

[50] J. Garriga, O. Pujolàs and T. Tanaka, *Moduli effective action in warped brane world compactifications*, *Nucl. Phys.* **B 655** (2003) 127 [hep-th/0111277] [INSPIRE].

[51] E. Megias, O. Pujolàs and M. Quirós, *On dilatons and the LHC diphoton excess*, *JHEP* **05** (2016) 137 [arXiv:1512.06106] [INSPIRE].

JHEP10(2019)202

4.2 Paper 2: Exploring the conformal transition from above and below

Published for SISSA by Springer

Received: *January 25, 2024*
Revised: *July 2, 2024*
Accepted: *July 31, 2024*
Published: *August 20, 2024*

Exploring the conformal transition from above and below

Alex Pomarol and **Lindber Salas**

IFAE and BIST, Universitat Autònoma de Barcelona,
08193 Bellaterra, Barcelona, Spain
Dept. de Física, Universitat Autònoma de Barcelona,
08193 Bellaterra, Barcelona, Spain

E-mail: alex.pomarol@uab.cat, lsalas@ifae.es

Abstract: We consider conformal transitions arising from the merging of IR and UV fixed points, expected to occur in QCD with a large enough number of flavors. We study the smoothness of physical quantities across this transition, being mostly determined by the logarithmic breaking of conformal invariance. We investigate this explicitly using holography where approaching the conformal transition either from outside or inside the conformal window (perturbed by a mass term) is characterized by the same dynamics. The mass of spin-1 mesons and F_π are shown to be continuous across the transition, as well as the dilaton mass. This implies that the lightness of the dilaton cannot be a consequence of the spontaneous breaking of scale invariance when leaving the conformal window. Our analysis suggests that the light scalar observed in QCD lattice simulations is a $q\bar{q}$ meson that becomes light since the $q\bar{q}$-operator dimension reaches its minimal value.

Keywords: AdS-CFT Correspondence, Effective Field Theories of QCD, Lattice QCD, Scale and Conformal Symmetries

ArXiv ePrint: 2312.08332

Open Access, © The Authors.
Article funded by SCOAP^3.

https://doi.org/10.1007/JHEP08(2024)149

JHEP08(2024)149

Contents

1 Introduction

A conformal field theory (CFT) can depart from its IR fixed point in various way as we vary the parameters of the model. Either because the IR fixed point goes to zero, to infinity or it merges with a UV fixed point. We are interested in conformal transitions characterized by this third case, the merging of the IR fixed point with a UV fixed point.

It has been speculated [1] that this is the case for SU(N_c) gauge theories as QCD at the lower edge of the conformal window –see figure 1. As we decrease the number of flavors N_F from the Banks-Zaks fixed point at $N_F = \frac{11}{2}N_c$, where QCD enters into the conformal window, to some critical value $N_F = N_F^{crit}$, QCD is expected to loose conformality by an IR-UV fixed point merging. Interestingly, in the last years lattice simulations have been providing abundant data on the properties of QCD at different values of N_F and quark masses M_q, helping to better understand this conformal transition [2–10]. A particularly intriguing feature is the presence of a very light 0^{++} state when QCD is close to (but outside) the conformal transition. It has been speculated that this state could be a dilaton, the Goldstone associated to the spontaneous breaking of scale invariance.

We will consider CFTs in the large-N_c limit. It has been argued in [11, 12] that when these models are close to the conformal transition, they must contain a scalar operator $\mathcal{O}_\Phi$ whose dimension gets close to 2, becoming imaginary when leaving the conformal window. For QCD, where in the large-N_c limit $N_F^{crit}/N_c \equiv x_{crit}$ becomes a continuous parameter, $\mathcal{O}_\Phi$ corresponds to the $q\bar{q}$ operator.

JHEP08(2024)149

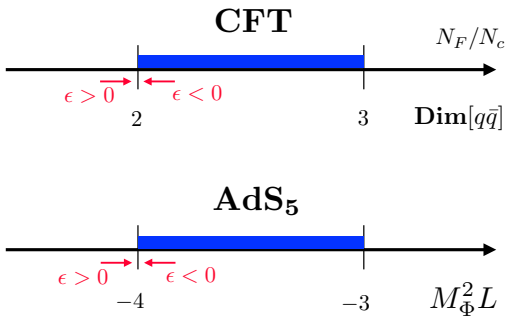

Figure 1. QCD conformal window and the holographic equivalent.

We are interested in understanding how the physical quantities change as we move across the conformal transition for nonzero quark masses.[1] Using holography [24–26] we will show how the meson mass spectrum is mostly dictated by chiral and conformal invariance and the way this is broken. We will show that spin-1 meson masses and F_π are continuous across the transition, while the masses of the scalar mesons, f_0 and a_0, show a jump due to a logarithmic breaking of conformal invariance.

The mass of the dilaton, corresponding to a glueball, is also found to be smooth across the transition, implying that this must be light at both sides of the conformal window. This implies that the lightness of the dilaton cannot only be a consequence of the spontaneous breaking of the conformal symmetry when leaving the conformal window. We will argue that this disfavors this state as the light 0^{++} scalar found in lattice simulations.

On the other hand, we will consider the possibility that the lightness of the 0^{++} scalar found in lattice simulations is a $q\bar{q}$ meson whose mass is small due to the fact that $\text{Dim}[\mathcal{O}_\Phi] \to 2$ at the conformal edge. This is the closest value to the unitary bound $\text{Dim}[\mathcal{O}_\Phi] \geq 1$ where a scalar is expected to become massless since the operator $\mathcal{O}_\Phi$ decouples from the CFT [27]. We will also understand why the breaking of the chiral symmetry is smaller as we move inside the conformal window, as lattice simulations seem to suggest.

Although some of these properties could also be derived following 4D CFT approaches, as for example in [28] or [29], we will see that it is much easier to derive them using holography.

Previous studies of how the meson masses change across the conformal transition in a holographic model (with nonzero quark masses) were presented in [30]. Here, we aim to explain the reason behind the pattern of the mass spectrum and its discontinuities across the conformal transition, providing also a comparison with the pattern observed in lattice simulations.

2 Conformal transition by fixed-point merging

Following [1], we will consider that the conformal transition occurs when an IR fixed point merges with a UV fixed point. For theories at large-N_c, it can be shown [11, 12] that close

[1] Effective field theories (EFTs) for a light dilaton have been widely developed [13–23]. Nevertheless, these are limited to small M_q values and cannot be used to describe the conformal transition.

JHEP08(2024)149

to the transition the theories must have a marginal operator $\mathcal{O}_f$

$$f(\mu)\mathcal{O}_f \ \in \mathcal{L}\,, \tag{2.1}$$

whose coupling f has a beta function given by

$$\beta_f \simeq \epsilon + (f - f_*)^2\,. \tag{2.2}$$

For $\epsilon < 0$ this beta function has two zeros corresponding to an IR and a UV fixed point that merge to a single fixed point at $\epsilon = 0$, that disappears for $\epsilon > 0$. This marks the conformal transition. In QCD we expect $\epsilon \propto x_{crit} - x$.

Therefore, as we approach the conformal transition ($\epsilon \to 0$), the theory can be in two different phases depending on the sign of ϵ:

- For $\epsilon < 0$, eq. (2.2) gives us

$$f(\mu) \simeq f_* - \frac{1}{\ln \mu/\mu_0}\,, \tag{2.3}$$

  and f will run towards the IR, $\mu/\mu_0 \to 0$, approaching f_* where the theory becomes conformal, $\beta_f \to 0$. Here μ_0 is an arbitrary scale related with the value of f at the UV.

- For $\epsilon > 0$, there are no possible zeros for β_f. In this case, we have

$$f(\mu) \simeq f_* + \sqrt{\epsilon}\tan\left(\sqrt{\epsilon}\ln\frac{\mu}{\mu_0}\right)\,, \tag{2.4}$$

  and $f(\mu)$ runs slowly when $f \sim f_*$, behaving almost as a CFT, but it blows up at some IR scale $\mu_{\rm IR}$ determined by

$$\sqrt{\epsilon}\ln\frac{\mu_{\rm IR}}{\mu_0} \simeq -\frac{\pi}{2}\,. \tag{2.5}$$

  Therefore conformality is never reached. In fact, the dimension of $\mathcal{O}_f$, formally given by

$$\mathrm{Dim}[\mathcal{O}_f] = 4 + \frac{d\beta_f}{df} \simeq 4 + 2\sqrt{-\epsilon}\,, \tag{2.6}$$

  becomes complex for $\epsilon > 0$.

These two phases corresponds to the two sides of the conformal lower edge shown in figure 1.

It has also been shown in [11, 12] that for theories in the large-N_c limit, $\mathcal{O}_f$ must be a double-trace operator, made of the squared of a single-trace operator $\mathcal{O}_\Phi$, i.e., $\mathcal{O}_f = |\mathcal{O}_\Phi|^2$. Since in the large N_c, $\mathrm{Dim}[\mathcal{O}_f] = 2\mathrm{Dim}[\mathcal{O}_\Phi]$, we have from eq. (2.6)

$$\mathrm{Dim}[\mathcal{O}_\Phi] = 2 + \sqrt{-\epsilon}\,. \tag{2.7}$$

In QCD, as argued in [1], $\mathcal{O}_\Phi$ is expected to be the operator made of quarks, $q\bar{q}$, whose dimension will go from ~ 3 when entering the conformal window at the upper edge to 2 at the lower edge (see figure 1). The fact that $\mathcal{O}_\Phi$ reaches the lowest dimension at the conformal transition can explain the existence of a relative light scalar meson (with respect to the vector one, m_ρ) [31]. Indeed, $\mathrm{Dim}[\mathcal{O}_\Phi]$ gets at the edge of the conformal transition the closest value to $\mathrm{Dim}[\mathcal{O}_\Phi] = 1$ (unitarity bound) at which the scalar operator decouples from the CFT [27], becoming then insensitive to the CFT IR scale.

JHEP08(2024)149

All the above properties of this conformal transition find a beautiful implementation in holographic models by the use of the correspondence (or duality) between strongly-coupled CFT_4 (in the large N_c and large 'tHooft coupling[2]) and weakly-coupled five-dimensional Anti-de-Sitter theories (AdS_5) [24–26]. Operators in the CFT_4 ($\mathcal{O}_\Phi$) correspond to scalar fields in the AdS_5 (Φ) where dimensions and masses are related via the AdS/CFT relation [24–26]:

$$\mathrm{Dim}[\mathcal{O}_\Phi] = 2 + \sqrt{4 + M_\Phi^2 L^2}\,. \tag{2.8}$$

Eq. (2.8) tells us that the conformal transition must occurs when the 5D scalar mass $M_\Phi^2 L^2$ becomes smaller than -4 (see figure 1). Indeed, in this case the mass is below the Breitenlohner-Freedman (BF) bound that determines the stability of a scalar in AdS_5. For $M_\Phi^2 < -4/L^2$ the scalar Φ becomes tachyonic, turning on in the 5D bulk [31, 35, 36] (for earlier work in $D < 5$ see [37, 38]).[3]

2.1 Probing the conformal phase by $M_q\mathcal{O}_\Phi$

We are interested in understanding the properties of the mass spectrum at the two sides of the conformal edge. Since the spectrum in the conformal phase is continuous, we will perturb the theory by adding to the Lagrangian the term

$$\Delta\mathcal{L} = M_q\mathcal{O}_\Phi \qquad (M_q \geq 0)\,, \tag{2.9}$$

that explicitly breaks scale invariance. In QCD this corresponds to add a mass to the quarks, $M_q q\bar{q}$, that not only breaks conformal invariance but also the chiral symmetry; this is also done in lattice simulations.

A nonzero M_q allows to probe the physical properties of the theory inside the conformal window, as the mass spectrum becomes discrete and can be compared with the one at the other side of the edge of the transition. All the masses are expected to be proportional to $M_q^{1/(4-\mathrm{Dim}[\mathcal{O}_\Phi])}$, referred as "hyperscaling". At the conformal edge where $\mathrm{Dim}[\mathcal{O}_\Phi] \to 2$, we then have

$$m_i = a_i\sqrt{M_q}\,, \tag{2.10}$$

where a_i are constants that depend on the parameters of the model such as N_F/N_c. Obviously, the ratio of masses is independent of M_q.

The presence of M_q in the conformal theory ($\epsilon < 0$) brings also a logarithmic divergence that can be easily understood from scale invariance [41]. Since $\dim[\mathcal{O}_\Phi] \to 2$, the two-point function in momentum space is given by

$$\int d^4x e^{ip\cdot x}\langle\mathcal{O}_\Phi(x)\mathcal{O}_\Phi(0)\rangle \sim \int d^4x \frac{1}{|x|^4} \sim \ln\Lambda\,. \tag{2.11}$$

Therefore we expect a logarithmic breaking of conformal invariance in $\langle\mathcal{O}_\Phi\rangle$ proportional to M_q. Notice however that M_q does not enter into the log, so eq. (2.10) is always guaranteed.

[2]It has been recently shown [32–34] that higher spin decouple from low-energy observables, making holography a good approach even for models where the 'tHooft coupling is not very large.

[3]Alternatively, one could consider holographic models of complex CFTs, as done in [39, 40].

JHEP08(2024)149

From outside the conformal window ($\epsilon > 0$), the situation is the following. If we add eq. (2.9) and increase M_q over the scale $\mu_{\rm IR}$ defined in eq. (2.5), the coupling $f(\mu)$ will not reach the regime $\mu \sim \mu_{\rm IR}$ where it blows up, and $f(\mu) \simeq f_*$ similarly as for $\epsilon < 0$. Therefore in the limit $M_q \gg \mu_{\rm IR}$ the mass spectrum outside the conformal window must smoothly tend to eq. (2.10).

Before moving to the holographic model, we must remark that our analysis using holography shares many features of that in [28] based on the Schwinger-Dyson equation for the renormalized fermion self-energy. It is also related to the approach taken in [29] where the theory is assumed to be conformal deep in the IR.

3 A five-dimensional model for the conformal transition

A holographic model with the properties of described above was presented in [31] (for other models, see [30, 35, 36, 42–61]). This consists in a $\mathrm{SU}(N_F)_L \otimes \mathrm{SU}(N_F)_R$ gauge theory in 5D with a complex scalar Φ transforming as a $(\mathbf{N_F},\overline{\mathbf{N}}_\mathbf{F})$.[4] This scalar plays the role of the $q\bar{q}$ operator in 4D QCD. Imposing parity ($L \leftrightarrow R$), the action is given by

$$S_5 = \int d^4x \int dz\, \sqrt{g}\, M_5 \left[\frac{1}{\kappa^2}\left(\mathcal{R} + \Lambda_5\right) + \mathcal{L}_5\right], \tag{3.1}$$

where the Lagrangian is given by

$$\mathcal{L}_5 = -\frac{1}{4}\,\mathrm{Tr}\left[L_{MN}L^{MN} + R_{MN}R^{MN}\right] + \frac{1}{2}\,\mathrm{Tr}\,|D_M\Phi|^2 - V_\Phi(\Phi)\,, \tag{3.2}$$

with L_{MN}, R_{MN} being the field-strength of the $\mathrm{SU}(N_F)_L$ and $\mathrm{SU}(N_F)_R$ gauge bosons respectively, and the indices run over the five dimensions, $M = \{\mu, 5\}$. We parametrize the fields as $\Phi = \Phi_s + T_a\Phi_a$ with $\mathrm{Tr}[T_aT_b] = \delta_{ab}$. The fields Φ_s and Φ_a will respectively transform as singlet and adjoint under $\mathrm{SU}(N_F)_V$, the remaining symmetry after $\Phi \neq 0$ breaks the chiral symmetry. The covariant derivative is defined as

$$D_M\Phi = \partial_M\Phi + ig_5L_M\Phi - ig_5\Phi R_M\,, \tag{3.3}$$

and the potential is given by[5]

$$V_\Phi(\Phi) = \frac{1}{2}M_\Phi^2\,\mathrm{Tr}\,|\Phi|^2 + \frac{1}{4}\lambda_1\,\mathrm{Tr}\,|\Phi|^4 + \frac{1}{4}\lambda_2(\mathrm{Tr}\,|\Phi|^2)^2\,. \tag{3.4}$$

The 5D metric in conformal coordinates is defined as

$$ds^2 = a(z)^2(\eta_{\mu\nu}dx^\mu dx^\nu - dz^2)\,, \tag{3.5}$$

where $\eta_{\mu\nu} = \mathrm{diag}(1,-1,-1,-1)$ and $a(z)$ is the warp factor. Before the scalar Φ turns on, the presence of Λ_5 leads to an AdS_5 geometry:

$$a(z) = \frac{L}{z}\,, \tag{3.6}$$

[4] With respect to [31], we are neglecting the $\mathrm{U}(1)_B$ gauge sector that does not play any role in the discussion.

[5] We notice that one can absorb one coupling into M_5, as we will do later –see footnote 6.

JHEP08(2024)149

where $L^2 = 12/\Lambda_5$ is the squared AdS curvature radius. The 5D space will be cut off by an IR-brane at some point $z = z_{\rm IR}$ to be determined dynamically. Also a UV-boundary at $z = z_{\rm UV}$ will be needed to regularize the theory. The limit $z_{\rm UV} \to 0$ will be taken in a proper way to provide finite physical quantities [24–26].

The dimension of $\mathcal{O}_\Phi$, eq. (2.7), is related by eq. (2.8) to the 5D mass of Φ:

$$M_\Phi^2 = -\frac{4+\epsilon}{L^2}\,. \tag{3.7}$$

When $\epsilon < 0$ the mass of Φ is above the BF bound and Φ does not turn on, as we will see in section 3.1.2. Nevertheless, for $\epsilon > 0$ the mass is below the BF bound and Φ turns on in the 5D bulk [31], breaking the conformal and chiral symmetry. Therefore, as in the strongly-coupled model described in section 2, we have two phases separated by the sign of ϵ (see figure 1):

- $\epsilon > 0 \;\Rightarrow\;$ non-AdS$_5$ (non-CFT$_4$) phase.
- $\epsilon < 0 \;\Rightarrow\;$ AdS$_5$ (CFT$_4$) phase.

The presence of the IR-brane add extra parameters to the theory as Φ might also have a potential on the IR-boundary. Following the EFT criteria of [31], we have

$$\mathcal{L}_{\rm IR} = -a^4 \tilde{V}_b(\Phi)\big|_{z_{\rm IR}}, \qquad \tilde{V}_b(\Phi) = \frac{\Lambda_4}{\kappa^2} + \frac{1}{2} m_b^2 \,{\rm Tr}\,|\Phi|^2\,. \tag{3.8}$$

3.1 The $\phi(z)$ profile

The conformal and the chiral symmetry breaking ${\rm SU}(N_F)_L \otimes {\rm SU}(N_F)_R \to {\rm SU}(N_F)_V$ is trigger by a nonzero profile for $\phi = {\rm Tr}|\Phi|$. From eq. (3.2), the equation of motion for ϕ is determined to be

$$-\frac{1}{a^5}\left(\partial_5\, a^3 \partial_5 - a^3 \partial^\mu \partial_\mu\right)\phi + M_\Phi^2\,\phi + \lambda\,\phi^3 = 0\,, \tag{3.9}$$

where $\lambda \equiv \lambda_1 + N_F \lambda_2$ and the warp factor is determined by the Einstein equations [31]:

$$-\frac{\dot{a}}{a^2} = \sqrt{\frac{1}{L^2} + \frac{\hat{\kappa}^2 L^2}{12}\left(\frac{\dot{\phi}^2}{2a^2} - V(\phi)\right)}\,, \tag{3.10}$$

with $\dot{\phi} \equiv \partial_z \phi$ and $\hat{\kappa}^2$ being the 5D gravitational strength. Notice that a nonzero $\hat{\kappa}^2$ induces a mixing between the singlet sector of Φ and the gravitational sector. This corresponds in the dual theory to a mixing of the $q\bar{q}$ mesons with the glueballs.

The boundary conditions are the following. At the UV-boundary we fix

$$L\phi\big|_{z_{\rm UV}} = z_{\rm UV}^{{\rm Dim}[M_q]} M_q\,. \tag{3.11}$$

M_q plays the role of the quark mass in the dual gauge theory, eq. (2.9). Using eq. (2.8) we can write the dimension of M_q as

$${\rm Dim}[M_q] = 4 - {\rm Dim}[\mathcal{O}_\Phi]\,, \tag{3.12}$$

so at the conformal edge we have ${\rm Dim}[M_q] \to 2$. For $M_q \neq 0$, ϕ turns on independently of the sign of ϵ, and the conformal and chiral symmetry are broken inside the 5D bulk. For $M_q = 0$,

JHEP08(2024)149

the field $\phi(z)$ gets a nonzero profile only when we are outside the conformal window ($\epsilon > 0$), as we will explicitly see later. At the IR-brane we must impose the boundary condition determined by the model. We have [31]

$$\left(\frac{M_5}{a}\dot{\phi} + \partial_\phi V_b\right)\Big|_{z_{\rm IR}} = 0\,, \qquad \left(-\frac{6M_5}{\hat{\kappa}^2 L^2}\frac{\dot{a}}{a^2} + V_b\right)\Big|_{z_{\rm IR}} = 0\,. \tag{3.13}$$

The first one is the IR condition for ϕ, while the second one is the junction condition that determines the position of the IR-brane $z_{\rm IR}$.

Although we will present in the next section results with no approximations, it is instructive to consider the case in which the profile of ϕ can be solved analytically. For this, we will take the approximation that ϕ is small such that the quartic term can be neglected as well as the feedback of ϕ on the metric, i.e., the 5D space is AdS_5. Eq. (3.13) reduces in this case to

$$\dot{\phi}(z_{\rm IR}) = -\frac{m_b^2 L}{z_{\rm IR} M_5}\phi_{\rm IR}\,, \quad \phi(z_{\rm IR}) = \phi_{\rm IR}\,, \tag{3.14}$$

where we have introduced the parameter $\phi_{\rm IR}$ related to other parameters of the model (a combination of $\hat{\kappa}^2$, m_b^2, Λ_4 and the sign of λ [31]).[6] We will restrict to $m_b^2 > -2M_5/L$ that guarantees that the conformal symmetry is not broken by the IR-boundary potential.

3.1.1 Towards the conformal transition from outside ($\epsilon > 0$)

With the above approximations, we can solve ϕ analytically. For $\epsilon > 0$, the two solutions are $z^{2\pm i\sqrt{\epsilon}}$ that we can write as

$$\phi(z) = \frac{A}{L^3} z^2 \sin\left(\sqrt{\epsilon}\ln\frac{z}{z_{\rm UV}} + \beta\right)\,, \tag{3.15}$$

where A and β are dimensionless constants to be determined by the boundary conditions. From eq. (3.11) and eq. (3.13), we get

$$M_q = \frac{A}{L^2}\sin\beta\,, \tag{3.16}$$

and

$$\tan\left(\sqrt{\epsilon}\ln\frac{z_{\rm IR}}{z_{\rm UV}} + \beta\right) = -\frac{\sqrt{\epsilon}}{\tilde{m}_b^2}\,, \tag{3.17}$$

where $\tilde{m}_b^2 \equiv 2 + m_b^2 L/M_5$. In the limit $\epsilon \to 0$, eq. (3.17) tells us that $\sin(\sqrt{\epsilon}\ln z_{\rm IR}/z_{\rm UV} + \beta) \to \sqrt{\epsilon}$. Therefore expanding eq. (3.17) around z_c determined by[7]

$$\sqrt{\epsilon}\ln\frac{z_c}{z_{\rm UV}} + \beta = n\pi\,, \quad n = 1, 2, \ldots\,, \tag{3.18}$$

we get

$$\ln\frac{z_{\rm IR}}{z_c} = -\frac{1}{\tilde{m}_b^2} < 0\,. \tag{3.19}$$

[6] By field redefinitions we can absorb $|\lambda|$ in other parameters. Therefore, with no loss of generality, we can consider $\lambda = \pm 1$.

[7] The solution for $n = 1$ corresponds to a global minimum, while $n > 1$ just gives local minima (corresponding to a surviving discrete conformal invariance).

JHEP08(2024)149

Notice that the limit $\epsilon \to 0$ must be taken with $z_{\rm UV} \to 0$ according to eq. (3.18). Using eq. (3.14) and eq. (3.19) we finally get

$$\phi(z) = -\phi_{\rm IR}\, \tilde{m}_b^2 \left(\frac{z}{z_{\rm IR}}\right)^2 \ln \frac{z}{a\, z_{\rm IR}}\,, \tag{3.20}$$

where $a = \mathrm{Exp}[1/\tilde{m}_b^2]$. It is interesting to remark that eq. (3.20) is valid for any value of M_q. In the particular case $M_q = 0$, we have from eq. (3.16) that $\beta = 0$ but $A \neq 0$, corresponding to a spontaneous breaking of the conformal and chiral symmetry.

The above is in accordance with the discussion in section 2 where for $\epsilon > 0$ it was shown that $f(\mu)$ runs as eq. (2.4) and diverges at the scale $\mu_{\rm IR} \sim 1/z_c$ for $\mu_0 \sim \mathrm{Exp}[-\pi/(2\sqrt{\epsilon})]/z_{\rm UV}$.

3.1.2 Towards the conformal transition from inside ($\epsilon < 0$)

Let us now consider the solution of ϕ from the other side of the conformal edge, $\epsilon < 0$. In this case the two possible solutions are $z^{2\pm\sqrt{|\epsilon|}}$ that in the limit $\epsilon \to 0$ leads to z^2 and $z^2 \ln z$. We can then write the most general solution as

$$\phi = \frac{z^2}{L^3} \hat{A} \ln \frac{z}{z_0}\,, \tag{3.21}$$

where $\hat{A}$ and z_0 are the two parameters to be fixed by the boundary conditions. Eq. (3.11) gives

$$M_q = \frac{\hat{A}}{L^2} \ln \frac{z_{\rm UV}}{z_0}\,. \tag{3.22}$$

From the IR-brane boundary conditions we get, similarly to eq. (3.19),

$$\ln \frac{z_{\rm IR}}{z_0} = -\frac{1}{\tilde{m}_b^2} < 0\,, \tag{3.23}$$

that leads exactly to eq. (3.20). We notice however an important difference in this case with respect to the $\epsilon > 0$ case. From eq. (3.22) we have that $M_q = 0$ requires $z_0 \to z_{\rm UV}$, but this is incompatible with eq. (3.23). In other words, there is no nonzero solution for ϕ when $M_q = 0$. As expected, the model flows to the conformal phase for $M_q = 0$.

We can then conclude from the above analysis that approaching the conformal transition $\epsilon \to 0$ from inside the conformal window ($\epsilon < 0$) or outside ($\epsilon > 0$) gives the same profile for ϕ (eq. (3.20)) and, as a consequence, the spontaneous conformal and chiral breaking driven by ϕ at the IR have to be felt equally in both sides of the transition, independently of the value of $M_q \neq 0$.

4 Mass spectrum

Let us discuss here what differences we expect in the mass spectrum of the theory when we approach the conformal edge from inside or outside the conformal window. We will back up our arguments with the mass spectrum calculated in the holographic model with no approximations. For the numerical analysis we will take the benchmark values

$$\phi_{\rm IR} = 1\,, \quad \lambda = 1\,, \quad N_F \lambda_2 = -2\,, \quad \tilde{m}_b^2 = 1\,, \ \hat{\kappa} = 1\,, \quad g_5 = 1.52\,. \tag{4.1}$$

The mass spectrum would change by varying these values, but the qualitative picture will be the same. For other values of the parameter space see [31].

JHEP08(2024)149

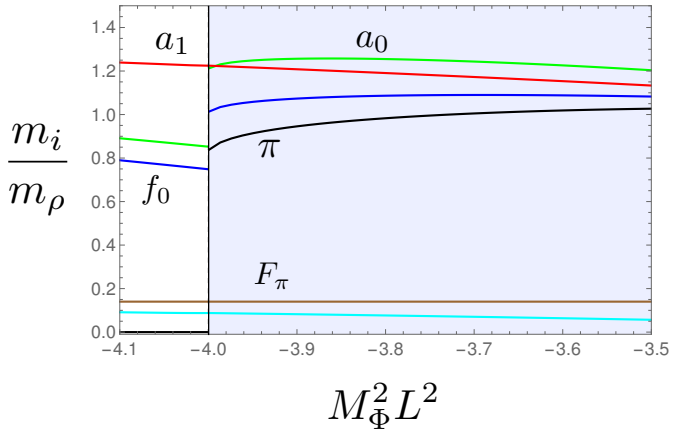

Figure 2. Mass spectrum of mesons, normalized to m_ρ, as a function of the 5D scalar mass or equivalently $Dim[q\bar{q}]$ defined in eq. (2.8). The values of the model are given in eq. (4.1). We vary the value of $\phi_{\rm IR}$ to keep F_π/m_ρ fixed. The sky-blue line corresponds to the dilaton/radion (glueball). For $M_\Phi^2 L^2 < -4$ we have $M_q = 0$, while for $M_\Phi^2 L^2 > -4$ we have $M_q \neq 0$.

4.1 Spin-1 states

It is clear that vector states, coming from the Kaluza-Klein (KK) decomposition of $V_M = (L_M + R_M)/\sqrt{2}$ are not much affected by the scalar $\phi(z)$ since they do not couple to it. They can only notice a nonzero ϕ from the feedback of this on the metric. This clearly affects the KK spectrum, but this is expected to be quite universal for the different type of states. For this reason, we will use the mass of the lightest vector state, the ρ, to normalize the other masses.

The axial-vector $A_M = (L_M - R_M)/\sqrt{2}$ couple to ϕ through the covariant derivative, and therefore a nonzero ϕ splits the masses of the KK of A_M from those of V_M. Since ϕ has the same profile at both sides of the conformal edge independently of M_q, as shown in eq. (3.20), we expect the masses of the axial-vectors to be smooth across the transition. Similarly for F_π, defined as the axial-vector two-point correlator at zero momentum [31], we expect this quantity to be independent of M_q and smooth across the transition.

In figure 2 we show the mass of the lightest axial-vector, a_1 as well as F_π normalized to m_ρ. We indeed see that these values are smooth across the transition. To show that these physical quantities are also independent of M_q, we plot in figure 3 the predictions of the holographic model as a function of M_q for $\epsilon > 0$. We remark again that this is obvious for $\epsilon < 0$ (hyperscaling –see also [62]) but not for $\epsilon > 0$. Indeed we see in figure 3 that a_1 and F_π (normalized to m_ρ) do not vary as we move M_q.

4.2 The dilaton/radion

It has been claimed that approaching the conformal edge from below, the theory could have a light scalar, the dilaton, associated to the spontaneous breaking of the conformal invariance. This has been partly supported by lattice results [2–7] that have seen a 0^{++} state below the ρ mass for values of N_F where one expects to be outside (but close to) the conformal window. In [31] it was shown that in holographic models the radion, that corresponds to the dilaton

JHEP08(2024)149

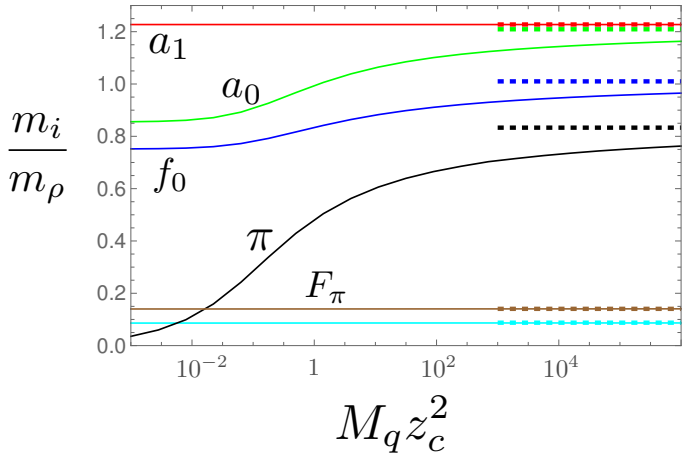

Figure 3. Mass spectrum of mesons outside the conformal window $\epsilon > 0$ ($\epsilon \to 0$), normalized the m_ρ, as a function of M_q in units of $1/z_c$ defined in eq. (3.18). In dashed-lines the values for $\epsilon < 0$. The sky-blue line corresponds to the dilaton/radion (glueball).

in the 4D dual theory, was the lightest state of the spectrum, although not parametrically lighter than the others (see also [35, 36, 42–61]). This state arises from the KK decomposition of the AdS_5 gravitons, and therefore should be considered a glueball state (it mixes with the mesons from Φ but the mixing comes out to be small [31], always smaller than 20%).

Since we showed that the profile of ϕ is the same at both sides of the conformal transition, we must also expect a light radion/dilaton inside the conformal window (for $M_q \neq 0$) as long as we are close to the lower edge. We find that this is indeed the case. As it can be appreciated in figure 2 the radion/dilaton mass is smooth across the transition and is also light inside the conformal window. The reason for this lightness can be found in [31] since the argument given there can also be applied at the other side of the transition (for $\epsilon < 0$). This surprising result shows that this light dilaton has nothing to do with the spontaneous breaking of the conformal symmetry.

Another important property of the radion/dilaton is that its mass (normalized to m_ρ) is practically independent of M_q, since the profile of ϕ, given in eq. (3.20), is the same for any value of M_q. This is shown in figure 3 by a sky-blue line.

4.3 Scalar mesons

Let us now analyze the mass spectrum of the fluctuations of Φ corresponding to $q\bar{q}$ mesons. Although they can in principle mix with the glueballs, we find that in our holographic model this mixing is small. Let us start with the radial excitations and consider later the angular fluctuations corresponding to the Goldstones.

4.3.1 Radial fluctuations: 0^{++} states

To understand the dependence on the sign of ϵ, we will first calculate the scalar-scalar correlator on the AdS_5 boundary at $z = z_{UV} \to 0$. To obtain analytical expressions, we will work in the approximation where the quartic couplings and the feedback on the metric are

JHEP08(2024)149

neglected. At this level the singlet and adjoint scalars are degenerate. Following [63, 64], we have (neglecting an overall factor)

$$\Pi_S(p) = M_5 L \left[2 + z_{\rm UV} \frac{\partial_z J_{\sqrt{-\epsilon}}(ipz) + b(p)\partial_z Y_{\sqrt{-\epsilon}}(ipz)}{J_{\sqrt{-\epsilon}}(ipz) + b(p) Y_{\sqrt{-\epsilon}}(ipz)} \right]_{z=z_{\rm UV}} , \tag{4.2}$$

where J_n and Y_n are Bessel functions of order n and p is the Euclidean momentum, and

$$b(p) = - \frac{z\partial_z J_{\sqrt{-\epsilon}}(ipz) + \tilde{m}_b^2 J_{\sqrt{-\epsilon}}(ipz)}{z\partial_z Y_{\sqrt{-\epsilon}}(ipz) + \tilde{m}_b^2 Y_{\sqrt{-\epsilon}}(ipz)} \bigg|_{z=z_{\rm IR}} . \tag{4.3}$$

- **$\epsilon < 0$:** let us take the limit $\epsilon \to 0$ from inside the conformal window with $M_q \neq 0$ such that $z_{\rm IR}$ is fixed at some finite value. The scalar-scalar correlator eq. (4.2) defined at $z_{\rm UV} \to 0$ simplifies to

$$\Pi_S(p) = M_5 L \left[2 + \frac{2b(p)}{\pi + 2b(p)(\gamma + \ln(ipz_{\rm UV}/2))} \right] + \cdots , \tag{4.4}$$

  where

$$b(p) = - \frac{ipz_{\rm IR} J_1(ipz_{\rm IR}) - \tilde{m}_b^2 J_0(ipz_{\rm IR})}{ipz_{\rm IR} Y_1(ipz_{\rm IR}) - \tilde{m}_b^2 Y_0(ipz_{\rm IR})} . \tag{4.5}$$

  For large momentum $pz_{\rm IR} \gg 1$, eq. (4.4) gives

$$\Pi_S(p) \simeq M_5 L \left[2 + \frac{1}{\gamma + \ln(pz_{\rm UV}/2)} \right] . \tag{4.6}$$

  The origin of the logarithm is expected from the discussion in section 2. The theory contains the marginal term $f(\mu)\,{\rm Tr}[\mathcal{O}_\Phi \mathcal{O}_\Phi]$ where f runs according to eq. (2.3). For $pz_{\rm UV} \to 0$ the log-dependent term goes to zero and the theory enters into the conformal regime.

  Therefore the mass spectrum of the scalars are not sensitive to $\ln z_{\rm UV}$ terms. Using the fact that a scalar-scalar correlator in a large-N_c theory can also be written as a sum over infinitely narrow resonances

$$\Pi_S(p) = \sum_{i=1}^{\infty} \frac{F_{S_i}^2 m_{S_i}^2}{p^2 + m_{S_i}^2} , \tag{4.7}$$

  we can obtain the mass spectrum by looking at the poles of eq. (4.4). Taking $\tilde{m}_b^2 = 1$ we find that the lightest resonance, that we named as in QCD f_0, is given by $m_{f_0} \simeq 1.26/z_{\rm IR}$, much lighter that the ρ meson mass that in the approximation that we are taking here is $m_\rho \simeq 2.4/z_{\rm IR}$. In fact, we find that $m_{f_0}/m_\rho < 1$ is true for any value of $\tilde{m}_b^2 \geq 0$.

  The reason of why the lightest scalar meson is lighter than the ρ is tied to the fact that the mass of M_Φ^2 is taking at the conformal edge the lowest possible value ($M_\Phi^2 L^2 \to -4$) [31]. We can see this analytically by taking the limit $m_{S_i} z_{\rm IR} \gg 1$. We find

$$m_{S_i} \simeq \left(i - \frac{3}{4} + \frac{\sqrt{-\epsilon}}{2} \right) \frac{\pi}{z_{\rm IR}} , \quad i = 1, 2, \cdots , \tag{4.8}$$

JHEP08(2024)149

that shows that the lightest state mass minimizes for $\epsilon = 0$. As we already said, this can also be understood from the CFT point of view. Close to the conformal lower edge the dimension of $\mathcal{O}_\Phi = q\bar{q}$ takes the closest value to the unitarity bound ($\text{Dim}[q\bar{q}] > 1$) where a scalar is expected to become massless since $\mathcal{O}_\Phi$ decouples from the CFT [27].

- **$\epsilon > 0$:** let us now consider the limit $\epsilon \to 0$ from outside the conformal window. We recall that we have to take this limit such that eq. (3.18) is kept fixed. This leads to

$$\Pi_S(p) \simeq M_5 L \left[2 + \frac{2b(p)}{\pi + 2b(p)(\gamma + \ln(ipz_c/2) + \tilde{M}_q)} \right] , \tag{4.9}$$

where $\tilde{M}_q = M_q z_{\text{IR}}^2/(L\phi_{\text{IR}}\tilde{m}_b^2)$. Notice that it is now $z_c \sim z_{\text{IR}}$ that regulate the logarithm and not z_{UV} as in the $\epsilon < 0$ case. This means that the logarithmic breaking of conformal invariance remains at low-energies. For large values of M_q however this term tends to zero and eq. (4.9) approaches eq. (4.4). This was expected from the discussion in section 2: the presence of a large M_q sets a mass gap to the theory much larger than the scale z_c; the IR flow "stops" when the theory is (almost) a CFT, much before the coupling $f(\mu)$ blows up. The theory in this case has to have the same behavior as that for $\epsilon < 0$.

The scalar meson masses are determined by the poles of eq. (4.9). We get

$$b(m_{S_i}) = -\frac{\pi/2}{\gamma + \ln(m_{S_i} z_c/2) + \tilde{M}_q} . \tag{4.10}$$

Taking the approximation $m_{S_i} z_{\text{IR}} \gg 1$ and using eq. (3.19), we obtain

$$m_{S_i} \simeq (i - \frac{3}{4})\frac{\pi}{z_{\text{IR}}} - \frac{\pi/2}{\gamma + \ln(m_{S_i} z_{\text{IR}}/2) + \frac{1}{\tilde{m}_b^2} + \tilde{M}_q} \frac{1}{z_{\text{IR}}} , \quad i = 1, 2, \cdots . \tag{4.11}$$

Notice that the masses are sensitive to a logarithmic conformal breaking (there is no a simple scaling with $1/z_{\text{IR}}$), different from the case $\epsilon < 0$. Nevertheless, as expected, eq. (4.11) tends to eq. (4.8) for $M_q \to \infty$.

The numerical results (with no approximations) for the masses of the lightest scalar singlet (f_0) and adjoint (a_0) are shown in figure 2. The masses are different at the two sides of the conformal transition due to the log terms discussed above. The dependence on M_q for $\epsilon > 0$ is shown in figure 3. As M_q grows, the masses tend to the values for $\epsilon < 0$ (hyperscaling case), shown as dashed lines.

4.3.2 Angular fluctuations: the pions

Let us finally comment on the angular fluctuations of Φ, the pions. These are the only states sensitive to the UV-boundary condition and therefore the ones that clearly distinguish among the two limits towards the conformal edge. As explained above, for $\epsilon > 0$ and $M_q = 0$ the model shows spontaneous chiral symmetry breaking and we expect the pions to be massless. On the other side, $\epsilon < 0$, the chiral breaking is explicit (UV driven by M_q) and the pions should have a mass as large as the other mesons, following hyperscaling eq. (2.10). This is shown in figure 3. It is interesting to remark that we find $m_\pi < m_{f_0}$ for any value of M_q and for any value of the parameters of the model.

JHEP08(2024)149

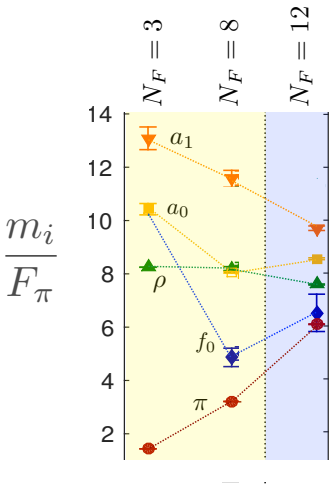

Figure 4. Lattice results from [4, 5] for the QCD meson masses normalized to F_π for different values of N_F. See [4, 5] for the values of the quark masses. For $N_F = 3$ we have identified $m_{f_0} \sim m_{a_0}$.

4.4 Moving further inside the conformal window

As M_Φ^2 moves from -4 to -3, corresponding to an increase of $\text{Dim}[q\bar{q}]$ from 2 to 3, we are getting further inside the conformal window (see figure 1). We expect the scalar mesons to become heavier since we are moving away from the unitarity bound ($\text{Dim}[q\bar{q}] > 1$).

On the other hand, the explicit chiral breaking is dictated by M_q whose dimension moves from 2 to 1. As a consequence, the profile of ϕ, that grows as

$$\phi \sim M_q \, z^{\text{Dim}[M_q]} \,, \tag{4.12}$$

becomes flatter and spreads more into the AdS_5 space. To keep F_π/m_ρ constant, the flatter the ϕ profile, the smaller ϕ_{IR} must be. This implies that the effect of ϕ on the IR ($z \sim z_{\text{IR}}$) becomes relatively weaker. Since the spectrum of resonances is determined by the fields at $z \sim z_{\text{IR}}$, we expect that they will notice less the chiral breaking driven by ϕ. This is indeed seen in figure 2 where, as M_Φ^2 moves towards -3, we have $m_{a_1} \to m_\rho$ and $m_{a_0} \to m_{f_0} \to m_\pi$. This behavior is also observed in lattice simulations as we will see below.

5 Comparison with lattice simulations

There are several lattice simulations of SU(3) QCD at large values of N_F. In [2, 3, 6, 7] lattice simulations for $N_F = 8$ were provided, while results for $N_F = 12$ were given in [8–10]. In [4, 5] the value of N_F was effectively made to vary from 8 to 12 by varying the quark masses. In figure 4 we show the results of [4, 5] for $N_F = 3, 8$ and 12.

It is highly supported that QCD with $N_F = 8$ flavors is outside the conformal window, while it is inside for $N_F = 12$. The main indication comes from the pion mass that it is seen to go to zero with M_q for $N_F = 8$ and shows hyperscaling for $N_F = 12$ [4, 5], as it can be appreciated in figure 4. Therefore we can compare our results inside and outside the conformal window with those of lattice for $N_F = 8$ and $N_F = 12$ respectively.

JHEP08(2024)149

Figure 4 shows the following general features:

- The scalars are the lightest states for $N_F = 8$ where we expect QCD to be outside (but close) to the conformal window.
- The chiral-breaking mass splittings diminish as N_F increases and we move inside the conformal window ($m_{a_1} \to m_\rho$, $m_{a_0} \to m_{f_0} \to m_\pi$).

These properties are quite close to the ones derived in our holographic model. Increasing N_F is equivalent to increasing M_Φ^2 in holographic models and figure 2 shows that chiral breaking effects become weaker. Also the scalar f_0 is predicted to be light close to the conformal transition. Nevertheless, our holographic model also predicts a light radion/dilaton that was advocated in [31] to be associated with the lightest scalar seen in lattice simulation. Nevertheless, the radion/dilaton is predicted to be mostly a glueball whose mass is smooth as we cross the conformal transition (sky-blue line in figure 2). This is in contradiction with lattice results that seem to suggest that the lightest 0^{++} scalar is a $q\bar{q}$ meson, not a glueball, since its mass tends to m_π for large N_f. The light glueball present in our holographic model could be then a feature of the simple IR-brane setup that might be absent in more realistic holographic models. For example, there are no light glueballs in the holographic model of [30]. We leave this investigation for the future.

Another important feature derived from our analysis is the dependence of the meson masses with M_q, shown in figure 3. This property might offer an additional hint to the nature of the light scalar: $q\bar{q}$ meson if its mass has a M_q dependence (see eq. (4.11)), or a glueball if not. In figure 5 we show our predictions for the masses of f_0, π and glueball (normalized to F_π) as a function of M_q, and compare them with the lattice predictions of [65].[8] Unfortunately, at present lattice results are not accurate enough to clearly distinguish any dependence with M_q, with the exception of m_π. Figure 5 however seems to slightly favor f_0 as the lattice 0^{++} state in front of a glueball state.

6 Conclusions

We have analyzed how the physical properties of a system change when approaches a conformal transition from both sides of the conformal edge. The derived properties seem to be generic for large-N_c models where the conformal transition occurs by the merging of an IR and a UV fixed point. We have obtained the following features:

- The dilaton (mostly a glueball) is light at both sides of the conformal transition, showing that has nothing to do with the spontaneous breaking of conformal invariance. This is very different from the pion that is massless outside the conformal window but massive inside due respectively to the spontaneous and explicit breaking of the chiral symmetry.
- The scalar meson f_0 (mostly a $\bar{q}q$ state) is light close to the conformal edge, being lighter when approaching it from outside the conformal window than from inside –see

[8] We have fitted the lowest value of m_π/F_π in [65] to our prediction in order to normalize our M_q with that in [65].

JHEP08(2024)149

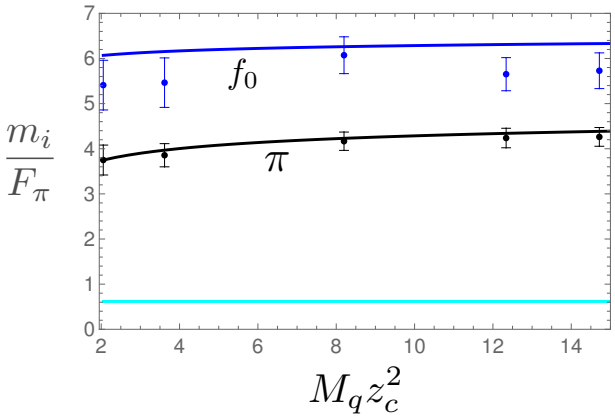

Figure 5. Predictions for meson masses normalized to F_π as a function of M_q in units of $1/z_c$ defined in eq. (3.18). The sky-blue line corresponds to the dilaton/radion (glueball). Data points are lattice results from [65].

figure 3. Its mass shows a dependence with M_q predicted as in eq. (4.11) that can be parametrized as

$$\frac{m_{f_0}}{m_\rho} = \frac{a_{f_0}}{a_\rho} - \frac{\alpha_1}{\alpha_2 \ln \frac{m_{f_0}}{m_\rho} + M_q}\,, \tag{6.1}$$

where a_i are the hyperscaling values (eq. (2.10)) and α_i are constants.

- Our model predicts $m_\pi < m_{f_0}$ inside the conformal window.
- Spin-1 meson masses as well as F_π are practically smooth across the conformal transition and independent of M_q as shown in figure 3.
- Chiral symmetry breaking effects become smaller as we move further inside the conformal window, i.e., $m_{a_1} \to m_\rho$ and $m_{a_0} \to m_{f_0} \to m_\pi$. This is because the dimension of M_q, responsible for the chiral and conformal symmetry breaking, decreases.

Most of these generic properties seem to be followed by QCD as we increase N_F as lattice results show in figure 4.

Models close to the conformal transition can also be useful for physics beyond the SM [31]. In particular, if this phase transition occurs in the early universe, a supercooled epoch can generate interesting signal [66, 67]. These applications are left for the future.

Acknowledgments

We would like to thank Oriol Pujolas for collaborating at the early stages of this work. LS also thanks Leandro Da Rold for useful correspondence. The authors acknowledge support from the Departament de Recerca i Universitats from Generalitat de Catalunya to the Grup de Recerca "Grup de Física Teòrica UAB/IFAE" (Codi: 2021 SGR 00649). This work has also been supported by the research grant PID2020-115845GB-I00/AEI/10.13039/501100011033.

JHEP08(2024)149

Open Access. This article is distributed under the terms of the Creative Commons Attribution License (CC-BY4.0), which permits any use, distribution and reproduction in any medium, provided the original author(s) and source are credited.

References

[1] D.B. Kaplan, J.-W. Lee, D.T. Son and M.A. Stephanov, *Conformality lost*, *Phys. Rev. D* **80** (2009) 125005 [arXiv:0905.4752] [INSPIRE].

[2] LatKMI collaboration, *Light flavor-singlet scalars and walking signals in $N_f = 8$ QCD on the lattice*, *Phys. Rev. D* **96** (2017) 014508 [arXiv:1610.07011] [INSPIRE].

[3] LatKMI collaboration, *Light composite scalar in eight-flavor QCD on the lattice*, *Phys. Rev. D* **89** (2014) 111502 [arXiv:1403.5000] [INSPIRE].

[4] R.C. Brower et al., *Composite Higgs model at a conformal fixed point*, *Phys. Rev. D* **93** (2016) 075028 [arXiv:1512.02576] [INSPIRE].

[5] A. Hasenfratz, C. Rebbi and O. Witzel, *Large scale separation and resonances within LHC range from a prototype BSM model*, *Phys. Lett. B* **773** (2017) 86 [arXiv:1609.01401] [INSPIRE].

[6] T. Appelquist et al., *Strongly interacting dynamics and the search for new physics at the LHC*, *Phys. Rev. D* **93** (2016) 114514 [arXiv:1601.04027] [INSPIRE].

[7] Lattice Strong Dynamics collaboration, *Nonperturbative investigations of SU(3) gauge theory with eight dynamical flavors*, *Phys. Rev. D* **99** (2019) 014509 [arXiv:1807.08411] [INSPIRE].

[8] Z. Fodor et al., *Twelve massless flavors and three colors below the conformal window*, *Phys. Lett. B* **703** (2011) 348 [arXiv:1104.3124] [INSPIRE].

[9] Y. Aoki et al., *Lattice study of conformality in twelve-flavor QCD*, *Phys. Rev. D* **86** (2012) 054506 [arXiv:1207.3060] [INSPIRE].

[10] LatKMI collaboration, *Light composite scalar in twelve-flavor QCD on the lattice*, *Phys. Rev. Lett.* **111** (2013) 162001 [arXiv:1305.6006] [INSPIRE].

[11] E. Pomoni and L. Rastelli, *Large N field theory and AdS tachyons*, *JHEP* **04** (2009) 020 [arXiv:0805.2261] [INSPIRE].

[12] V. Gorbenko, S. Rychkov and B. Zan, *Walking, weak first-order transitions, and complex CFTs*, *JHEP* **10** (2018) 108 [arXiv:1807.11512] [INSPIRE].

[13] M. Golterman and Y. Shamir, *Low-energy effective action for pions and a dilatonic meson*, *Phys. Rev. D* **94** (2016) 054502 [arXiv:1603.04575] [INSPIRE].

[14] M. Golterman and Y. Shamir, *Effective pion mass term and the trace anomaly*, *Phys. Rev. D* **95** (2017) 016003 [arXiv:1611.04275] [INSPIRE].

[15] M. Golterman and Y. Shamir, *Large-mass regime of the dilaton-pion low-energy effective theory*, *Phys. Rev. D* **98** (2018) 056025 [arXiv:1805.00198] [INSPIRE].

[16] M. Golterman and Y. Shamir, *Explorations beyond dilaton chiral perturbation theory in the eight-flavor SU(3) gauge theory*, *Phys. Rev. D* **102** (2020) 114507 [arXiv:2009.13846] [INSPIRE].

[17] M. Golterman, E.T. Neil and Y. Shamir, *Application of dilaton chiral perturbation theory to $N_f = 8$, SU(3) spectral data*, *Phys. Rev. D* **102** (2020) 034515 [arXiv:2003.00114] [INSPIRE].

[18] A. Freeman, M. Golterman and Y. Shamir, *Dilaton chiral perturbation theory at next-to-leading order*, *Phys. Rev. D* **108** (2023) 074506 [arXiv:2307.00940] [INSPIRE].

JHEP08(2024)149

[19] T. Appelquist, J. Ingoldby and M. Piai, *Dilaton EFT framework for lattice data*, *JHEP* **07** (2017) 035 [arXiv:1702.04410] [INSPIRE].

[20] T. Appelquist, J. Ingoldby and M. Piai, *Analysis of a dilaton EFT for lattice data*, *JHEP* **03** (2018) 039 [arXiv:1711.00067] [INSPIRE].

[21] T. Appelquist, J. Ingoldby and M. Piai, *Nearly conformal composite Higgs model*, *Phys. Rev. Lett.* **126** (2021) 191804 [arXiv:2012.09698] [INSPIRE].

[22] T. Appelquist, J. Ingoldby and M. Piai, *Composite two-Higgs doublet model from dilaton effective field theory*, *Nucl. Phys. B* **983** (2022) 115930 [arXiv:2205.03320] [INSPIRE].

[23] T. Appelquist, J. Ingoldby and M. Piai, *Dilaton effective field theory*, *Universe* **9** (2023) 10 [arXiv:2209.14867] [INSPIRE].

[24] J.M. Maldacena, *The large N limit of superconformal field theories and supergravity*, *Adv. Theor. Math. Phys.* **2** (1998) 231 [hep-th/9711200] [INSPIRE].

[25] S.S. Gubser, I.R. Klebanov and A.M. Polyakov, *Gauge theory correlators from noncritical string theory*, *Phys. Lett. B* **428** (1998) 105 [hep-th/9802109] [INSPIRE].

[26] E. Witten, *Anti-de Sitter space and holography*, *Adv. Theor. Math. Phys.* **2** (1998) 253 [hep-th/9802150] [INSPIRE].

[27] B. Grinstein, K.A. Intriligator and I.Z. Rothstein, *Comments on unparticles*, *Phys. Lett. B* **662** (2008) 367 [arXiv:0801.1140] [INSPIRE].

[28] A.G. Cohen and H. Georgi, *Walking beyond the rainbow*, *Nucl. Phys. B* **314** (1989) 7 [INSPIRE].

[29] R. Zwicky, *QCD with an infrared fixed point: the pion sector*, *Phys. Rev. D* **109** (2024) 034009 [arXiv:2306.06752] [INSPIRE].

[30] M. Jarvinen, *Massive holographic QCD in the Veneziano limit*, *JHEP* **07** (2015) 033 [arXiv:1501.07272] [INSPIRE].

[31] A. Pomarol, O. Pujolas and L. Salas, *Holographic conformal transition and light scalars*, *JHEP* **10** (2019) 202 [arXiv:1905.02653] [INSPIRE].

[32] J. Albert and L. Rastelli, *Bootstrapping pions at large N*, *JHEP* **08** (2022) 151 [arXiv:2203.11950] [INSPIRE].

[33] C. Fernandez, A. Pomarol, F. Riva and F. Sciotti, *Cornering large-N_c QCD with positivity bounds*, *JHEP* **06** (2023) 094 [arXiv:2211.12488] [INSPIRE].

[34] T. Ma, A. Pomarol and F. Sciotti, *Bootstrapping the chiral anomaly at large N_c*, *JHEP* **11** (2023) 176 [arXiv:2307.04729] [INSPIRE].

[35] D. Kutasov, J. Lin and A. Parnachev, *Conformal phase transitions at weak and strong coupling*, *Nucl. Phys. B* **858** (2012) 155 [arXiv:1107.2324] [INSPIRE].

[36] D. Kutasov, J. Lin and A. Parnachev, *Holographic walking from tachyon DBI*, *Nucl. Phys. B* **863** (2012) 361 [arXiv:1201.4123] [INSPIRE].

[37] K. Jensen, A. Karch, D.T. Son and E.G. Thompson, *Holographic Berezinskii-Kosterlitz-Thouless transitions*, *Phys. Rev. Lett.* **105** (2010) 041601 [arXiv:1002.3159] [INSPIRE].

[38] N. Iqbal, H. Liu, M. Mezei and Q. Si, *Quantum phase transitions in holographic models of magnetism and superconductors*, *Phys. Rev. D* **82** (2010) 045002 [arXiv:1003.0010] [INSPIRE].

[39] A.F. Faedo, C. Hoyos, D. Mateos and J.G. Subils, *Holographic complex conformal field theories*, *Phys. Rev. Lett.* **124** (2020) 161601 [arXiv:1909.04008] [INSPIRE].

JHEP08(2024)149

[40] A.F. Faedo, C. Hoyos, D. Mateos and J.G. Subils, *Multiple mass hierarchies from complex fixed point collisions*, *JHEP* **10** (2021) 246 [arXiv:2106.01802] [INSPIRE].

[41] E. Witten, *Multitrace operators, boundary conditions, and AdS/CFT correspondence*, hep-th/0112258 [INSPIRE].

[42] L. Vecchi, *The conformal window of deformed CFT's in the planar limit*, *Phys. Rev. D* **82** (2010) 045013 [arXiv:1004.2063] [INSPIRE].

[43] D. Elander and M. Piai, *Light scalars from a compact fifth dimension*, *JHEP* **01** (2011) 026 [arXiv:1010.1964] [INSPIRE].

[44] S.P. Kumar, D. Mateos, A. Paredes and M. Piai, *Towards holographic walking from N=4 super Yang-Mills*, *JHEP* **05** (2011) 008 [arXiv:1012.4678] [INSPIRE].

[45] M. Jarvinen and E. Kiritsis, *Holographic models for QCD in the Veneziano limit*, *JHEP* **03** (2012) 002 [arXiv:1112.1261] [INSPIRE].

[46] N. Evans and K. Tuominen, *Holographic modelling of a light technidilaton*, *Phys. Rev. D* **87** (2013) 086003 [arXiv:1302.4553] [INSPIRE].

[47] J. Erdmenger, N. Evans and M. Scott, *Meson spectra of asymptotically free gauge theories from holography*, *Phys. Rev. D* **91** (2015) 085004 [arXiv:1412.3165] [INSPIRE].

[48] D. Elander, R. Lawrance and M. Piai, *Hyperscaling violation and electroweak symmetry breaking*, *Nucl. Phys. B* **897** (2015) 583 [arXiv:1504.07949] [INSPIRE].

[49] N. Evans, P. Jones and M. Scott, *Soft walls in dynamic AdS/QCD and the technidilaton*, *Phys. Rev. D* **92** (2015) 106003 [arXiv:1508.06540] [INSPIRE].

[50] D. Arean, I. Iatrakis, M. Jarvinen and E. Kiritsis, *CP-odd sector and θ dynamics in holographic QCD*, *Phys. Rev. D* **96** (2017) 026001 [arXiv:1609.08922] [INSPIRE].

[51] K. Bitaghsir Fadafan, W. Clemens and N. Evans, *Holographic gauged NJL model: the conformal window and ideal walking*, *Phys. Rev. D* **98** (2018) 066015 [arXiv:1807.04548] [INSPIRE].

[52] D. Elander, M. Piai and J. Roughley, *Holographic glueballs from the circle reduction of Romans supergravity*, *JHEP* **02** (2019) 101 [arXiv:1811.01010] [INSPIRE].

[53] Y. Buyukdag, *Light scalar modes from holographic deformations*, *Phys. Rev. D* **102** (2020) 106018 [arXiv:1911.12328] [INSPIRE].

[54] D. Elander, M. Frigerio, M. Knecht and J.-L. Kneur, *Holographic models of composite Higgs in the Veneziano limit. Part I. Bosonic sector*, *JHEP* **03** (2021) 182 [arXiv:2011.03003] [INSPIRE].

[55] D. Elander, M. Piai and J. Roughley, *Probing the holographic dilaton*, *JHEP* **06** (2020) 177 [*Erratum ibid.* **12** (2020) 109] [arXiv:2004.05656] [INSPIRE].

[56] D. Elander, M. Piai and J. Roughley, *Dilatonic states near holographic phase transitions*, *Phys. Rev. D* **103** (2021) 106018 [arXiv:2010.04100] [INSPIRE].

[57] D. Elander, M. Piai and J. Roughley, *Light dilaton in a metastable vacuum*, *Phys. Rev. D* **103** (2021) 046009 [arXiv:2011.07049] [INSPIRE].

[58] D. Elander, M. Piai and J. Roughley, *Coulomb branch of N=4 SYM and dilatonic scions in supergravity*, *Phys. Rev. D* **104** (2021) 046003 [arXiv:2103.06721] [INSPIRE].

[59] D. Elander, A. Fatemiabhari and M. Piai, *Toward minimal composite Higgs models from regular geometries in bottom-up holography*, *Phys. Rev. D* **107** (2023) 115021 [arXiv:2303.00541] [INSPIRE].

JHEP08(2024)149

[60] J. Cruz Rojas, D.K. Hong, S.H. Im and M. Järvinen, *Holographic light dilaton at the conformal edge*, *JHEP* **05** (2023) 204 [arXiv:2302.08112] [INSPIRE].

[61] D. Elander, A. Fatemiabhari and M. Piai, *Phase transitions and light scalars in bottom-up holography*, *Phys. Rev. D* **108** (2023) 015021 [arXiv:2212.07954] [INSPIRE].

[62] N. Evans and M. Scott, *Hyper-scaling relations in the conformal window from dynamic AdS/QCD*, *Phys. Rev. D* **90** (2014) 065025 [arXiv:1405.5373] [INSPIRE].

[63] L. Da Rold and A. Pomarol, *Chiral symmetry breaking from five dimensional spaces*, *Nucl. Phys. B* **721** (2005) 79 [hep-ph/0501218] [INSPIRE].

[64] L. Da Rold and A. Pomarol, *The scalar and pseudoscalar sector in a five-dimensional approach to chiral symmetry breaking*, *JHEP* **01** (2006) 157 [hep-ph/0510268] [INSPIRE].

[65] LSD collaboration, *Hidden conformal symmetry from the lattice*, *Phys. Rev. D* **108** (2023) L091505 [arXiv:2305.03665] [INSPIRE].

[66] P. Baratella, A. Pomarol and F. Rompineve, *The supercooled universe*, *JHEP* **03** (2019) 100 [arXiv:1812.06996] [INSPIRE].

[67] C. Csáki, M. Geller, Z. Heller-Algazi and A. Ismail, *Relevant dilaton stabilization*, *JHEP* **06** (2023) 202 [arXiv:2301.10247] [INSPIRE].

JHEP08(2024)149

4.3 Paper 3: $g_\mu - 2$ from Vector-Like Leptons in Warped Space

JHEP

Published for SISSA by Springer

Received: January 25, 2017
Accepted: April 24, 2017
Published: May 3, 2017

$g_\mu - 2$ from Vector-like leptons in warped space

Eugenio Megías,[a,b] **Mariano Quirós**[c,d] **and Lindber Salas**[c]

[a] *Max-Planck-Institut für Physik (Werner-Heisenberg-Institut), Föhringer Ring 6, D-80805, Munich, Germany*

[b] *Departamento de Física Teórica, Universidad del País Vasco UPV/EHU, Apartado 644, 48080 Bilbao, Spain*

[c] *Institut de Física d'Altes Energies (IFAE), The Barcelona Institute of Science and Technology (BIST), Campus UAB, 08193 Bellaterra (Barcelona), Spain*

[d] *ICREA, Pg. Lluís Companys 23, 08010 Barcelona, Spain*

E-mail: emegias@mppmu.mpg.de, quiros@ifae.es, lsalas@ifae.es

Abstract: The experimental value of the anomalous magnetic moment of the muon, as well as the LHCb anomalies, point towards new physics coupled non-universally to muons and electrons. Working in extra dimensional theories, which solve the electroweak hierarchy problem with a warped metric, strongly deformed with respect to the AdS_5 geometry at the infra-red brane, the LHCb anomalies can be solved by imposing that the bottom and the muon have a sizable amount of compositeness, while the electron is mainly elementary. Using this set-up as starting point we have proven that extra physics has to be introduced to describe the anomalous magnetic moment of the muon. We have proven that this job is done by a set of vector-like leptons, mixed with the physical muon through Yukawa interactions, and with a high degree of compositeness. The theory is consistent with all electroweak indirect, direct and theoretical constraints, the most sensitive ones being the modification of the $Z\bar{\mu}\mu$ coupling, oblique observables and constraints on the stability of the electroweak minimum. They impose lower bounds on the compositeness ($c \lesssim 0.37$) and on the mass of the lightest vector-like lepton ($\gtrsim 270\,\text{GeV}$). Vector-like leptons could be easily produced in Drell-Yan processes at the LHC and detected at $\sqrt{s} = 13\,\text{TeV}$.

Keywords: Phenomenology of Field Theories in Higher Dimensions, Phenomenology of Large extra dimensions

ArXiv ePrint: 1701.05072

Open Access, © The Authors.
Article funded by SCOAP[3].

doi:10.1007/JHEP05(2017)016

JHEP05(2017)016

Contents

1 Introduction

In spite of the fact that, so far, LHC has found no direct evidence of new physics (NP) beyond the Standard Model (BSM), there are several hints of lepton flavor universality NP. Two of them are related to the muon lepton flavor, as the $B \to K^* \mu^+ \mu^-$ anomalies [1, 2] and the anomalous magnetic moment (AMM) of the muon [3], so one could suspect that both of them could be related to the same kind of NP.

JHEP05(2017)016

Moreover, as the Standard Model (SM) has a naturalness problem (the so-called hierarchy problem) it would be rewarding to accommodate the solutions to present (or future) experimental anomalies within theories solving the hierarchy problem. The most popular solutions to the hierarchy problem are provided by supersymmetric theories (where the electroweak scale is protected by supersymmetry) and by theories with a warped extra dimension [4] (where the electroweak scale is provided by the Planck scale after warping along the extra dimension).[1]

We will concentrate on the latter class of theories, i.e. in theories with a warped extra dimension. In particular we will consider theories with two branes, an ultra-violet (UV) and an infra-red (IR) brane, and a stabilizing field ϕ strongly deforming the AdS_5 metric near the IR-brane. This strong deformation makes it possible to accommodate the SM in the bulk, without an additional custodial gauge symmetry, consistently with all electroweak and flavor constraints, thanks to a naked metric singularity in the extra dimension (soft-wall metric) outside the physical interval [5–14]. We have recently shown that in this theory one can easily accommodate the LHCb anomalies provided that the left-handed muon (and bottom quark) has some degree of compositeness [15].

In this paper we will consider the other muon anomaly: the AMM of the muon. At the tree level the muon predicts a magnetic moment $\vec{M}_\mu = g_\mu \frac{e}{2m_\mu}\vec{S}_\mu$ with gyromagnetic ratio $g_\mu = 2$. Loop effects predict a deviation with respect to the tree level value which is parameterized by the ratio (AMM)

$$a_\mu = \frac{g_\mu - 2}{2}\,. \tag{1.1}$$

The SM gives a very precise prediction of the AMM of the muon [16]. In particular a recent update of the hadronic vacuum polarization contribution to the AMM [17] yields a value $a_\mu^{\rm SM}$ which deviates with respect to the experimental determination $a_\mu^{\rm exp}$ [3] by $\sim 3.6\,\sigma$, i.e.

$$\Delta a_\mu \equiv a_\mu^{\rm exp} - a_\mu^{\rm SM} = (2.74 \pm 0.76) \times 10^{-9}. \tag{1.2}$$

There are a number of proposals aiming to explain the experimental value of the AMM of the muon by means of new BSM physics. Many of these proposal invoke physics unrelated to the solution of the hierarchy problem, as introducing Z' gauge bosons, extra fermions, scalars, vectors, or lepto-quarks. For some recent papers see refs. [18–23] and references therein. There are also a number of explanations of the AMM of the muon in the context of supersymmetric theories, which essentially select the space of supersymmetric parameters such that there can be enhanced contributions to Δa_μ. For a review of supersymmetric contributions to Δa_μ see ref. [24].

In this work we will consider a possible explanation of the AMM of the muon, in the context of theories solving the hierarchy problem by means of a warped extra dimension. We will do that in soft-wall metric models, where the SM fields can propagate in the bulk of the extra dimensions without invoking an extra gauge custodial symmetry, as described

[1] In particular theories with a warped extra dimension are dual to theories with a strongly coupled sector and a composite Higgs, which are by themselves theories solving the hierarchy problem as, at the compositeness scale, the Higgs melts into its components.

JHEP05(2017)016

in refs. [5–14]. As these theories can accommodate the fermion flavor problem of the SM, by means of particular values of the parameters localizing the fermions along the extra dimension, we will adopt the particular configuration of these parameters which provide a natural solution to the LHCb anomaly, as done in ref. [15]. This configuration will settle a starting point for analyzing the AMM of the muon. The outline of the rest of this paper will be as follows.

In section 2 we introduce the model of warped extra dimension we will be using throughout this paper. We show the consistency of the model with the main electroweak constraints, in particular the oblique observables and the $Z\bar{\mu}\mu$ coupling. We also show how the model can accommodate the LHCb anomalies, which motivates the choice of the localizing (compositeness) parameters in the muon sector which will be used in the rest of the paper. Finally we show that the minimal version of the model is unable to explain the AMM of the muon, which motivates the introduction of vector-like leptons (VLL) with a Yukawa mixing to the muon sector. The formalism of VLL propagating in the bulk of the extra dimension, and their boundary conditions, is covered in section 3. We show that masses $\gtrsim 1\,\text{TeV}$ imply fermions localized toward the IR brane, i.e. fermions with a certain degree of compositeness in the dual theory. The gauge interactions of VLL with the gauge boson Z and the Kaluza-Klein (KK)-modes Z_n, γ_n are studied in section 4. In particular the couplings of VLL with the KK-modes are very strong in the deep IR (for VLL localized toward the IR brane) while they are very week for VLL localized toward the UV brane. The former behavior will partly determine the posterior explanation of the AMM of the muon. The mixing of VLL with the muon through Yukawa interactions will be studied in section 5. In particular the physical mass eigenstates will be found by diagonalization of the mixed VLL-muon mass matrix, through some unitary matrices $U_{L,R}$, providing some mixing angles between the sector of VLL and that of the muon. The gauge couplings studied in section 4 will be then modified by the presence of the mixing in the matrices $U_{L,R}$. As the mixing between VLL and the muon sector must be small as implied by electroweak constraints, the corresponding entries in the matrices $U_{L,R}$ must be small which allows an explicit analytical approximation for $U_{L,R}$ as performed in section 6. This analytical approximation will simplify all couplings and will allow a much simpler treatment and understanding of further calculations in this paper. Moreover as electroweak constraints in the muon sector are very strong the accuracy of our analytical approximation will show up to be an extremely efficient one. A further simplification (this time a purely instrumental one) will be done in section 7, where we will impose a simplifying assumption: the localization parameters of doublet (c_L) and singlet (c_R) VLL are equal ($c_L = c_R \equiv c$). This assumption reduces the number of free parameters and allows a simplification of the matrices $U_{L,R}$. Using this particular case we will study the five-dimensional (5D) Yukawa couplings and found to lie in the perturbative region. In section 8 we single out the strongest electroweak constraint: the $Z\bar{\mu}\mu$ coupling, which gets modified by the mixing of the muon with VLL. We have proven that it constrains the absolute value of the off-diagonal elements of the unitary matrices U_L^{31} and U_R^{21} to be $\lesssim 0.02$, which justifies *a posteriori* the approximation done in section 6. Using the previous constraints we have computed in section 9 the contribution of VLL and the vectors Z, W, Z_n, γ_n, W_n, and the Higgs H, fields to the AMM of

JHEP05(2017)016

the muon. We have shown the region in the parameter space where the value of the AMM can be in agreement with the experimental result of eq. (1.2). In particular we have proven that the agreement implies that VLL have a high degree of compositeness, i.e. that they are localized toward the IR brane (in particular that $c \lesssim 0.42$). The rest of constraints (except for the $Z\bar{\mu}\mu$ constraint) are analyzed in section 10. We study constraints from oblique observables, from LHC data on the $H \to \gamma\gamma$ decay when VLL run inside the loop, from the stability of the electroweak minimum as VLL accelerate the running of the Higgs quartic coupling towards negative values, and finally from collider phenomenology as the VLL can be pair produced by Drell-Yan processes at hadron colliders. All these constraints reduce the size of the region allowed by VLL and leave a permitted region where $c \lesssim 0.37$ and the mass of VLL is $\gtrsim 270\,\text{GeV}$. Finally our conclusions, and some comments about possible extensions of this work, are drawn in section 11.

2 The model

We will review in this section the main aspects of the 5D warped model proposed and developed in refs. [5–14]. We assume the Higgs doublet to be a 5D field, so that it propagates in the bulk. Splitting the degrees of freedom into Goldstone modes $\chi(x,y)$, vacuum expectation (background) value $h(y)$ and physical fluctuations $\xi(x,y)$ we can rewrite the Higgs field as

$$H(x,y) = e^{i\chi(x,y)} \begin{pmatrix} 0 \\ h(y) + \frac{1}{\sqrt{2}}\xi(x,y) \end{pmatrix}. \tag{2.1}$$

Electroweak symmetry breaking (EWSB) is triggered by an IR brane potential, whereas additional mass terms are introduced for the Higgs in the bulk and at the UV brane. The full Higgs potential is then

$$V(H) = M^2(\phi)|H|^2 + M_0|H|^2\delta(y) + \left(-M_1|H|^2 + \gamma|H|^4\right)\delta(y-y_1)\,, \tag{2.2}$$

with

$$M^2(\phi) = \alpha k\left[\alpha k - \frac{2}{3}W(\phi)\right]. \tag{2.3}$$

where ϕ is the 5D bulk propagating field which stabilizes the size of the extra dimension at the value $y = y_1$, k a parameter with mass dimension related to the curvature along the fifth dimension [5], and $W(\phi)$ the superpotential which fixes the gravitational background metric $A(y)$ such that

$$ds^2 = e^{-2A(y)}\eta_{\mu\nu}dx^\mu dx^\nu + dy^2\,. \tag{2.4}$$

The dimensionless parameter α controls the localization of the Higgs wavefunction and can thus be connected to the amount of tuning related to the hierarchy problem.[2] The Higgs background $h(y)$ has the required exponential shape

$$h(y) = h_0 e^{\alpha k y} \tag{2.5}$$

[2] In fact solving the whole hierarchy problem amounts to fixing $A(y_1) \simeq 35$.

JHEP05(2017)016

and it can be easily checked that the fine-tuning is avoided for large enough values of α, i.e.

$$\alpha \gtrsim \alpha_1 = \frac{2A_1}{ky_1}\,, \tag{2.6}$$

where $A_1 \equiv A(y_1)$, which correspond to localizing the Higgs background profile towards the IR brane.

The SM fermions are realized in our scenario as chiral zero modes of 5D fermions. The localization of the different fermions is determined by their 5D (Dirac) mass term. The mass term for the 5D fermions can be conveniently chosen as $M_{f_{L,R}}(y) = \mp c_{f_{L,R}} W(\phi)/6$ where the upper (lower) sign applies for fields with left-handed (right-handed) zero modes [11].

In this paper we will primarily focus in the leptonic sector and, in particular, in the second generation of leptons. We will introduce the notation for the 5D leptons as

$$\begin{pmatrix} \nu_i \\ \ell_i \end{pmatrix}, \quad E_i \tag{2.7}$$

where i is a generation index, the doublets have hypercharge $Y = -1/2$ and the singlets hypercharge $Y = -1$. In the following we will just consider the second lepton generation ($i = 2$) and will drop the generation index. We will impose boundary conditions such that the zero mode of ℓ has only left-handed chirality ℓ_L and the zero mode of E only right-handed chirality E_R, where the contribution from the zero-modes is

$$\ell_L(x,y)_L = \ell_L(y)\mu_L(x) + \cdots\,, \quad E_R(x,y) = E_R(y)\mu_R(x) + \cdots \tag{2.8}$$

and the ellipses indicate the contribution from the non-zero KK-modes The 5D wave functions for the zero modes are given by

$$\ell_L(y) = \frac{e^{(2-c_{\mu_L})A(y)}}{\left(\int dy\, e^{A(1-2c_{\mu_L})}\right)^{1/2}}, \quad E_R(y) = \frac{e^{(2-c_{\mu_R})A(y)}}{\left(\int dy\, e^{A(1-2c_{\mu_R})}\right)^{1/2}} \tag{2.9}$$

where c_{μ_L} provides the 5D Dirac mass of the doublet and c_{μ_R} that of the singlet.

In this paper we will use the superpotential formalism [25] and consider the 5D gravitational background $A(y)$ determined by the superpotential [14]

$$W(\phi) = 6k\left(1 + e^{a_0\phi}\right)^{b_0} \tag{2.10}$$

where a_0 and b_0 are real dimensionless parameters. This model has been analyzed thoroughly for different values of the superpotential parameters in refs. [14, 26]. The main feature of this kind of gravitational (soft-wall) models is that the 5D metric has a naked singularity [5] outside (but near) the physical interval and their prediction for electroweak observables is greatly suppressed with respect to that of the AdS_5 case [6], as we will now review.

JHEP05(2017)016

2.1 Oblique corrections from KK-modes

The S and T parameters, contributing to oblique electroweak observables, are given by the general expressions [27]

$$S = -16\pi\Pi'_{3Y}(0), \quad T = \frac{4\pi}{s_W^2 c_W^2}\left[\Pi_{11}(0) - \Pi_{33}(0)\right]. \tag{2.11}$$

Their contribution from the gauge KK modes was already considered in refs. [14]. They are given by the following expressions [7]

$$\begin{aligned}
\alpha_{EM}\Delta T &= s_W^2 \frac{m_Z^2}{\rho^2} k^2 y_1 \int_0^{y_1} \left[1 - \Omega_h(y)\right]^2 e^{2A(y)-2A_1} dy\,, \\
\alpha_{EM}\Delta S &= 8 c_W^2 s_W^2 \frac{m_Z^2}{\rho^2} k^2 y_1 \int_0^{y_1} \left(1 - \frac{y}{y_1}\right)\left[1 - \Omega_h(y)\right] e^{2A(y)-2A_1} dy\,, \\
\alpha_{EM}\Delta U &\simeq 0\,,
\end{aligned} \tag{2.12}$$

where $\rho \equiv k e^{-A(y_1)}$ and

$$\Omega_h(y) = \frac{\omega(y)}{\omega(y_1)}, \quad \omega(y) = \int_0^y h^2(\bar{y}) e^{-2A(\bar{y})} d\bar{y}\,. \tag{2.13}$$

These expressions include the leading contributions, which are due to the tree-level mixing of the SM gauge bosons with the massive vector KK modes.

We show in figure 1 the KK contribution to the oblique parameters, for $m_{KK} = 2\,\text{TeV}$ (where m_{KK} is the mass of the first KK mode of gauge bosons in the absence of electroweak breaking) and $b_0 = 1.5$, as a function of a_0.[3] In particular we can see from figure 1 that for values $a_0 \simeq 0.2$, their contribution is tiny: $\Delta S \simeq 0.0257$, $\Delta T \simeq 0.0244$. Therefore this small contribution, and possibly other kind of new physics contributing to the parameters ΔS and ΔT, as we will see in the next section, leaves room to accommodate the experimental values [16]:

$$S = 0.07 \pm 0.08, \quad T = 0.1 \pm 0.07, \quad (91\%\ \text{correlation})\,. \tag{2.14}$$

In this paper we will then consider, from now on, the particular set of 'gravitational' parameters given by:

$$a_0 = 0.2,\ b_0 = 1.5,\ \alpha = \alpha_1,\ A_1 = 35,\ m_{KK} = 2\,\text{TeV}. \tag{2.15}$$

2.2 $\delta g_{Z\bar{\mu}\mu}$ from KK-modes

As the new physics considered in this paper concerns the muon sector, an obvious strong effect is on modifications of the coupling of the Z gauge boson with the physical muon. The main correction in this theory to $\delta g_{\mu_{L,R}}/g_{\mu_{L,R}}$ comes from the mixing of the Z gauge boson with its KK-modes and from the mixing of the muon zero mode with its KK modes. The resulting effect can be written as [11]

$$\delta g_{\mu_{L,R}} = -g^{\text{SM}}_{\mu_{L,R}} m_Z^2 \widehat{\alpha}_{\mu_{L,R}} \pm \frac{g}{c_W}\frac{v^2}{2}\widehat{\beta}_{\mu_{L,R}}\,, \tag{2.16}$$

[3] For other values of m_{KK} and the parameter b_0 see ref. [14].

JHEP05(2017)016

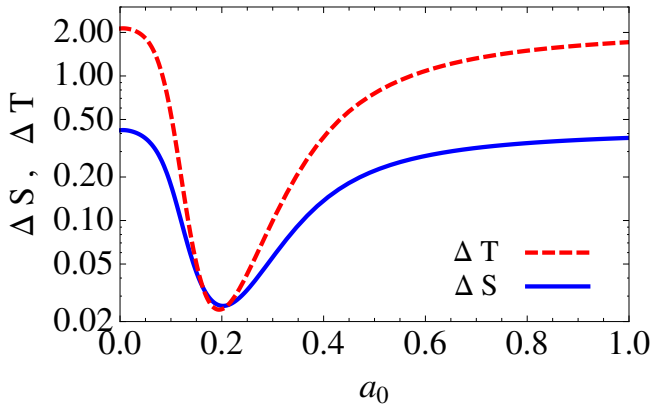

Figure 1. Contribution to the S and T parameters from the gauge KK modes as a function of a_0. We have considered $b_0 = 1.5$ and $m_{KK} = 2\,\text{TeV}$.

where

$$\widehat{\alpha}_{\mu_{L,R}} = y_1 \int_0^{y_1} e^{2A} \left(\Omega_h - \frac{y}{y_1}\right) \left(\Omega_{\mu_{L,R}} - 1\right) dy\,,$$
$$\widehat{\beta}_{\mu_{L,R}} = Y_\mu^2 \int_0^{y_1} e^{2A} \left(\frac{d\Omega_{\mu_{R,L}}}{dy}\right)^{-1} \left(\Gamma_\mu - \Omega_{\mu_{R,L}}\right)^2 dy\,, \tag{2.17}$$

with Y_μ the muon Yukawa coupling and

$$\Omega_{\mu_{L,R}} = \frac{\int_0^y e^{(1-2c_{\mu_{L,R}})A} dy}{\int_0^{y_1} e^{(1-2c_{\mu_{L,R}})A} dy}\,, \qquad \Gamma_\mu = \frac{\int_0^y h e^{-(c_{\mu_L}+c_{\mu_R})A} dy}{\int_0^{y_1} h e^{-(c_{\mu_L}+c_{\mu_R})A} dy}\,. \tag{2.18}$$

It is easy to recognize that the two terms in eq. (2.16) correspond, respectively, to the effects of the massive vectors and of the fermion KK modes.

For the metric we are considering in this paper with $a_0 = 0.2$ and $b_0 = 1.5$, and for the KK gauge bosons with mass $m_{KK} = 2\,\text{TeV}$, the values we obtain for $\delta g_{\mu_{L,R}}/g_{\mu_{L,R}}$ are shown in the plot of figure 2. We can see that for $c_{\mu_R} \gtrsim 0.5$, the experimental constraint $|\delta g_{\mu_{L,R}}/g_{\mu_{L,R}}| \lesssim 10^{-3}$ [16] imposes $c_{\mu_L} \gtrsim 0.4$. In the rest of this paper we will fix $c_{\mu_L} = 0.4$, a value consistent with the LHCb anomaly as we will see in the following.

2.3 The $B \to K^* \mu^+ \mu^-$ anomaly from KK-modes

We have recently shown that this theory can naturally accommodate the LHCb anomaly if the muon has a certain degree of compositeness [15, 28]. In fact the contribution to the Wilson coefficient of the relevant $\Delta F = 1$ operator $\mathcal{O}_9 = (\bar{s}_L \gamma_\mu b_L)(\bar{\mu}\gamma^\mu \mu)$ can be written as

$$\Delta C_9 = -\sum_{X=Z,\gamma} \sum_n \frac{\sqrt{2}\pi g_{\mu_V}^{X_n} (g_{b_L}^{X_n} - g_{s_L}^{X_n})}{G_F \alpha M_n^2} \tag{2.19}$$

where the fitted values from experimental data are $\Delta C_9 \in [-1.67, -0.39]$ [29–31]. The couplings $g_{\mu_V}^{X_n}$, $g_{b_L}^{X_n}$ and $g_{s_L}^{X_n}$ are provided by the overlapping of the wave functions of the

JHEP05(2017)016

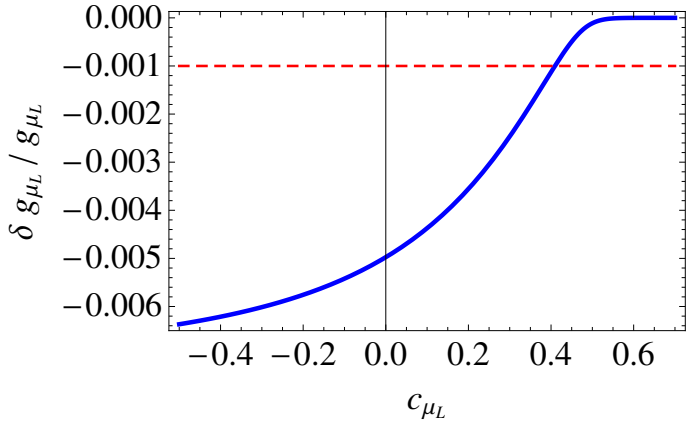

Figure 2. Contribution to $\delta g_{\mu_L}/g_{\mu_L}$ from KK modes. The horizontal dashed line corresponds to $|\delta g_{\mu_L}/g_{\mu_L}| = 10^{-3}$. We have considered $c_{\mu_R} = 0.5$.

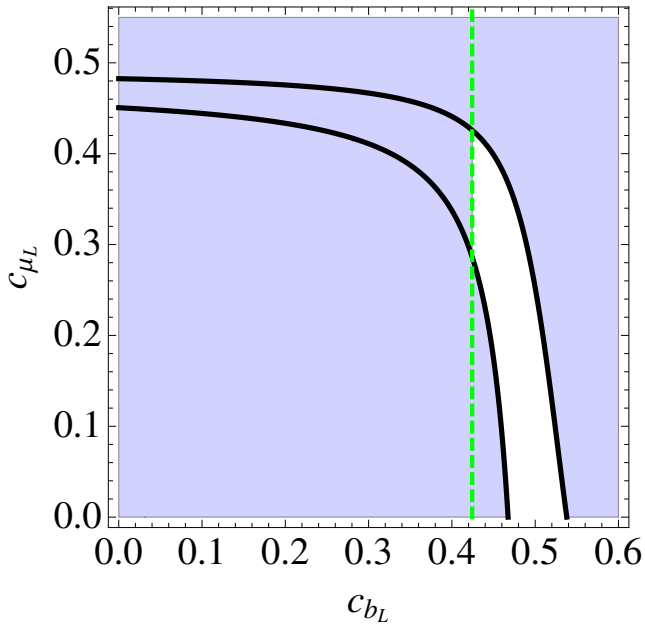

Figure 3. Region in the plane (c_{b_L}, c_{μ_L}) that accommodates $\Delta C_9 \in [-1.67, -0.39]$. We have also indicated the bound (vertical line) from flavor physics in the botton sector corresponding to $c_{b_L} > 0.424$ (see refs. [15, 28] for further details). We have considered $c_{\mu_R} = 0.5$, $c_{s_L} = 0.6$.

corresponding fermion and the KK-gauge bosons. For the calculation of $g^X_{b_L}$ we choose $c_{b_L} = 0.44$ (a value passing all the constrains in ref. [15]). Moreover for the values that we will consider in the present paper, $c_{\mu_L} = 0.4$ and $c_{\mu_R} = 0.5$, we obtain a value $\Delta C_9 = -0.464$ which is consistent with an explanation of the LHCb anomaly and passes all the precision tests from ref. [15]. We show in figure 3 the parameter space region in the (c_{b_L}, c_{μ_L}) plane that allows to fit the flavor anomalies.

JHEP05(2017)016

2.4 Δa_μ from muon KK-modes

The theory described in section 2 provides a framework where the (minimal) Standard Model propagates in the warped extra dimension thus solving the Higgs hierarchy problem, consistently with all electroweak precision data, and providing a solution to the quark and lepton flavor problem by fermion localization in the extra dimension, consistently with flavor data [11]. Moreover, as was shown in the previous section and in ref. [15], the theory could accommodate some of the recently observed flavor anomalies, in particular the $B \to K^* \mu^+ \mu^-$ anomaly.

The other anomaly in the muon sector, as explained in section 1, is the experimental value of the muon anomalous magnetic moment a_μ. The exchange of muon KK-modes along with Z and γ KK-modes, in diagrams similar to those of figure 8 (with obvious modifications), should be good candidates to explain the experimental value required for Δa_μ. However because of the structure of the 5D muon sector in eqs. (2.8) and (2.9) the chirality flip in the triangular diagram contributing to Δa_μ is suppressed by an $\mathcal{O}(m_\mu/m_{KK})$ factor leading to a too small effect unable to cope with the experimental result.[4] There are in the literature similar scenarios in Randall-Sundrum models that are unable to accommodate the experimental value of Δa_μ by at least one order of magnitude, see e.g. [32, 33].

As a consequence, the theory we are considering has to be enlarged to reproduce the experimental value of the muon anomalous magnetic moment. We will provide, in the rest of this paper, an extra sector, containing vector like leptons propagating in the bulk of the extra dimension, which mix with the muon sector through Yukawa interactions, providing the required sizable chirality flip in Δa_μ. As we will see next, the required mixing is consistent with all present experimental and theoretical constraints in the very sensitive muon sector.

3 Vector like leptons

We will now introduce vector-like leptons

$$D(x,y) = \begin{pmatrix} N(x,y) \\ L(x,y) \end{pmatrix}_{-1/2}, \quad R(x,y)_{-1} \tag{3.1}$$

transforming as a doublet and a singlet under $\mathrm{SU}(2)_L$, respectively, and with the same hypercharge as the SM leptons. We will give them 5D Dirac masses $M_{L,R}(y)$ depending on the constants c_L and c_R, and boundary conditions such that the zero modes are four-dimensional (4D) Dirac spinors with mass eigenvalues $M_{\mathcal{L}}(c_L)$ and $M_{\mathcal{R}}(c_R)$, respectively.

In order to figure out what are the boundary conditions (BC) that we need to impose to generate $M_{\mathcal{L},\mathcal{R}} \neq 0$, we write the zero modes decomposition as

$$\begin{aligned} &N_{L,R}(x,y) = N_{L,R}(y)\mathcal{N}_{L,R}(x), \quad L_{L,R}(x,y) = L_{L,R}(y)\mathcal{L}_{L,R}(x) \\ &R_{L,R}(x,y) = R_{L,R}(y)\mathcal{R}_{L,R}(x) \end{aligned} \tag{3.2}$$

[4] We thank Giuliano Panico for a discussion on this point.

JHEP05(2017)016

where the wave functions are normalized such that

$$\int e^{-3A} L_{L,R}^2(y) dy = \int e^{-3A} R_{L,R}^2(y) dy = 1\,, \tag{3.3}$$

and $N_{L,R}(y) \equiv L_{L,R}(y)$ from the $\mathrm{SU}(2)_L$ invariance. Defining the new functions

$$\widehat{L}_{L,R}(y) = e^{-2A} L_{L,R}(y), \quad \widehat{R}_{L,R}(y) = e^{-2A} R_{L,R}(y), \tag{3.4}$$

the Dirac equations for $\widehat{L}_{L,R}$ and $\widehat{R}_{L,R}$ are written as

$$\begin{aligned} M_{\mathcal{L}} e^{A} \widehat{L}_{R,L}(y) &= (M_L(y) \mp \partial_y) \widehat{L}_{L,R}(y), \\ M_{\mathcal{R}} e^{A} \widehat{R}_{R,L}(y) &= (M_R(y) \mp \partial_y) \widehat{R}_{L,R}(y). \end{aligned} \tag{3.5}$$

Imposing the BC as[5]

$$\begin{aligned} (M_L + \partial_y) \widehat{L}_L|_{y=0} = 0, \qquad & \widehat{L}_L|_{y=y_1} = 0, \\ \widehat{L}_R|_{y=0} = 0, \quad & (M_L - \partial_y) \widehat{L}_R|_{y=y_1} = 0, \end{aligned} \tag{3.6}$$

and similarly

$$\begin{aligned} (M_R + \partial_y) \widehat{R}_L|_{y=0} = 0, \qquad & \widehat{R}_L|_{y=y_1} = 0, \\ \widehat{R}_R|_{y=0} = 0, \quad & (M_R - \partial_y) \widehat{R}_R|_{y=y_1} = 0. \end{aligned} \tag{3.7}$$

it is easy to see that $M_{\mathcal{L},\mathcal{R}} \neq 0$. The proof goes as follows: assuming $M_{\mathcal{L}} = 0$, then from (3.5) we would have the solution

$$\widehat{L}_{L,R}(y) = \widehat{n}_{L,R} e^{\pm \int^y M_L dy}, \tag{3.8}$$

where $\widehat{n}_{L,R}$ are constants determined by (3.6). The BC $(M_L + \partial_y)\widehat{L}_L|_{y=0} = 0$ and $(M_L - \partial_y)\widehat{L}_R|_{y=y_1} = 0$ are automatically satisfied by the Dirac equation (3.5), while the BC $\widehat{L}_L|_{y=y_1} = 0$, $\widehat{L}_R|_{y=0} = 0$ result in $\widehat{n}_{L,R} = 0$. Thus, imposing BC such as (3.6) necessarily guarantees $M_{\mathcal{L}} \neq 0$ for non-trivial solutions ($\widehat{L}_{L,R}(y) \neq 0$). In the same way imposing the BC (3.7) we have $M_{\mathcal{R}} \neq 0$. In this work we conveniently choose $M_{L,R}(y) = -c_{L,R} W(\phi)/6$ that results in a continuous spectrum for the 4D zero modes as we can see in figure 4.

4 Gauge interactions

In this section we will describe the gauge interactions of the charged $[\mathcal{L}(x),\ \mathcal{R}(x)]$ and neutral $[\mathcal{N}(x)]$ components of the VLL with zero and non-zero KK modes of gauge bosons.

[5] We thank O. Pujolas for discussions on this point.

JHEP05(2017)016

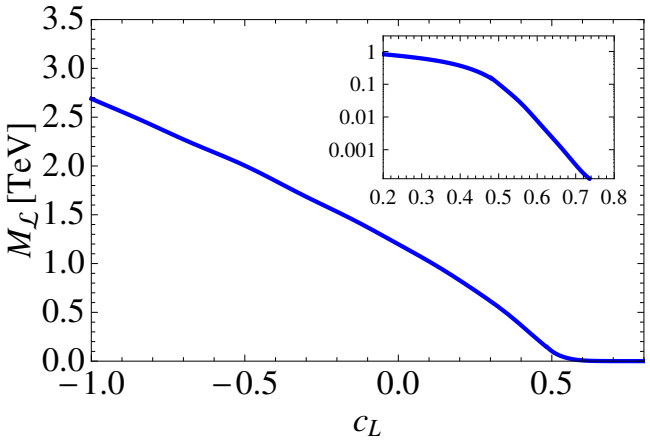

Figure 4. VLL mass $M_{\mathcal{L}}$ as a function of the parameter c_L. The inserted figure corresponds to a logarithmic plot in the regime in which $M_{\mathcal{L}}$ is small. The same plot would apply of course for $M_{\mathcal{R}}$ as a function of c_R.

Neutral currents. Before EWSB the Lagrangian describing the interactions of the charged leptons $\mu_L(x), \mu_R(x)$ and the charged VLL zero modes in the doublet $\mathcal{L}_{L,R}(x)$ and the singlet $R_{L,R}(x,y)$ $(\mu(x), \mathcal{L}(x), \mathcal{R}(x))$ with the Z gauge boson and the KK modes of the gauge bosons (Z_n, γ_n), with $n \geq 1$, is given by

$$\begin{aligned}\mathcal{L} = \sum_{X=Z,Z_n,\gamma_n} \mathcal{L}_X, \quad \mathcal{L}_X = X_\mu \left(\bar{\mu}_L(x)\ \bar{\mathcal{L}}_L(x)\ \bar{\mathcal{R}}_L(x)\right) \gamma^\mu G_L^X \begin{pmatrix} \mu_L(x) \\ \mathcal{L}_L(x) \\ \mathcal{R}_L(x) \end{pmatrix} \\ + X_\mu \left(\bar{\mu}_R(x)\ \bar{\mathcal{L}}_R(x)\ \bar{\mathcal{R}}_R(x)\right) \gamma^\mu G_R^X \begin{pmatrix} \mu_R(x) \\ \mathcal{L}_R(x) \\ \mathcal{R}_R(x) \end{pmatrix}\end{aligned} \tag{4.1}$$

where the coupling matrices $G_{L,R}^X$ are diagonal but not proportional to the identity

$$G_{L,R}^X = \begin{pmatrix} g^X_{\mu_{L,R}} & 0 & 0 \\ 0 & g^X_{\mathcal{L}_{L,R}} & 0 \\ 0 & 0 & g^X_{\mathcal{R}_{L,R}} \end{pmatrix} \tag{4.2}$$

and we will restrict ourselves to the lightest mode $n = 1$, although the generalization to higher KK modes is trivial. The couplings in (4.2) are given by

$$\begin{aligned} g^Z_{f_2} &= \frac{1}{c_W}\left(-\frac{1}{2} + s_W^2\right) g f^Z_{f_2}, \quad && f_2 = \mu_L, \mathcal{L}_{L,R} \\ g^{Z_n}_{f_1} &= \frac{s_W^2}{c_W} g f^{Z_n}_{f_1}, && f_1 = \mu_R, \mathcal{R}_{L,R} \\ g^{\gamma_n}_{f_{1,2}} &= -s_W g f^{\gamma_n}_{f_{1,2}} \end{aligned} \tag{4.3}$$

JHEP05(2017)016

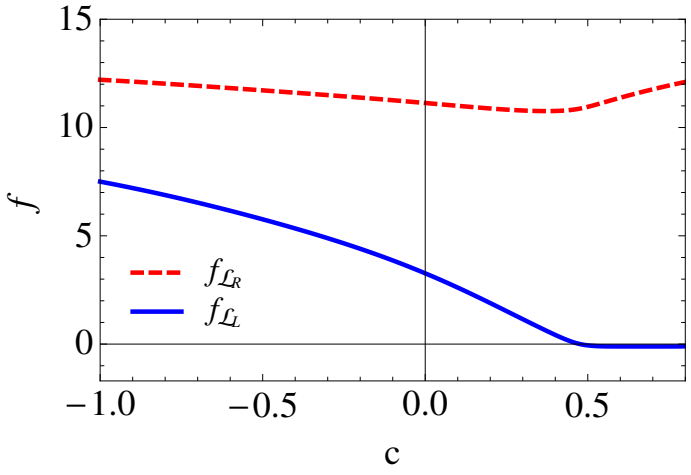

Figure 5. Coupling of Z_1, γ_1 with VLL as a function of $c = c_{L,R}$.

where $f^X_{f_{L,R}}$ is defined for $f = \mu, \mathcal{L}, \mathcal{R}$ as

$$f^X_{f_{L,R}} = \frac{\sqrt{y_1}\int e^{-3A} f_X(y) f^2_{L,R}(y)}{\left[\int f^2_X(y)\right]^{1/2} \int e^{-3A} f^2_{L,R}(y)} \quad (X = Z_n, \gamma_n), \quad f^Z_{f_{L,R}} = 1 \tag{4.4}$$

with $f_L(y) = \ell_L(y), L_L(y), R_L(y)$ and $f_R(y) = E_R(y), L_R(y), R_R(y)$. We show in figure 5 the profile of $f^{Z_1,\gamma_1}_{\mathcal{L}_L}$ and $f^{Z_1,\gamma_1}_{\mathcal{L}_R}$ defined in eq. (4.4).

Charged currents. The interaction Lagrangian of the neutral leptons $\mathcal{N}_{L,R}(x)$ with the charged leptons $\mathcal{L}_{L,R}(x)$ and the W-gauge boson and its KK excitations is given by

$$\mathcal{L}_W = \sum_{n\geq 0} W^\mu_n(x) \left(g^{W_n}_{\mathcal{N}_L} \bar{\mathcal{N}}_L(x) \gamma_\mu \mathcal{L}_L(x) + g^{W_n}_{\mathcal{N}_R} \bar{\mathcal{N}}_R(x) \gamma_\mu \mathcal{L}_R(x) \right) + \text{h.c.} \tag{4.5}$$

where

$$g^{W_0}_{\mathcal{N}_{L,R}} = \frac{g}{\sqrt{2}}, \quad g^{W_n}_{\mathcal{N}_{L,R}} = \frac{g}{\sqrt{2}} f^W_{\mathcal{N}_{L,R}} \quad (n \geq 1) \tag{4.6}$$

and

$$f^W_{\mathcal{N}_{L,R}} = \frac{\sqrt{y_1}\int e^{-3A} f_W(y) L_{L,R}(y) N_{L,R}(y)}{\left[\int f^2_W(y)\right]^{1/2} \int e^{-3A} L_{L,R}(y) N_{L,R}(y)} \,. \tag{4.7}$$

Notice that by neglecting the tiny effect of electroweak symmetry breaking, $f_{W_n}(y) = f_{Z_n,\gamma_n}(y)$, an approximation already used in the neutral current interaction.

JHEP05(2017)016

5 Yukawa interactions

We will now introduce the 5D Yukawa couplings as[6]

$$e^{4A}\mathcal{L}_Y = h(y)\left(\widehat{Y}_{\ell E}\bar{\ell}_L(x,y)E_R(x,y) + \widehat{Y}_{\ell R}\bar{\ell}_L(x,y)R_R(x,y)\right. \\ \left. + \widehat{Y}_{LE}\bar{L}_L(x,y)E_R(x,y) + \widehat{Y}_{LR}(\bar{L}_L(x,y)R_R(x,y) + \bar{R}_L(x,y)L_R(x,y))\right) + \text{h.c.} \tag{5.1}$$

where the $\widehat{Y}s$ are 5D Yukawa couplings with mass dimension $-1/2$.

By expanding the 5D fermions in the KK components and keeping the zero modes, we get the 4D fermion mass matrix

$$\mathcal{L}_m = \left(\bar{\mu}_L(x)\ \bar{\mathcal{L}}_L(x)\ \bar{\mathcal{R}}_L(x)\right)\cdot\mathcal{M}\cdot\begin{pmatrix}\mu_R(x)\\ \mathcal{L}_R(x)\\ \mathcal{R}_R(x)\end{pmatrix} + \text{h.c.} \tag{5.2}$$

where

$$\mathcal{M} = \begin{pmatrix} c_{\ell E} & 0 & c_{\ell R}\\ c_{LE} & M_{\mathcal{L}} & c_{LR}\\ 0 & c_{RL} & M_{\mathcal{R}}\end{pmatrix} \tag{5.3}$$

with entries given by

$$c_{JK} = \widehat{Y}_{JK}v\frac{\displaystyle\int e^{\alpha k y - 4A}J_L(y)K_R(y)dy}{\left[\displaystyle\int e^{2\alpha k y - 2A}\int e^{-3A}J_L^2(y)\int e^{-3A}K_R^2(y)\right]^{1/2}}\,, \tag{5.4}$$

for $J = \ell, L, R$ and $K = E, L, R$ with $\widehat{Y}_{RL} \equiv \widehat{Y}_{LR}$, and $v = 174\,\text{GeV}$.

We can now go to the mass eigenstate basis $(\mu, \mathcal{L}, \mathcal{R}) \to (\widetilde{\mu}, \widetilde{\mathcal{L}}, \widetilde{\mathcal{R}})$ defined as

$$\begin{pmatrix}\mu_{L,R}(x)\\ \mathcal{L}_{L,R}(x)\\ \mathcal{R}_{L,R}(x)\end{pmatrix} = U_{L,R}\begin{pmatrix}\widetilde{\mu}_{L,R}(x)\\ \widetilde{\mathcal{L}}_{L,R}(x)\\ \widetilde{\mathcal{R}}_{L,R}(x)\end{pmatrix}, \tag{5.5}$$

where U_L (U_R) is the unitary transformation that diagonalizes $\mathcal{M}\mathcal{M}^\dagger$ ($\mathcal{M}^\dagger\mathcal{M}$), such that the diagonalized mass matrix reads as

$$U_L^\dagger\mathcal{M}U_R \equiv \text{diag}(m_\mu, M_{\widetilde{\mathcal{L}}}, M_{\widetilde{\mathcal{R}}})\,. \tag{5.6}$$

In the same way the interaction of the fermions with the 4D Higgs field $H(x)$ can be written as[7]

$$\mathcal{L}_{Hff} = H(x)\left(\bar{\widetilde{\mu}}_L(x)\ \bar{\widetilde{\mathcal{L}}}_L(x)\ \bar{\widetilde{\mathcal{R}}}_L(x)\right)\frac{Y}{\sqrt{2}}\begin{pmatrix}\widetilde{\mu}_R(x)\\ \widetilde{\mathcal{L}}_R(x)\\ \widetilde{\mathcal{R}}_R(x)\end{pmatrix} + \text{h.c.} \tag{5.7}$$

[6] We are assuming that VLL in eq. (3.1) have lepton number $L_\mu = 1$, so they can only mix through the Higgs with themselves and with the second generation leptons. Moreover the couplings between the VLL and the SM leptons could have been avoided by the simple introduction of a discrete symmetry, as in ref. [34], an assumption we are not doing in this paper. Had we introduced it, as we will see, we would have failed to encompass the experimental value of the muon AMM.

[7] In the limit $m_h \ll m_{KK}$ we used $\xi(x,y) = h(y)H(x)/v$.

JHEP05(2017)016

where the matrix of 4D Yukawa couplings Y is given by

$$Y = \frac{1}{v} U_L^\dagger \begin{pmatrix} c_{\ell E} & 0 & c_{\ell R} \\ c_{LE} & 0 & c_{LR} \\ 0 & c_{RL} & 0 \end{pmatrix} U_R. \tag{5.8}$$

Neutral currents. From eq. (4.1) the interactions of the Z gauge boson, and the KK bosons Z_n^μ, γ_n^μ, with the mass eigenstates can be written as

$$\begin{aligned} \mathcal{L} = \sum_{X=Z,Z_n,\gamma_n} \mathcal{L}_X, \quad \mathcal{L}_X = X_\mu \left(\bar{\widetilde{\mu}}_L(x) \; \bar{\widetilde{\mathcal{L}}}_L(x) \; \bar{\widetilde{\mathcal{R}}}_L(x) \right) \gamma^\mu U_L^\dagger G_L^X U_L \begin{pmatrix} \widetilde{\mu}_L(x) \\ \widetilde{\mathcal{L}}_L(x) \\ \widetilde{\mathcal{R}}_L(x) \end{pmatrix} \\ + X_\mu \left(\bar{\widetilde{\mu}}_R(x) \; \bar{\widetilde{\mathcal{L}}}_R(x) \; \bar{\widetilde{\mathcal{R}}}_R(x) \right) \gamma^\mu U_R^\dagger G_R^X U_R \begin{pmatrix} \widetilde{\mu}_R(x) \\ \widetilde{\mathcal{L}}_R(x) \\ \widetilde{\mathcal{R}}_R(x) \end{pmatrix} \end{aligned} \tag{5.9}$$

where the matrices $U_{L,R}^\dagger G_{L,R}^X U_{L,R}$ create a mixing between the muon and the VLL.

The interaction Lagrangian with mass eigenstates involving at least one light state, $\widetilde{\mu}_{L,R}$, then reads as

$$\begin{aligned} \mathcal{L}_X = X_\mu \Big(& g^X_{\widetilde{\mu}_L} \bar{\widetilde{\mu}}_L \gamma^\mu \widetilde{\mu}_L + g^X_{\widetilde{\mathcal{L}}_L} \bar{\widetilde{\mu}}_L \gamma^\mu \widetilde{\mathcal{L}}_L + g^X_{\widetilde{\mathcal{R}}_L} \bar{\widetilde{\mu}}_L \gamma^\mu \widetilde{\mathcal{R}}_L \\ & + g^X_{\widetilde{\mu}_R} \bar{\widetilde{\mu}}_R \gamma^\mu \widetilde{\mu}_R + g^X_{\widetilde{\mathcal{L}}_R} \bar{\widetilde{\mu}}_R \gamma^\mu \widetilde{\mathcal{L}}_R + g^X_{\widetilde{\mathcal{R}}_R} \bar{\widetilde{\mu}}_R \gamma^\mu \widetilde{\mathcal{R}}_R \Big) + \text{h.c.} \end{aligned} \tag{5.10}$$

where the couplings with mass eigenstates are then given by

$$\begin{aligned} g^X_{\widetilde{\mu}_L} &= g^X_{\mu_L} U_L^{11} U_L^{11} + g^X_{\mathcal{L}_L} U_L^{21} U_L^{21} + g^X_{\mathcal{R}_L} U_L^{31} U_L^{31} \\ g^X_{\widetilde{\mathcal{L}}_L} &= g^X_{\mu_L} U_L^{11} U_L^{12} + g^X_{\mathcal{L}_L} U_L^{21} U_L^{22} + g^X_{\mathcal{R}_L} U_L^{31} U_L^{32} \\ g^X_{\widetilde{\mathcal{R}}_L} &= g^X_{\mu_L} U_L^{11} U_L^{13} + g^X_{\mathcal{L}_L} U_L^{21} U_L^{23} + g^X_{\mathcal{R}_L} U_L^{31} U_L^{33} \\ g^X_{\widetilde{\mu}_R} &= g^X_{\mu_R} U_R^{11} U_R^{11} + g^X_{\mathcal{L}_R} U_R^{21} U_R^{21} + g^X_{\mathcal{R}_R} U_R^{31} U_R^{31} \\ g^X_{\widetilde{\mathcal{L}}_R} &= g^X_{\mu_R} U_R^{11} U_R^{12} + g^X_{\mathcal{L}_R} U_R^{21} U_R^{22} + g^X_{\mathcal{R}_R} U_R^{31} U_R^{32} \\ g^X_{\widetilde{\mathcal{R}}_R} &= g^X_{\mu_R} U_R^{11} U_R^{13} + g^X_{\mathcal{L}_R} U_R^{21} U_R^{23} + g^X_{\mathcal{R}_R} U_R^{31} U_R^{33} \end{aligned} \tag{5.11}$$

and the corresponding vector and axial couplings are $g_{V,A} = \frac{1}{2}(g_L \pm g_R)$.

Charged currents. From eq. (4.5) the interaction of the neutral lepton $\mathcal{N}(x)$ with the physical (mass eigenstate) muon $\widetilde{\mu}(x)$ is given by

$$\mathcal{L}_W = \sum_{n \geq 0} W_n^\mu(x) \left(g^{W_n}_{\widetilde{\mu}_L} \bar{\mathcal{N}}_L(x) \gamma_\mu \widetilde{\mu}_L(x) + g^{W_n}_{\widetilde{\mu}_R} \bar{\mathcal{N}}_R(x) \gamma_\mu \widetilde{\mu}_R(x) \right) + \text{h.c.} \tag{5.12}$$

where

$$g^{W_n}_{\widetilde{\mu}_{L,R}} = U^{21}_{L,R} g^{W_n}_{\mathcal{N}_{L,R}} \tag{5.13}$$

and the vector and axial couplings are given by

$$g^W_{V,A} = \frac{1}{2} \left(U_L^{21} g^W_{\mathcal{N}_L} \pm U_R^{21} g^W_{\mathcal{N}_R} \right), \quad \left(g_V^W\right)^2 - \left(g_A^W\right)^2 = U_L^{21} U_R^{21} g^W_{\mathcal{N}_L} g^W_{\mathcal{N}_R} \tag{5.14}$$

JHEP05(2017)016

6 Analytic expressions of $U_{L,R}$

If the entries $c_{\ell E}$, $c_{\ell R}$ and c_{LE} in the mass matrix (5.3) are much smaller than the other entries (as we will see in section 8 it happens in this theory), the mass matrix $\mathcal{M}$ can be expanded as follows:

$$\mathcal{M} = \mathcal{M}^0 + \delta M^0 \equiv \begin{pmatrix} 0 & 0 & 0 \\ 0 & M_{\mathcal{L}} & c_{LR} \\ 0 & c_{RL} & M_{\mathcal{R}} \end{pmatrix} + \begin{pmatrix} c_{\ell E} & 0 & c_{\ell R} \\ c_{LE} & 0 & 0 \\ 0 & 0 & 0 \end{pmatrix} \tag{6.1}$$

which will allow us to use a perturbative approach to find the matrices U_L,U_R that diagonalize, respectively, $\mathcal{M}\mathcal{M}^\dagger$ and $\mathcal{M}^\dagger\mathcal{M}$. The resulting diagonalization matrices, $U_{L,R}$, are then given, to first order in the small parameters, by

$$U_{L,R} = \begin{pmatrix} 1 & U^{12}_{L,R} & U^{13}_{L,R} \\ U^{21}_{L,R} & \cos\theta_{L,R} & \sin\theta_{L,R} \\ U^{31}_{L,R} & -\sin\theta_{L,R} & \cos\theta_{L,R} \end{pmatrix} \tag{6.2}$$

where

$$\begin{pmatrix} U^{21}_{L,R} \\ U^{31}_{L,R} \end{pmatrix} = -\begin{pmatrix} \cos\theta_{L,R} & \sin\theta_{L,R} \\ -\sin\theta_{L,R} & \cos\theta_{L,R} \end{pmatrix} \begin{pmatrix} U^{12}_{L,R} \\ U^{13}_{L,R} \end{pmatrix} \tag{6.3}$$

with

$$\begin{aligned} U^{12}_L &= \frac{(c_{LR}\cos\theta_L - M_R \sin\theta_L)}{M^2_{\widetilde{\mathcal{L}}}} c_{\ell R}, & U^{13}_L &= \frac{(c_{LR}\sin\theta_L + M_R \cos\theta_L)}{M^2_{\widetilde{\mathcal{R}}}} c_{\ell R} \\ U^{12}_R &= \frac{(M_L\cos\theta_R - c_{LR} \sin\theta_R)}{M^2_{\widetilde{\mathcal{L}}}} c_{LE}, & U^{13}_R &= \frac{(M_L\sin\theta_R + c_{LR} \cos\theta_R)}{M^2_{\widetilde{\mathcal{R}}}} c_{LE} \end{aligned} \tag{6.4}$$

and the angles $\theta_{L,R}$ are given by

$$\begin{aligned} \sin 2\theta_L &= \frac{2(c_{RL}M_{\mathcal{L}} + c_{LR}M_{\mathcal{R}})}{|M^2_{\widetilde{\mathcal{L}}} - M^2_{\widetilde{\mathcal{R}}}|} \\ \sin 2\theta_R &= \frac{2(c_{LR}M_{\mathcal{L}} + c_{RL}M_{\mathcal{R}})}{|M^2_{\widetilde{\mathcal{L}}} - M^2_{\widetilde{\mathcal{R}}}|}. \end{aligned} \tag{6.5}$$

In this approximation the mass eigenvalues are then given by

$$\begin{aligned} m_\mu &= c_{\ell E} + \frac{c_{\ell R} c_{LE}}{M_{\widetilde{\mathcal{L}}} M_{\widetilde{\mathcal{R}}}}\, c_{RL} \\ M^2_{\widetilde{\mathcal{L}},\widetilde{\mathcal{R}}} &= \frac{1}{2}\Bigg\{ M^2_{\mathcal{L}} + M^2_{\mathcal{R}} + c^2_{RL} + c^2_{LR} \\ &\qquad \mp \sqrt{\left((M_{\mathcal{L}} + M_{\mathcal{R}})^2 + (c_{LR} - c_{RL})^2\right)\left((M_{\mathcal{L}} - M_{\mathcal{R}})^2 + (c_{LR} + c_{RL})^2\right)} \Bigg\} \end{aligned} \tag{6.6}$$

JHEP05(2017)016

From eq. (5.11) the interactions of the Z gauge boson and the neutral KK bosons Z_n^μ, γ_n^μ with the mass eigenstates can be written as

$$\begin{aligned}
g^X_{\widetilde{\mu}_L} &= g^X_{\mu_L} + g^X_{\mathcal{L}_L} U^{21}_L U^{21}_L + g^X_{\mathcal{R}_L} U^{31}_L U^{31}_L \\
g^X_{\widetilde{\mu}_R} &= g^X_{\mu_R} + g^X_{\mathcal{L}_R} U^{21}_R U^{21}_R + g^X_{\mathcal{R}_R} U^{31}_R U^{31}_R \\
g^X_{\widetilde{\mathcal{L}}_L} &= \cos\theta_L (g^X_{\mathcal{L}_L} - g^X_{\mu_L}) U^{21}_L - \sin\theta_L (g^X_{\mathcal{R}_L} - g^X_{\mu_L}) U^{31}_L \\
g^X_{\widetilde{\mathcal{L}}_R} &= \cos\theta_R (g^X_{\mathcal{L}_R} - g^X_{\mu_R}) U^{21}_R - \sin\theta_R (g^X_{\mathcal{R}_R} - g^X_{\mu_R}) U^{31}_R \\
g^X_{\widetilde{\mathcal{R}}_L} &= \sin\theta_L (g^X_{\mathcal{L}_L} - g^X_{\mu_L}) U^{21}_L + \cos\theta_L (g^X_{\mathcal{R}_L} - g^X_{\mu_L}) U^{31}_L \\
g^X_{\widetilde{\mathcal{R}}_R} &= \sin\theta_R (g^X_{\mathcal{L}_R} - g^X_{\mu_R}) U^{21}_R + \cos\theta_R (g^X_{\mathcal{R}_R} - g^X_{\mu_R}) U^{31}_R .
\end{aligned} \tag{6.7}$$

Notice that

$$g^X_{\widetilde{\mu}_{L,R}} = g^X_{\mu_{L,R}} + \cdots$$

where the ellipsis denotes (subleading) terms which are quadratic in the small perturbations.

The interactions of the W gauge boson and the charged KK modes W_n with the mass eigenstates in terms of the elements of $U_{L,R}$ were already given in eq. (5.13).

7 The case $c_L = c_R \equiv c$

As we have seen in the previous sections the mass eigenvalues and mixing angles in the muon/VLL sector depend on the two real parameters c_L and c_R, which determine the localization along the extra dimension, respectively, of the doublet and singlet VLL. In this section we will consider the particularly simple case where $c_L = c_R \equiv c$.[8] In this case we will be able to write all the functions c_{JK} in term of the function c_{LR} and the parameter c. This will be achieved by setting values for the elements U^{31}_L, U^{21}_R in order to satisfy the experimental bounds for $\delta g^Z_{\mu_{L,R}}$, as we will see in eq. (8.3).

For $c_R = c_L$ we have $M_{\mathcal{L}}(c) = M_{\mathcal{R}}(c) \equiv M(c)$ and the 5D wave functions are related to each other as $N_{L,R}(y) = L_{L,R}(y) = R_{L,R}(y)$ resulting in

$$c_{LR} = c_{RL} \text{ and } \theta_L = \theta_R = \pi/4. \tag{7.1}$$

Equation (7.1) and the explicit form for the matrix $U_{L,R}$ enable us to write

$$\begin{aligned}
M_{\widetilde{\mathcal{L}}}(c, c_{LR}) &= M(c) - c_{LR} \\
M_{\widetilde{\mathcal{R}}}(c, c_{LR}) &= M(c) + c_{LR}
\end{aligned} \tag{7.2}$$

and

$$\begin{aligned}
c_{\ell E} &= m_\mu - 2\frac{M_{\widetilde{\mathcal{R}}} M_{\widetilde{\mathcal{L}}} (M_{\widetilde{\mathcal{R}}} - M_{\widetilde{\mathcal{L}}})}{(M_{\widetilde{\mathcal{R}}} + M_{\widetilde{\mathcal{L}}})^2} U^{31}_L U^{21}_R \\
c_{\ell R} &= -2\frac{M_{\widetilde{\mathcal{R}}} M_{\widetilde{\mathcal{L}}}}{M_{\widetilde{\mathcal{R}}} + M_{\widetilde{\mathcal{L}}}} U^{31}_L \\
c_{LE} &= -2\frac{M_{\widetilde{\mathcal{R}}} M_{\widetilde{\mathcal{L}}}}{M_{\widetilde{\mathcal{R}}} + M_{\widetilde{\mathcal{L}}}} U^{21}_R .
\end{aligned} \tag{7.3}$$

[8] The general case $c_L \neq c_R$ can be worked out straightforwardly.

JHEP05(2017)016

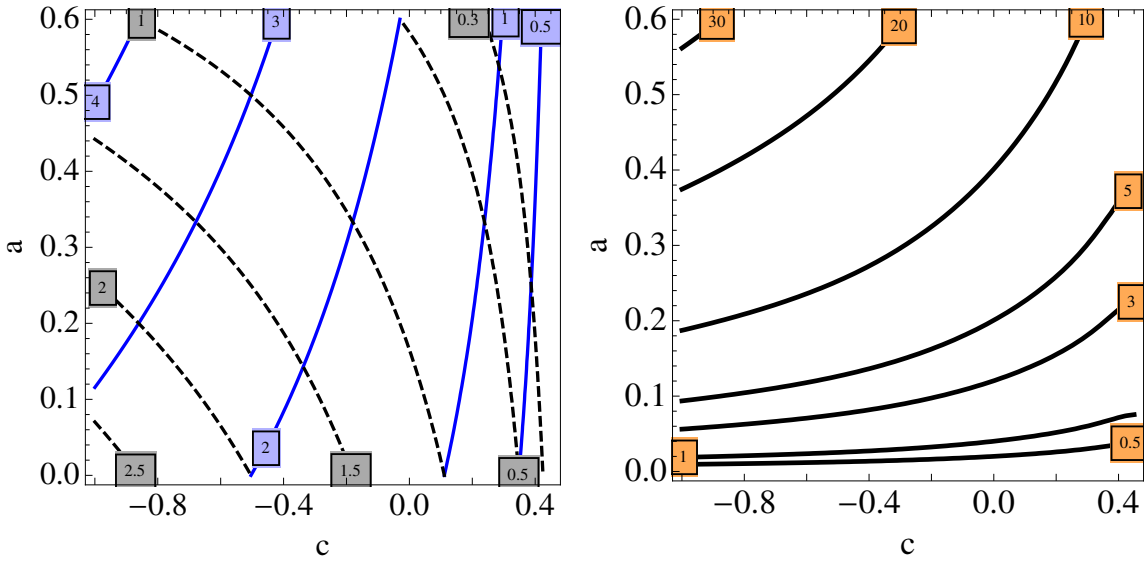

Figure 6. Left panel: contour plot of $M_{\widetilde{\mathcal{L}}}$ (dashed black) and $M_{\widetilde{\mathcal{R}}}$ (solid blue) in the plane (c, a). The labels of the contours are in TeV. Right panel: contour plot of Yukawa coupling in 5D, $\sqrt{k}\widehat{Y}_{LR}$ in the plane (c, a). We have considered $c_{\mu_L} = 0.4$, $c_{\mu_R} = 0.5$.

Then setting values for the elements U_L^{31}, U_R^{21} consistently with experimental bounds we can write all the functions c_{JK} in term of the parameters c and the function c_{LR}. Moreover by defining the parameter β as

$$\beta = -\frac{M_{\widetilde{\mathcal{R}}} - M_{\widetilde{\mathcal{L}}}}{M_{\widetilde{\mathcal{R}}} + M_{\widetilde{\mathcal{L}}}} \tag{7.4}$$

we get

$$U_L^{21} = \beta U_L^{31}, \quad U_R^{31} = \beta U_R^{21}. \tag{7.5}$$

We will change the independent parameters from (c, c_{LR}) to (c, a) by introducing the convenient parametrization

$$a \equiv c_{LR}/M(c) \tag{7.6}$$

and present the results for the mass eigenvalues in the plane (c, a) in the left panel of figure 6. In the absence of a theory predicting the 5D Yukawa couplings we will consider them as output from the different constraints. In particular, using the variable a from eq. (7.6), implies an implicit assumption for the 5D Yukawa coupling $\widehat{Y}_{LR}$. The required values of $\widehat{Y}_{LR}$ are shown as contour plots in the plane (c, a) in the right panel of figure 6. The condition of perturbativity of the 5D theory would imply an upper bound on the 5D Yukawa couplings such that $\sqrt{k}\widehat{Y}_{LR} \lesssim 4\pi$ which already excludes the upper left corner of the parameter region in the plane (c, a), as we can see from the right panel of figure 6. Nevertheless this region, as we will see, is also excluded by electroweak constraints which in fact rule out the region $\sqrt{k}\widehat{Y}_{LR} \gtrsim 4$.

Gauge and Yukawa couplings, in the particular case we are considering in this section, also take simplified values which we now describe.

JHEP05(2017)016

7.1 Gauge couplings

The couplings with the Z gauge boson and the neutral KK bosons Z_n, γ_n can be written, from eq. (6.7), as

$$\begin{aligned} g^X_{\widetilde{\mathcal{L}}_L} &= \frac{U^{31}_L}{\sqrt{2}}\left[\beta(g^X_{\mathcal{L}_L} - g^X_{\mu_L}) - (\tan\alpha_X g^X_{\mathcal{L}_L} - g^X_{\mu_L})\right] \\ g^X_{\widetilde{\mathcal{L}}_R} &= \frac{U^{21}_R}{\sqrt{2}}\left[(g^X_{\mathcal{L}_R} - g^X_{\mu_R}) - \beta(\tan\alpha_X g^X_{\mathcal{L}_R} - g^X_{\mu_R})\right] \\ g^X_{\widetilde{\mathcal{R}}_L} &= \frac{U^{31}_L}{\sqrt{2}}\left[\beta(g^X_{\mathcal{L}_L} - g^X_{\mu_L}) + (\tan\alpha_X g^X_{\mathcal{L}_L} - g^X_{\mu_L})\right] \\ g^X_{\widetilde{\mathcal{R}}_R} &= \frac{U^{21}_R}{\sqrt{2}}\left[(g^X_{\mathcal{L}_R} - g^X_{\mu_R}) + \beta(\tan\alpha_X g^X_{\mathcal{L}_R} - g^X_{\mu_R})\right] \end{aligned} \tag{7.7}$$

with

$$\tan\alpha_X = \begin{cases} \frac{g^{Z,\mathrm{SM}}_{\mu_R}}{g^{Z,\mathrm{SM}}_{\mu_L}} & \text{if } X = Z,\, Z_n \\ 1 & \text{if } X = \gamma_n. \end{cases} \tag{7.8}$$

where $g^{Z,\mathrm{SM}}_{\mu_{L,R}}$ denotes the SM (tree-level) Z coupling to the $\mu_{L,R}$ fields.

On the other hand, the couplings with the W gauge boson and the charged KK bosons W_n, eq. (5.13), are written as

$$g^{W_n}_{\widetilde{\mu}_L} = \beta U^{31}_L g^{W_n}_{N_L}, \quad g^{W_n}_{\widetilde{\mu}_R} = U^{21}_R g^{W_n}_{N_R}, \quad \left(g^{W_n}_V\right)^2 - \left(g^{W_n}_A\right)^2 = \beta U^{31}_L U^{21}_R g^{W_n}_{N_L} g^{W_n}_{N_R} \quad (n \geq 0) \tag{7.9}$$

7.2 Yukawa couplings

We can also write the 4D Yukawa couplings of the Higgs with mass eigenstates in eq. (5.8) as

$$Y = \frac{1}{v}\begin{pmatrix} c_{\ell E} & \frac{M_{\widetilde{\mathcal{R}}} U^{31}_L}{\sqrt{2}} & -\frac{M_{\widetilde{\mathcal{L}}} U^{31}_L}{\sqrt{2}} \\ -\frac{M_{\widetilde{\mathcal{R}}} U^{21}_R}{\sqrt{2}} & -\left(\frac{M_{\widetilde{\mathcal{R}}} - M_{\widetilde{\mathcal{L}}}}{2}\right) & 0 \\ -\frac{M_{\widetilde{\mathcal{L}}} U^{21}_R}{\sqrt{2}} & 0 & \frac{M_{\widetilde{\mathcal{R}}} - M_{\widetilde{\mathcal{L}}}}{2} \end{pmatrix} + \cdots \tag{7.10}$$

where the ellipsis refers to terms which are subleading (quadratic) in the small parameters U^{31}_L and U^{21}_R. As we will see below the tiny elements Y^{12}, Y^{21} and Y^{13}, Y^{31} will generate small (subleading) corrections to the muon anomalous magnetic moments while the diagonal elements Y^{22} and Y^{33} will contribute to the Higgs branching fractions of $H \to \gamma\gamma$ and will constrain the parameter space, or can be an indirect measurement of VLL if in the future there is an excess of $\gamma\gamma$ events.

8 $\delta g_{Z\bar{\mu}\mu}$ from VLL

As VLL mix with the muon sector, the most important effect of the presence of VLL is the modification of the coupling of the Z gauge boson with the physical muon. We have singled out this constraint as it will unambiguously determine part of the theory

JHEP05(2017)016

parameters. In particular we will see that it determines the size of the relevant mixing parameters U_L^{31} and U_R^{21}.

In the presence of the mixing (5.5) the SM coupling of the Z gauge boson with muons $g_{\mu_{L,R}}^{Z,\mathrm{SM}}$ gets modified. In fact we have defined the coupling matrix to Z gauge bosons in eq. (5.11). We can assume here, to leading order, that $f_Z(y) = 1$ so that the coupling matrices can be written as

$$\begin{aligned} G_L^Z &= G_L^{Z,\mathrm{SM}} + \delta G_L^Z = g_{\mu_L}^{Z,\mathrm{SM}} \left[\mathbb{I}_3 + \mathrm{diag}\left(0, 0, \frac{1}{2s_W^2 - 1}\right)\right] \\ G_R^Z &= G_R^{Z,\mathrm{SM}} + \delta G_R^Z = g_{\mu_R}^{Z,\mathrm{SM}} \left[\mathbb{I}_3 + \mathrm{diag}\left(0, -\frac{1}{2s_W^2}, 0\right)\right]. \end{aligned} \tag{8.1}$$

Going now to the mass eigenstates as in eq. (4.1)

$$\begin{aligned} \mathcal{L}_Z = Z_\mu \left(\overline{\widetilde{\mu}}_L(x)\ \overline{\widetilde{\mathcal{L}}}_L(x)\ \overline{\widetilde{\mathcal{R}}}_L(x)\right) \gamma^\mu U_L^\dagger G_L^Z U_L \begin{pmatrix} \widetilde{\mu}_L(x) \\ \widetilde{\mathcal{L}}_L(x) \\ \widetilde{\mathcal{R}}_L(x) \end{pmatrix} \\ + Z_\mu \left(\overline{\widetilde{\mu}}_R(x)\ \overline{\widetilde{\mathcal{L}}}_R(x)\ \overline{\widetilde{\mathcal{R}}}_R(x)\right) \gamma^\mu U_R^\dagger G_R^Z U_R \begin{pmatrix} \widetilde{\mu}_R(x) \\ \widetilde{\mathcal{L}}_R(x) \\ \widetilde{\mathcal{R}}_R(x) \end{pmatrix} \end{aligned} \tag{8.2}$$

we can write

$$\begin{aligned} \frac{\delta g_{\mu_L}^Z}{g_{\mu_L}^Z} &= -\frac{(U_L^{31})^2}{1 - 2s_W^2}, \\ \frac{\delta g_{\mu_R}^Z}{g_{\mu_R}^Z} &= -\frac{(U_R^{21})^2}{2s_W^2}. \end{aligned} \tag{8.3}$$

Using now the experimental bound $\left|\delta g_{\mu_{L,R}}^Z / g_{\mu_{L,R}}^Z\right| \lesssim 10^{-3}$ [16] we obtain for the relevant entries the upper bounds

$$|U_L^{31}|,\ |U_R^{21}| \lesssim 0.02\,. \tag{8.4}$$

Using these values we present in figure 7 the values for the Yukawa couplings $\widehat{Y}_{\ell E}$ (left panel), $\widehat{Y}_{\ell R}$ (middle panel) and $\widehat{Y}_{LR}$ (right panel) from eq. (7.3). A first observation is that the three 5D Yukawa couplings are in the perturbative regime for all values of the parameters in the (c, a) plane. In fact $\sqrt{k}\widehat{Y}_{\ell R}, \sqrt{k}\widehat{Y}_{LR} \lesssim 4$ while $0.005 \lesssim \sqrt{k}\widehat{Y}_{\ell E} \lesssim 0.02$. Moreover the small values of $\sqrt{k}Y_{\ell E}$ imply a certain degree of fine-tuning, as the mechanism to give mass to the muon in this model is somewhat different from the usual mechanism to give masses to fermions in Randall-Sundrum-like models (by means of different localizations in the extra dimension and anarchic $\mathcal{O}(1)$ 5D Yukawa couplings). In our case the muon mass is fixed by the first line in eq. (7.3), where the second term on the right-hand side is typically of $\mathcal{O}(\mathrm{GeV})$, as it has to be the left-hand side term, whose small Yukawa coupling pre-factor comes from the degree of compositeness of the muon as required in order to fit the LHCb anomaly. Finally the typical fine-tuning between both $\mathcal{O}(\mathrm{GeV})$ terms, to yield the physical muon mass ($\sim 0.1\,\mathrm{GeV}$) is then expected to be $\sim 10\%$.

JHEP05(2017)016

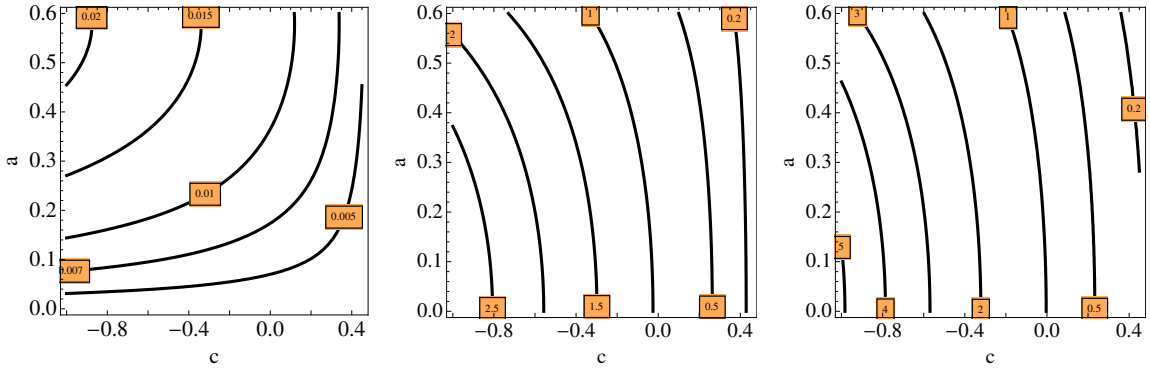

Figure 7. Contour plot of the 5D Yukawa couplings, $\sqrt{k}\widehat{Y}_{\ell E}$ (left panel) $\sqrt{k}|\widehat{Y}_{\ell R}|$ (middle panel), and $\sqrt{k}\widehat{Y}_{LE}$ (right panel) in the plane (c, a). We have considered $c_{\mu_L} = 0.4$, $c_{\mu_R} = 0.5$.

9 Δa_μ from VLL

Charged ($\widetilde{\mathcal{L}}$, $\widetilde{\mathcal{R}}$) and neutral ($\mathcal{N}$) vector like fermions contribute to the muon anomalous magnetic moment. Charged VLL make use of neutral current interactions with Z, Z_n, γ_n, H, and neutral ones make use of charged current interactions with W, W_n. They will therefore provide corresponding contributions to the muon AMM.

9.1 Charged VLL

Charged vector like fermions contribute in loops to the muon AMM as shown in figure 8. The relevant quantity for their contribution to Δa_μ is, in a very good approximation,[9] given by [18, 35]

$$\Delta a_\mu^C = \sum_{X=Z,Z^n,\gamma^n} \Delta a_\mu^X, \quad \Delta a_\mu^X \equiv \frac{1}{4\pi^2} K_X \tag{9.1}$$

where

$$K_X = \sum_{f=\widetilde{\mathcal{L}},\widetilde{\mathcal{R}}} \frac{m_\mu^2}{m_X^2} \left[\left(g_{f_V}^X\right)^2 - \left(g_{f_A}^X\right)^2 \right] \frac{M_f}{m_\mu} F_0\left(\frac{M_f}{m_X}\right) \tag{9.2}$$

and the function $F_0(x)$, given by

$$F_0(x) = \frac{1 - (3/4)x^2 - (1/4)x^6 + 3x^2 \log x}{(1-x^2)^3}, \tag{9.3}$$

is a monotonously decreasing function such that $F_0(0) = 1$ and $F_0(\infty) = 1/4$. Using the couplings in (5.11) we can write

$$K_X = \frac{m_\mu^2}{m_X^2} \left[g_{\widetilde{\mathcal{L}}_L}^X g_{\widetilde{\mathcal{L}}_R}^X \frac{M_{\widetilde{\mathcal{L}}}}{m_\mu} F_0\left(\frac{M_{\widetilde{\mathcal{L}}}}{m_X}\right) + g_{\widetilde{\mathcal{R}}_L}^X g_{\widetilde{\mathcal{R}}_R}^X \frac{M_{\widetilde{\mathcal{R}}}}{m_\mu} F_0\left(\frac{M_{\widetilde{\mathcal{R}}}}{m_X}\right) \right]. \tag{9.4}$$

[9] We are not considering subleading contributions coming from KK modes of VLL and from higher ($n \geq 2$) KK modes.

JHEP05(2017)016

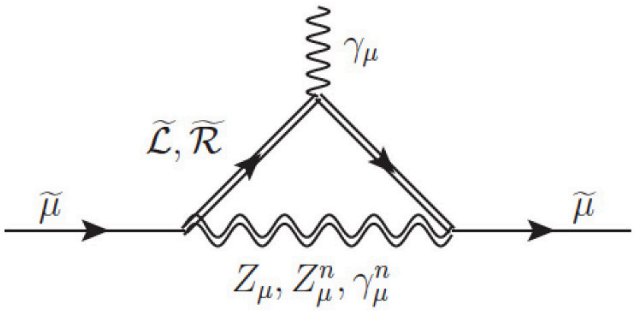

Figure 8. Diagrams contributing to Δa_μ^C from charged VLL.

In order to find a more explicit expression for Δa_μ, as function of (c, a), we first consider the contribution of KK-modes $X = Z_n, \gamma_n$ when $g^X_{\mathcal{L}_L} \gg g^X_{\mu_L}$ and $g^X_{\mathcal{L}_R} \gg g^X_{\mu_R}$. In this case we can write

$$\begin{aligned} g^X_{\widetilde{\mathcal{L}}_L} g^X_{\widetilde{\mathcal{L}}_R} &= \frac{U_R^{21} U_L^{31} g^X_{\mathcal{L}_L} g^X_{\mathcal{L}_R} (\beta - \tan\alpha_X)(1 - \beta \tan\alpha_X)}{2} \\ g^X_{\widetilde{\mathcal{R}}_L} g^X_{\widetilde{\mathcal{R}}_R} &= \frac{U_R^{21} U_L^{31} g^X_{\mathcal{L}_L} g^X_{\mathcal{L}_R} (\beta + \tan\alpha_X)(1 + \beta \tan\alpha_X)}{2} \end{aligned} \tag{9.5}$$

and

$$\begin{aligned} \Delta a_\mu^X = & \frac{m_\mu U_R^{21} U_L^{31} g^X_{\mathcal{L}_L} g^X_{\mathcal{L}_R}}{8\pi^2 m_X^2} \\ & \times \left\{ \beta(1 + \tan^2\alpha_X) \left[M_{\widetilde{\mathcal{L}}} F_0\left(\frac{M_{\widetilde{\mathcal{L}}}}{m_X}\right) + M_{\widetilde{\mathcal{R}}} F_0\left(\frac{M_{\widetilde{\mathcal{R}}}}{m_X}\right) \right] \right. \\ & \left. - \tan\alpha_X (1 + \beta^2) \left[M_{\widetilde{\mathcal{L}}} F_0\left(\frac{M_{\widetilde{\mathcal{L}}}}{m_X}\right) - M_{\widetilde{\mathcal{R}}} F_0\left(\frac{M_{\widetilde{\mathcal{R}}}}{m_X}\right) \right] \right\}. \end{aligned} \tag{9.6}$$

On the other hand the contribution from the Z gauge boson is given by

$$\Delta a_\mu^Z = \frac{m_\mu}{4\pi^2 m_Z^2} \frac{U_L^{31} U_R^{21}}{2} (g^Z_{\mu_L} - g^Z_{\mu_R})^2 \left[M_{\widetilde{\mathcal{L}}} F_0\left(\frac{M_{\widetilde{\mathcal{L}}}}{m_Z}\right) - M_{\widetilde{\mathcal{R}}} F_0\left(\frac{M_{\widetilde{\mathcal{R}}}}{m_Z}\right) \right]. \tag{9.7}$$

Notice that the contribution from the Z gauge boson is important as the relative enhancement ($\propto m_X^2/m_Z^2$) in Δa_μ is not compensated by the small Standard Model couplings.

Finally the Yukawa interactions in eq. (7.10) generate an extra contribution to Δa_μ mediated by the diagram of figure 8, where the line propagating gauge and KK bosons is replaced[10] by the Higgs propagator. The result is provided by the general expression [18, 35]

$$\Delta a_\mu^H = \sum_{f=\widetilde{\mathcal{L}},\widetilde{\mathcal{R}}} \frac{m_\mu^2}{192\pi^2 M_f^2} \left[\left(Y_{\widetilde{\mu}_L f_R}\right)^2 + \left(Y_{\widetilde{\mu}_R f_L}\right)^2 \right] F_2\left(\frac{M_f^2}{m_H^2}\right) \tag{9.8}$$

[10]Here we again neglect the tiny contribution from ($n \geq 1$) KK modes of the Higgs boson.

JHEP05(2017)016

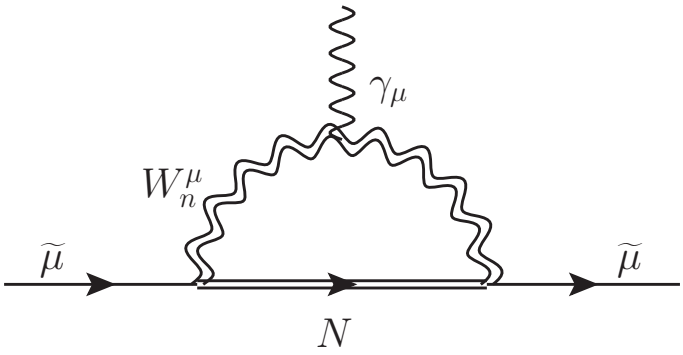

Figure 9. Diagrams contributing to Δa_μ^N from neutral VLL.

where

$$F_2(x) = \frac{x^4 - 6x^3 + 3x^2 + 2x + 6x^2 \log x}{(x-1)^4}\,. \tag{9.9}$$

For the case $c_L = c_R \equiv c$, using eq. (7.10) yields the result

$$\Delta a_\mu^H = \frac{m_\mu^2}{384\pi^2 v^2}\left[\left(U_L^{31}\right)^2 + \left(U_R^{21}\right)^2\right]\left[\frac{M_{\widetilde{\mathcal{R}}}^2}{M_{\widetilde{\mathcal{L}}}^2} F_2\left(\frac{M_{\widetilde{\mathcal{L}}}^2}{m_H^2}\right) + \frac{M_{\widetilde{\mathcal{L}}}^2}{M_{\widetilde{\mathcal{R}}}^2} F_2\left(\frac{M_{\widetilde{\mathcal{R}}}^2}{m_H^2}\right)\right]. \tag{9.10}$$

Notice that due to the strong suppression on the values of U_L^{31} and U_R^{21} in eq. (8.4) the Higgs contribution will be subleading, thus not contributing significantly to the $g_\mu - 2$ anomaly.

9.2 Neutral VLL

Moreover the contribution of the neutral vector like fermion $\mathcal{N}$ in loops to the anomalous magnetic moment of the muon $\Delta a_\mu^{\mathcal{N}}$ comes from the diagrams in figure 9. Similarly to the previous section we can now write $\Delta a_\mu^{\mathcal{N}}$ as

$$\Delta a_\mu^{\mathcal{N}} = \frac{1}{4\pi^2}\sum_{n\geq 0} K_{W_n} \tag{9.11}$$

with

$$K_{W_n} = \frac{m_\mu^2}{m_{W_n}^2} g_{\widetilde{\mu}_L}^{W_n} g_{\widetilde{\mu}_R}^{W_n} \frac{M}{m_\mu} F_1\left(\frac{M}{m_{W_n}}\right) \tag{9.12}$$

where $M = M(c)$ is the mass of the neutral VLL ($\mathcal{N}$) and

$$F_1(x) = \frac{-1 + (17/4)x^2 - 3x^4 - (1/4)x^6 + 5x^4 \log x}{(1-x^2)^3}\,. \tag{9.13}$$

Using now the results in eq. (5.13) we can write

$$\Delta a_\mu^{\mathcal{N}} = \sum_{n\geq 0} \frac{m_\mu U_R^{21} U_L^{31} g_{N_L}^{W_n} g_{N_R}^{W_n}}{4\pi^2 m_{W_n}^2} \beta M F_1\left(\frac{M}{m_{W_n}}\right). \tag{9.14}$$

JHEP05(2017)016

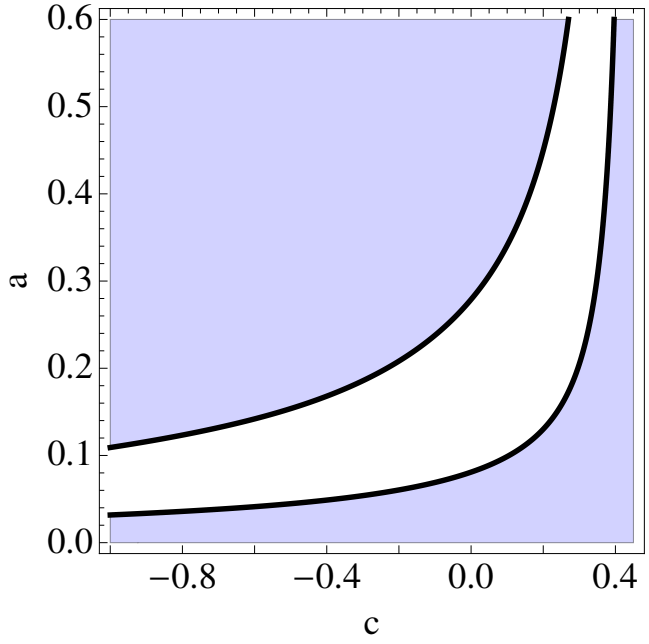

Figure 10. Contour plot of Δa_μ. We have considered $c_{\mu_L} = 0.4$, $c_{\mu_R} = 0.5$.

9.3 Numerical results

Summing up all the contributions we define the total contribution to Δa_μ as

$$\Delta a_\mu = \Delta a_\mu^C + \Delta a_\mu^H + \Delta a_\mu^{\mathcal{N}} \tag{9.15}$$

where Δa_μ^C (Δa_μ^H) is the contribution from the charged VLL ($\widetilde{\mathcal{L}}$, $\widetilde{\mathcal{R}}$) and the neutral gauge bosons (Z, Z_n, γ_n), and their KK modes (the Higgs boson), and $\Delta a_\mu^{\mathcal{N}}$ the contribution from the neutral VLL ($\mathcal{N}$) and the charged gauge boson and its KK modes (W, W_n). In figure 10 we show the 95% CL allowed region in the plane (c, a) which provides the experimental value for the muon AMM $\Delta a_\mu^{\text{exp}}$ given by eq. (1.2). Notice that, as parametrically[11] $\Delta a_\mu \propto U_L^{31} U_R^{21}$, the allowed region in the plane (c, a) is entirely determined by the mixing angles between the VLL and the muon, which in turn are determined from the electroweak bounds on the observable $\delta g_{L,R}$ in eq. (8.3).

We can see that the allowed region is localized towards the IR so that it implies a degree of compositeness for the VLL. In particular extending the results to the limiting region where $a \to 1$ we can see that the allowed region from the muon AMM implies the absolute upper bound $c \lesssim 0.42$. However as wee will see next still there are other experimental and theoretical constraints which restrict the allowed region for VLL to encompass the muon AMM.

[11] Except for the tiny (subleading) contribution from the Higgs boson in the loop which goes as $|U_L^{31}|^2 + |U_R^{21}|^2$.

JHEP05(2017)016

10 Other constraints

In this section we will present the main constraints from electroweak observables to VLL. First of all, VLL mix with the muon and thus are subject to strong constraints in the measurement of the $Z\bar{\mu}\mu$ coupling, as we already have explained in section 8. Second, the presence of VLL modify the universal (oblique) observables and thus their contribution can be encoded in their correction to the S, T and U observables [27]. This will constraint the allowed region in the (c, a) plane. The corresponding constraints coming from the correction to the electroweak observables from Kaluza-Klein modes of gauge bosons and fermions were already summarized in section 2 and will be taken into account in the present one. Moreover, the presence of VLL running in loops should contribute to the decay rate $\Gamma(H \to \gamma\gamma)$, which has been measured at LHC7 and 8 TeV, and is being measured at LHC13 TeV, and to the Higgs quartic coupling β-function triggering an instability of the electroweak vacuum faster than in the SM. Both effects, as we will see, will further constraint the allowed region. Finally we will need to take into account present experimental bounds from direct searches at LHC.

10.1 Oblique corrections

The relevant Lagrangian in the interaction basis is given by

$$\begin{aligned}\mathcal{L} \supset & \frac{g}{2} W_\mu^3 \left[\bar{\nu}_L \gamma^\mu \nu_L + \bar{N}\gamma^\mu N - \bar{\mu}\gamma^\mu \mu - \overline{\mathcal{L}}\gamma^\mu \mathcal{L}\right] \\ & - \frac{g'}{2} B_\mu \left[\bar{\nu}_L \gamma^\mu \nu_L + \bar{\mu}\gamma^\mu \mu + \bar{N}\gamma^\mu N + \overline{\mathcal{L}}\gamma^\mu \mathcal{L} + 2\,\overline{\mathcal{R}}\gamma^\mu \mathcal{R}\right] \\ & + \frac{g}{2} W_\mu^1 \left[\bar{\nu}_L \gamma^\mu \mu_L + \bar{N}\gamma^\mu \mathcal{L} + \text{h.c.}\right]. \end{aligned} \tag{10.1}$$

It can be written in the mass eigenstate basis $(\widetilde{\mu}, \widetilde{\mathcal{L}}, \widetilde{\mathcal{R}})$ by making the change

$$\begin{aligned}\mu_{L,R} &= U^{11}_{L,R}\widetilde{\mu}_{L,R} + U^{12}_{L,R}\widetilde{\mathcal{L}}_{L,R} + U^{13}_{L,R}\widetilde{\mathcal{R}}_{L,R}, \\ \mathcal{L}_{L,R} &= U^{21}_{L,R}\widetilde{\mu}_{L,R} + U^{22}_{L,R}\widetilde{\mathcal{L}}_{L,R} + U^{23}_{L,R}\widetilde{\mathcal{R}}_{L,R}, \\ \mathcal{R}_{L,R} &= U^{31}_{L,R}\widetilde{\mu}_{L,R} + U^{32}_{L,R}\widetilde{\mathcal{L}}_{L,R} + U^{33}_{L,R}\widetilde{\mathcal{R}}_{L,R}. \end{aligned} \tag{10.2}$$

After using the expressions for $U_{L,R}$ given in eq. (6.2), and neglecting the matrix elements U_L^{31} and U_R^{21} from eq. (8.4), we obtain

$$\mu \simeq \widetilde{\mu}, \quad \begin{pmatrix}\mathcal{L}_{L,R} \\ \mathcal{R}_{L,R}\end{pmatrix} \simeq \begin{pmatrix}\cos\theta_{L,R} & \sin\theta_{L,R} \\ -\sin\theta_{L,R} & \cos\theta_{L,R}\end{pmatrix} \begin{pmatrix}\widetilde{\mathcal{L}}_{L,R} \\ \widetilde{\mathcal{R}}_{L,R}\end{pmatrix} \tag{10.3}$$

which can be used to compute eq. (2.11). For the case considered in section 7, the contribution of VLL to the S and T observables can be written as [36]

$$\begin{aligned}\Delta S &= 8\pi \left[\Pi'(M) - \frac{3}{4}\left(\Pi'(M_{\widetilde{\mathcal{L}}}) + \Pi'(M_{\widetilde{\mathcal{R}}})\right) + \frac{1}{2}\Pi'(M_{\widetilde{\mathcal{L}}}, M_{\widetilde{\mathcal{R}}})\right] \\ \Delta T &= \frac{2\pi}{s_W^2 m_W^2}\left[\Pi(M, M_{\widetilde{\mathcal{L}}}) + \Pi(M, M_{\widetilde{\mathcal{R}}}) - \frac{1}{2}\Pi(M_{\widetilde{\mathcal{L}}}, M_{\widetilde{\mathcal{R}}})\right] \end{aligned} \tag{10.4}$$

JHEP05(2017)016

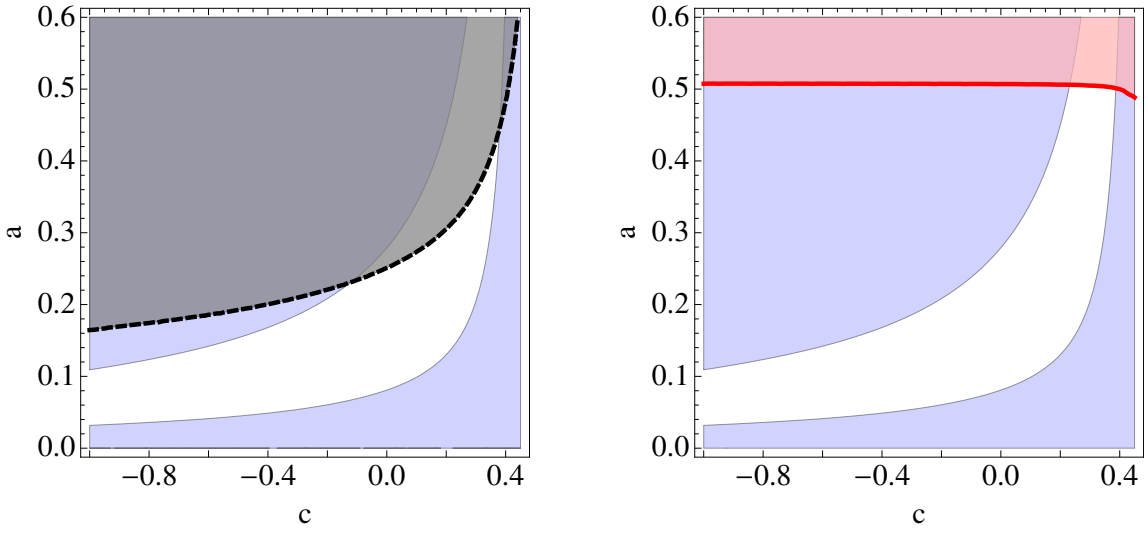

Figure 11. Bounds imposed by oblique observables (left panel) and by $H \to \gamma\gamma$ (right panel). The region allowed by the muon AMM is superimposed.

where the self-energies from fermions with masses m_a and m_b propagating in the loop, $\Pi(p^2; m_a, m_b)$ and $d\Pi(p^2; m_a, m_b)/dp^2$ are defined at $p^2 = 0$, as $\Pi(0; m_a, m_b) \equiv \Pi(m_a, m_b)$ and $d\Pi(p^2; m_a, m_b)/dp^2\big|_{p^2=0} \equiv \Pi'(m_a, m_b)$, with

$$\begin{aligned}
\Pi(m_a, m_b) = {} & \frac{1}{32\pi^2}\frac{1}{(m_a^2 - m_b^2)}\left[m_a^4 - m_b^4 - 2m_a^4 \log m_a^2 + 2m_b^4 \log m_b^2\right. \\
& \left. - 4m_a m_b (m_a^2 - m_b^2 - m_a^2 \log m_a^2 + m_b^2 \log m_b^2)\right] \\
\Pi'(m_a, m_b) = {} & \frac{1}{144\pi^2}\frac{1}{(m_a^2 - m_b^2)^3}\left[-2m_a^6 + 2m_b^6 + 18 m_a^2 m_b^2 (m_a^2 - m_b^2)\right. \\
& + 6m_a^4 (m_a^2 - 3m_b^2)\log m_a^2 - 6m_b^4 (m_b^2 - 3m_a^2)\log m_b^2 \\
& \left. - 9 m_a m_b (m_a^4 - m_b^4 - 2m_a^2 m_b^2 \log(m_a^2/m_b^2))\right]
\end{aligned} \tag{10.5}$$

and where $\Pi'(m_b) = \lim_{m_a \to m_b} \Pi'(m_a, m_b)$.

We will show our results in the plane (c, a). The region allowed by oblique parameters consistent with the experimental data [16], eq. (2.14), at 95% CL, is given in the left panel of figure 11, where the excluded region is shadowed, and we have superimposed (as we will do in all the plots from here on) the region allowed by the muon AMM. We can see that the universal (oblique) observables impose upper bounds on the parameters a and c, as $a \lesssim 0.42$ and $c \lesssim 0.39$. This condition imposes the mild bound on the mass of the lightest eigenstate as $M_{\widetilde{\mathcal{L}}} \gtrsim 230\,\text{GeV}$.

10.2 $H \to \gamma\gamma$

The interactions of the Higgs with the VLL (7.10) generate, when the charged VLL propagate in the loop, an extra contribution to the processes $H \to \gamma\gamma$. Taking only into account the contribution of the W boson, the top quark t and other extra fermions f, and neglecting

JHEP05(2017)016

the off-diagonal elements in (7.10), we can write [37]

$$\Gamma(H\to\gamma\gamma)=\frac{G_F\alpha^2 m_h^3}{128\sqrt{2}\pi^3}\left|A_1(\tau_W)+N_c Q_t^2 A_{1/2}(\tau_t)+\sum_{f=\widetilde{\mathcal{L}},\widetilde{\mathcal{R}}}\frac{vY_{ff}}{M_f}A_{1/2}(\tau_f)\right|^2 \tag{10.6}$$

where $N_c=3$ is the number of colors, $Q_t=+2/3$ is the top quark electric charge in units of $|e|$, $\tau_i\equiv 4m_i^2/m_H^2$, $i=W,t,f$, and

$$A_1(x)=-x^2\left[2x^{-2}+3x^{-1}+3(2x^{-1}-1)f(x^{-1})\right], \tag{10.7}$$

$$A_{1/2}(x)=2x^2\left[x^{-1}+(x^{-1}-1)f(x^{-1})\right] \tag{10.8}$$

with

$$f(x)=\begin{cases}\arcsin^2(\sqrt{x}), & 0<x<1\\ -\ln^2(\sqrt{x}+\sqrt{x-1})+\frac{1}{4}\pi^2+i\pi\ln\left(\sqrt{x}+\sqrt{x-1}\right), & x>1.\end{cases} \tag{10.9}$$

The observable measured by the ATLAS and CMS Collaborations at LHC is the Higgs signal strength $\widehat{\mu}$ defined as

$$\widehat{\mu}=\frac{\sigma(pp\to H)\cdot BR(H\to\gamma\gamma)\,|_{\rm obs}}{\sigma(pp\to H)\cdot BR(H\to\gamma\gamma)\,|_{\rm SM}} \tag{10.10}$$

with a combined value for ATLAS and CMS given by $\widehat{\mu}=1.09\pm 0.11$ [38].

The contribution of the charged VLL, $\widetilde{\mathcal{L}}$ and $\widetilde{\mathcal{R}}$, to $\widehat{\mu}$ is positive and its present experimental value already excludes a region in the plane (c,a) as it is shown in the right panel of figure 11. As it is clear from figure 11, the region excluded by $\widehat{\mu}$, at 95% CL, is inside the region already excluded by oblique observables and does not restrict further the region allowed by the muon AMM. However future measurements of the Higgs strength $\widehat{\mu}$ could possibly exclude additional regions in the plane (c,a). For instance a hypothetical (much stronger) bound as $\widehat{\mu}<1.01$ would translate into the upper bounds $c\lesssim 0.15$ and $a\lesssim 0.11$ which translate into the lower bound on the mass of the lightest VLL, $M_{\widetilde{\mathcal{L}}}\gtrsim 800\,\text{GeV}$.

10.3 The stability of the electroweak minimum

An important (theoretical) constraint is the (in)stability of the electroweak minimum for scales larger than the mass of VLL, and thus much larger than the electroweak scale. For large values of the Higgs field H, the tree-level Higgs potential can be approximated by

$$V_0(H)\simeq\lambda(\mu)|H|^4 \tag{10.11}$$

where $\mu\simeq|H|$. This effect already appears in the SM due to the contribution of the top quark to the renormalization group equations (RGE) of the Higgs quartic coupling λ in the 4D theory.

It is well known that in the SM, and for the measured values of the top quark and Higgs boson masses, the electroweak vacuum becomes unstable (i.e. $\lambda<0$) at a scale $\mu_I\simeq 10^{10}\,\text{GeV}$, although the tunneling lifetime from the electroweak vacuum to the false vacuum is much larger than the age of the universe [42–45].

JHEP05(2017)016

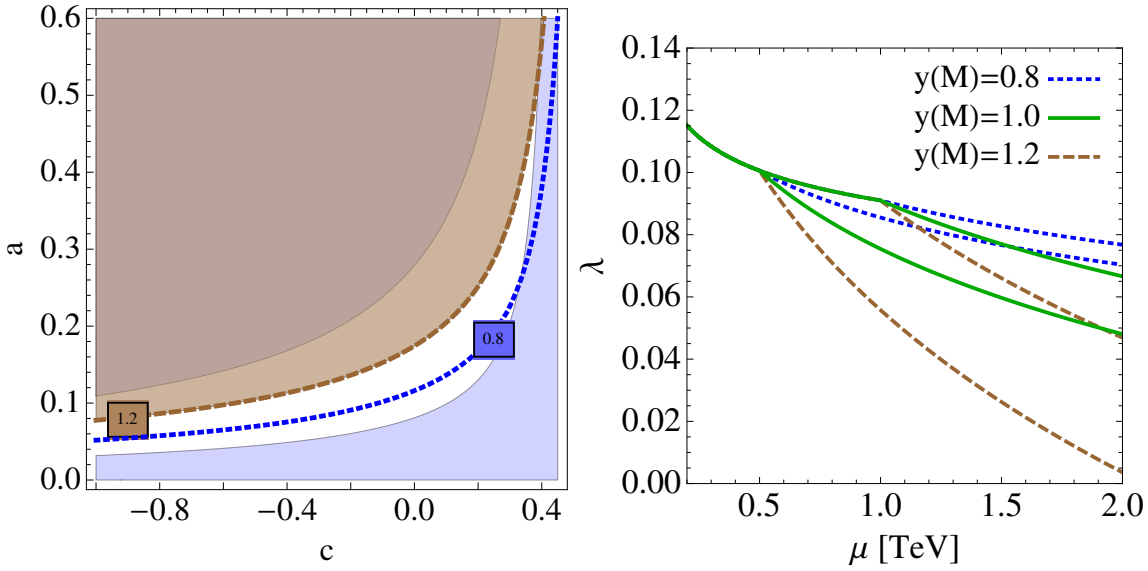

Figure 12. Left panel: contour plot of $y(c, a)$ in the plane (c, a). Right panel: RGE evolution of λ for $y(M) = 0.8$ (dotted blue lines), $y(M) = 1$ (solid red lines) and $y(M) = 1.2$ (dashed green lines). For every value of y, $M = 1\,\text{TeV}$ (upper line) and $M = 0.5\,\text{TeV}$ (lower line).

In the presence of VLL with Yukawa couplings $y(\mu)|_{\mu=M} \equiv aM(c)/v$ to the Higgs field, see eq. (7.10), the instability problem is more acute as the quartic coupling is driven faster to negative values. In fact VLL contribute to the SM RGE by [39, 40]

$$\Delta\beta_\lambda = \frac{1}{16\pi^2}(8\lambda y^2 - 4y^4), \;\; \Delta\beta_{h_t} = \frac{1}{16\pi^2} 2h_t y^2 \tag{10.12}$$

and for large values of the Yukawa coupling y, the (quartic) term y^4 in eq. (10.12) drives rapidly λ to negative values. Particles which are (almost) localized on the TeV brane, such as the Higgs, the top quark or the VLL, only contribute to the running above their mass and below the energy $\mu = m_{KK}$, where the theory is 4D [41]. For scales $\mu > m_{KK}$ they contribute like the bulk fields which represent their preonic constituents. From the holographic point of view this is due to the fact that TeV brane fields are the bound states of the near conformal field theory (CFT) at higher energy scales. In fact the running for $\mu > m_{KK}$ depends on the particular preonic constituents and it is thus very much model dependent. In this paper we will just present the 4D running of the Higgs quartic coupling, see the right panel of figure 12. The 5D running, and thus the full problem of the stability of the electroweak minimum, is model dependent and beyond the scope of the present paper, and it is postponed for a future work. We plot the running of λ for different values of the coupling $y(\mu)$ at the scale $\mu = M$, $y(M) = 0.8, 1, 1.2$ and for different values of M, $M = 0.5, 1\,\text{TeV}$. For scales $\mu < M$, VLL are decoupled and the running is purely the SM one. For scales $\mu > M$, VLL are integrated in and they contribute to β_λ triggering a quick descent of λ. As VLL are active only for $\mu > M$, the smaller the value of M, the faster λ goes to zero. In fact we can see that for $M = 0.5\,\text{TeV}$ the value of $\lambda(m_{KK})$ gets very close to zero for $y(M) = 1.2$, which puts an absolute upper bound on $y(M)$ as $y(M) \lesssim 1.2$. This

JHEP05(2017)016

bound translates into the upper bounds $c \lesssim 0.37$ and $a \lesssim 0.36$, i.e. a lower bound on the mass of the lightest VLL as $M_{\widetilde{\mathcal{L}}} \gtrsim 270\,\text{GeV}$. For larger values of M and/or smaller values of $y(M)$, $\lambda(m_{KK}) > 0$ and the theory is safe from the 4D point of view. Contour plots of $y(M)$ are shown in the left plot of figure 12.

10.4 Collider phenomenology

Heavy leptons can be produced in pairs at lepton colliders and by Drell-Yan processes at hadron colliders, and in particular at the LHC, with cross-sections $\sigma(pp \to Z^*/\gamma^* \to \widetilde{\mathcal{L}}^+\widetilde{\mathcal{L}}^-)$ which depend on the center of mass energy, the mass and the couplings of VLL to Z/γ. In our model VLL couple to electroweak gauge bosons with SM couplings. In particular VLL could have been produced at LEP2 in the process $e^+e^- \to Z/\gamma \to \widetilde{\mathcal{L}}^+\widetilde{\mathcal{L}}^-$ settling the lower bound $M_{\widetilde{\mathcal{L}}} > 101.2\,\text{GeV}$ [46]. More recently a search for heavy leptons decaying into Z and muons is done by the ATLAS collaboration [47] based on pp collision data taken at $\sqrt{s} = 8\,\text{TeV}$ with an integrated luminosity of $20.3\,\text{fb}^{-1}$. VLL are excluded at 95% CL for masses $M_{\widetilde{\mathcal{L}}} < 168\,\text{GeV}$. As we will see this relevant region is already excluded by the other constraints and after imposing that the correct value of the muon anomalous magnetic moment is reproduced.

Stronger bounds are expected in the future based on collisions at $\sqrt{s} = 13\,\text{TeV}$ although the production cross-section decreases very fast for larger values of the masses of the VLL. For instance it turns out that $\sigma(pp \to Z/\gamma^* \to \widetilde{\mathcal{L}}^+\widetilde{\mathcal{L}}^-) \lesssim \mathcal{O}(1)\,\text{fb}$ for $M_{\widetilde{\mathcal{L}}} \gtrsim 500\,\text{GeV}$ [39], and so a full-fledged collider study should be done to put bounds on $M_{\widetilde{\mathcal{L}}}$ based on $\sqrt{s} = 13\,\text{TeV}$ data.

Once the lightest VLL, $\widetilde{\mathcal{L}}$, is produced it decays through the channels $\widetilde{\mathcal{L}} \to \tilde{\mu}Z, \nu_L W, \tilde{\mu}H$. The relevant couplings are given by the Lagrangian

$$\begin{aligned}\mathcal{L}_{\text{VLL}} = {} & g^Z_{\widetilde{\mathcal{L}}_{L,R}} Z_\mu \overline{\widetilde{\mu}}_{L,R} \gamma^\mu \widetilde{\mathcal{L}}_{L,R} + g^W_{\widetilde{\mathcal{L}}_L} W_\mu \overline{\nu}_L \gamma^\mu \widetilde{\mathcal{L}}_L \\ & + \overline{\widetilde{\mu}} H \left(\frac{Y_{12}+Y_{21}}{2\sqrt{2}} - \gamma_5 \frac{Y_{12}-Y_{21}}{2\sqrt{2}} \right) \widetilde{\mathcal{L}} + \text{h.c.}\end{aligned} \tag{10.13}$$

where the matrix Y is defined in eq. (7.10) and

$$\begin{aligned} g^Z_{\widetilde{\mathcal{L}}_L} &= \frac{U_L^{31}}{\sqrt{2}}(g^Z_{\mu_L} - g^Z_{\mu_R}) = -U_L^{31}\frac{g}{2\sqrt{2}c_W}, \\ g^Z_{\widetilde{\mathcal{L}}_R} &= \frac{U_R^{21}}{\sqrt{2}}(g^Z_{\mu_L} - g^Z_{\mu_R}) = -U_R^{21}\frac{g}{2\sqrt{2}c_W} \\ g^W_{\widetilde{\mathcal{L}}_L} &= \frac{g(1+a)}{2}U_L^{31}, \qquad \frac{Y_{12} \pm Y_{21}}{2\sqrt{2}} = \frac{(1+a)M}{4v}\left(U_L^{31} \mp U_R^{21}\right). \end{aligned} \tag{10.14}$$

Two observations from eq. (10.14) are now in order

- As, from eq. (8.3), $|U_L^{31}|$, $|U_R^{21}| \lesssim 0.02$ the gauge couplings are tiny. In particular the gauge couplings with the Z and the W are $\lesssim 6 \times 10^{-3}$.
- The Yukawa coupling remains perturbative in the whole region where $M \lesssim 2.5\,\text{TeV}$, for which $|Y_{12}/(2\sqrt{2})|$, $|Y_{21}/(2\sqrt{2})| \lesssim 0.07$. In the opposite extreme, for light VLL, say $M \gtrsim 250\,\text{GeV}$, we find $|Y_{12}/(2\sqrt{2})|$, $|Y_{21}/(2\sqrt{2})| \gtrsim 0.007$.

JHEP05(2017)016

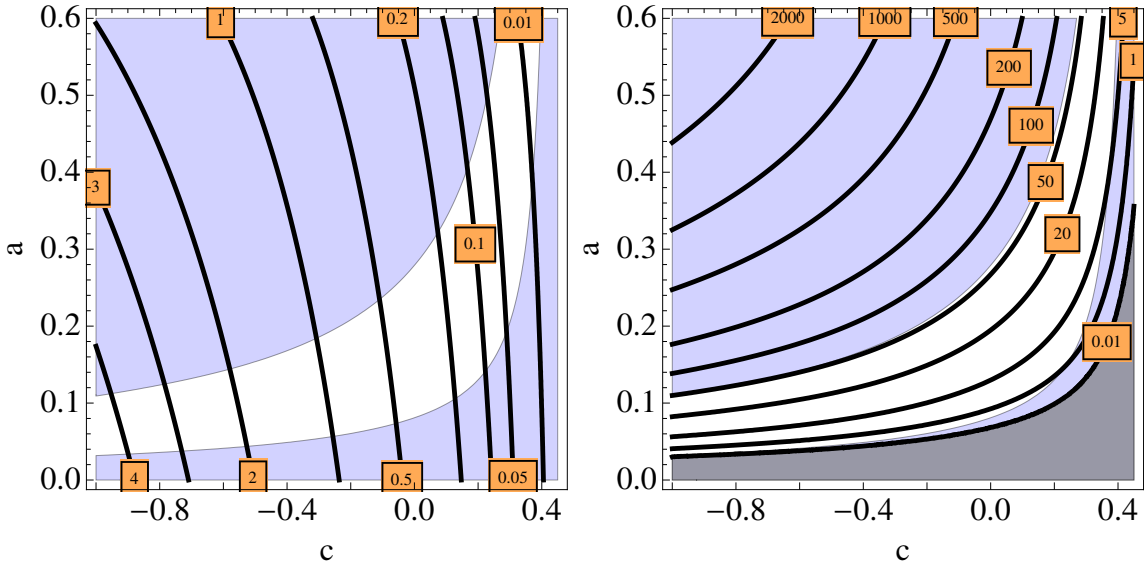

Figure 13. Left panel: contour plot of $\Gamma_{\widetilde{\mathcal{L}}}$ in GeV. Right panel: contour plot of $\Gamma_{\mathcal{N}}$ in GeV. The black shaded area in the right panel is the two-body excluded region $a < m_W/M$, corresponding to the three-body decay channel.

The decay width for the channel $\widetilde{\mathcal{L}} \to \widetilde{\mu} H$ is given by

$$\begin{aligned}\Gamma(\widetilde{\mathcal{L}} \to \widetilde{\mu} H) &= \frac{(|Y_{12}|^2 + |Y_{21}|^2)}{64\pi} M_{\widetilde{\mathcal{L}}} \left(1 - \frac{m_H^2}{M_{\widetilde{\mathcal{L}}}^2}\right)^2 \\ &= \frac{g^2(1-a^2)(1+a)}{256\pi} \frac{M^3}{m_W^2} \left(|U_L^{31}|^2 + |U_R^{21}|^2\right) \left(1 - \frac{m_H^2}{(1-a)^2 M^2}\right)^2, \end{aligned} \tag{10.15}$$

while the decay widths for the channels $\widetilde{\mathcal{L}} \to \widetilde{\mu} Z$ and $\widetilde{\mathcal{L}}_L \to \nu_L W$ are given by

$$\begin{aligned}\Gamma(\widetilde{\mathcal{L}}_L \to \nu_L W) &= \frac{\left(g^W_{\widetilde{\mathcal{L}}_L}\right)^2}{32\pi} \frac{M_{\widetilde{\mathcal{L}}}^3}{m_W^2} \left(1 - \frac{m_W^2}{M_{\widetilde{\mathcal{L}}}^2}\right)^2 \left(1 + 2\frac{m_W^2}{M_{\widetilde{\mathcal{L}}}^2}\right) \qquad (10.16) \\ &= \frac{g^2(1-a^2)^2(1-a)}{128\pi} |U_L^{31}|^2 \frac{M^3}{m_W^2} \left(1 - \frac{m_W^2}{(1-a)^2 M^2}\right)^2 \left(1 + 2\frac{m_W^2}{(1-a)^2 M^2}\right) \\ \Gamma(\widetilde{\mathcal{L}} \to \widetilde{\mu} Z) &= \frac{\left(g^Z_{\widetilde{\mathcal{L}}_L}\right)^2 + \left(g^Z_{\widetilde{\mathcal{L}}_R}\right)^2}{32\pi} \frac{M_{\widetilde{\mathcal{L}}}^3}{m_Z^2} \left(1 - \frac{m_Z^2}{M_{\widetilde{\mathcal{L}}}^2}\right)^2 \left(1 + 2\frac{m_Z^2}{M_{\widetilde{\mathcal{L}}}^2}\right) \qquad (10.17) \\ &= \frac{g^2(1-a)^3}{256\pi} \left(|U_L^{31}|^2 + |U_R^{21}|^2\right) \frac{M^3}{m_W^2} \left(1 - \frac{m_Z^2}{(1-a)^2 M^2}\right)^2 \left(1 + 2\frac{m_Z^2}{(1-a)^2 M^2}\right). \end{aligned}$$

The total width of the lightest VLL is given by $\Gamma_{\widetilde{\mathcal{L}}} = \Gamma(\widetilde{\mathcal{L}} \to \widetilde{\mu} H) + \Gamma(\widetilde{\mathcal{L}}_L \to \nu_L W) + \Gamma(\widetilde{\mathcal{L}} \to \widetilde{\mu} Z)$. We show in the left panel of figure 13 the plot of $\Gamma_{\widetilde{\mathcal{L}}}$ in the plane (c, a). Its mean free path is given by $c\tau = [1.97\,/\Gamma_{\widetilde{\mathcal{L}}}(GeV)] \times 10^{-10} \mu m$ so that in all cases the decay is extremely prompt, as the distance of the secondary decay vertex can never be resolved

JHEP05(2017)016

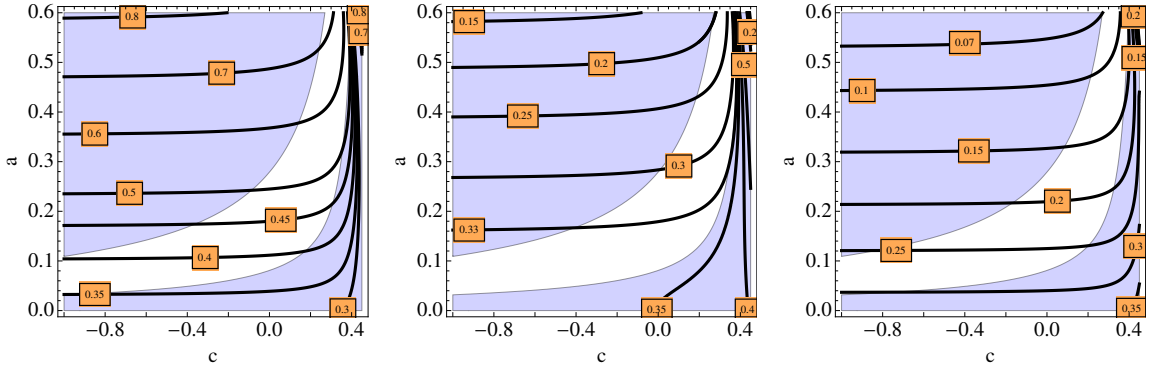

Figure 14. Branching ratios of the decays $\widetilde{\mathcal{L}} \to \widetilde{\mu} H$ (left panel), $\widetilde{\mathcal{L}}_L \to \nu_L W$ (middle panel) and $\widetilde{\mathcal{L}} \to \widetilde{\mu} Z$ (right panel).

from the interaction point.[12] From the partial expressions of the decay rates of $\widetilde{\mathcal{L}}$ into the different channels in eqs. (10.15), (10.16) and (10.17) we can decompose the total rate as $\Gamma_{\widetilde{\mathcal{L}}} = \Gamma_{\widetilde{\mathcal{L}}_L} + \Gamma_{\widetilde{\mathcal{L}}_R}$ where $\Gamma_{\widetilde{\mathcal{L}}_L}$ ($\Gamma_{\widetilde{\mathcal{L}}_R}$) is the term of $\Gamma_{\widetilde{\mathcal{L}}}$ proportional to $|U_L^{31}|^2$ ($|U_R^{21}|^2$). As we can see the ratio of contributions to $H : W : Z$ in $\Gamma_{\widetilde{\mathcal{L}}_L}$, in the limit of large values of M, is equal to $1 : 2 : 1$ in agreement with the Goldstone Boson Equivalence Theorem. The same happens for $\Gamma_{\widetilde{\mathcal{L}}_R}$, except that the W channel does not exist in $\Gamma_{\widetilde{\mathcal{L}}_R}$, as we are assuming only left-handed neutrinos in doublets. In figure 14 we show contour lines of the branching ratios corresponding to the different channels $\widetilde{\mathcal{L}} \to \widetilde{\mu} H$ (left panel), $\widetilde{\mathcal{L}}_L \to \nu_L W$ (middle panel) and $\widetilde{\mathcal{L}} \to \widetilde{\mu} Z$ (right panel). We see that in spite of the fact that gauge couplings are much smaller than the Yukawa couplings all the different branching ratios are of the same order of magnitude in most of the parameter space.

The next-to-lightest VLL is the (neutral) vector-like neutrino (VLN) $\mathcal{N}$ with a mass M. VLN are pair produced by Drell-Yan processes at the LHC via a Z gauge boson, $\sigma(pp \to Z \to \mathcal{N}\mathcal{N})$. When $a > m_W/M$ it decays into the channel $\mathcal{N} \to \widetilde{\mathcal{L}} W$. The region $a > m_W/M$ is shown in the right panel of figure 13 from where we can see that it overlaps with the allowed region from all previous constraints.[13] The relevant Lagrangian is

$$\mathcal{L}_{\rm VLN} = \frac{g}{2} W^\mu \overline{\mathcal{N}} \gamma_\mu \widetilde{\mathcal{L}} \tag{10.18}$$

and the decay width is given by

$$\Gamma(\mathcal{N} \to \widetilde{\mathcal{L}} W) = \frac{g^2}{64\pi} \frac{M^3}{m_W^2} \left\{ (2-a)^2 a^2 + [1 + (1-a)^2 - 6(1-a)] \frac{m_W^2}{M^2} - 2 \frac{m_W^4}{M^4} \right\} \beta(M)$$
$$\beta(M) = \sqrt{\left(a^2 - \frac{m_W^2}{M^2}\right)\left((2-a)^2 - \frac{m_W^2}{M^2}\right)} \,. \tag{10.19}$$

[12] The distance between the displaced vertices and the interaction point which can be resolved inside the detector is typically given by $c\tau \simeq (75 - 100)\,\mu m$. For displaced vertices such that $c\tau \lesssim 75\,\mu m$ the particle is called *prompt*. For displaced vertices such that $100\mu m < c\tau < (1-3)\,m$ the particle decays inside the detector and the displaced vertex can be reconstructed. For decay distances $c\tau > 3m$ the particle decays outside the detector and it is called *long-lived*. There are strong constraints on the mass of long-lived charged particles [48] which do not apply to our model.

[13] In the region $a < m_W/M$ the vector-like neutrino $\mathcal{N}$ decays through $\mathcal{N} \to \widetilde{\mathcal{L}} W^* \to \widetilde{\mathcal{L}} f_1 f_2$ in a three-body decay channel.

JHEP05(2017)016

The contour plot of $\Gamma_{\mathcal{N}} \simeq \Gamma(\mathcal{N} \to \widetilde{\mathcal{L}} W)$ is shown in the right panel of figure 13. We can see that its decay is also prompt.

11 Conclusions

In this paper we have assessed the capability of theories, solving the hierarchy problem by mean of a warped extra dimension, to solve some of the flavor anomalies which appear in the muon sector: in particular the $B \to K^* \mu^+ \mu^-$ LHCb anomaly and the anomalous magnetic moment of the muon a_μ. To do that we have considered a particular geometry in the warped dimension where the AdS_5 symmetry is strongly perturbed near the IR brane, with a naked singularity in the gravitational metric outside the physical interval (the so-called soft-wall metric). These models, where the minimal 5D SM propagates in the bulk of the extra dimension, have the advantage that, even in the absence of an extra gauge custodial symmetry in the bulk, the contribution to the electroweak observables is strongly suppressed for low values of the mass of gauge KK modes.

One possible solution to accommodate the LHCb anomaly requires the presence of massive vector gauge bosons which are strongly coupled to muons and very weakly coupled to electrons, thus breaking lepton universality. In the considered theory the massive vector gauge bosons are naturally identified with the KK modes of the Z and photon gauge bosons, whose couplings with fermions depend on their degree of (compositeness) IR localization: the more composite the fermions the more strongly coupled they are to KK modes. Thus a simple and natural solution to the LHCb anomaly is considering muons more composite than electrons. This solution has been proven to be consistent with all electroweak constraints by a simple choice of the localizing parameters for the muon and the bottom quark $c_{\mu_{L,R}}, c_{b_{L,R}}$. In particular the adopted values in this paper are

$$\begin{aligned} c_{\mu_L} &= 0.4, \quad & c_{\mu_R} &= 0.5 \\ c_{b_L} &= 0.44, \quad & c_{b_R} &= 0.58\,. \end{aligned}$$

Although this minimal theory has all the ingredients to also solve the muon AMM problem, it fails to provide a strong enough chirality flip to cope with the experimental value of a_μ. In order to do that we have enlarged the theory with a set of vector-like leptons, a doublet and a singlet, mixed with the muon sector through Yukawa interactions. The VLL propagate in the bulk with localizing parameters c_L and c_R for the doublet and singlet, respectively. The use of VLL (unmixed with the muon sector) has been often proposed in the past to increase the value of the width $H \to \gamma\gamma$ in order to cope with a possible deviation with respect to the SM prediction [39, 40]. In our case VLL are mixed with the muon sector, which implies strong constraints, not only from universal (oblique) observables but also from non-oblique ones, in particular from the $Z\overline{\mu}\mu$ coupling. This exercise has been performed in this paper where we show that a region in the space of parameters (c_L, c_R) is consistent with the muon AMM value and all experimental and theoretical constraints. The original region consistent with the muon AMM is in fact restricted by all electroweak constraints. For the particularly simple case of equal $c_L = c_R \equiv c$ the combined allowed

JHEP05(2017)016

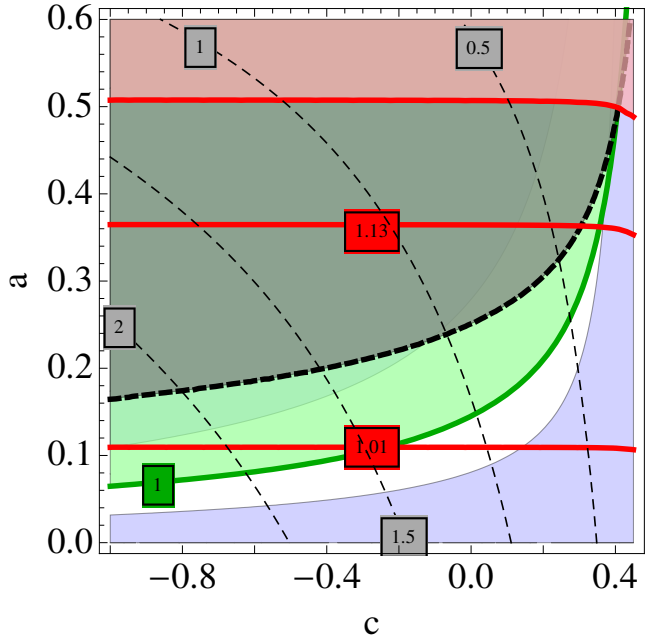

Figure 15. Contour plot of Δa_μ along with bounds from oblique corrections (dashed black line) stability bound (solid green line) and from the Higgs strength into diphotons (solid red upper bound). We have considered $c_{\mu_L} = 0.4$, $c_{\mu_R} = 0.5$.

region is given by the plot in figure 15, where we have superimposed the region allowed by electroweak precision observables (dashed black line) as well as the region allowed by the Higgs strength into diphotons (upper red solid line) and the region allowed by the stability of the electroweak vacuum (solid green line). As we can see the present bound from $H \to \gamma\gamma$ is superseded by the other constraints. However if in the future the Higgs strength approaches the SM value ($\widehat{\mu} = 1$) it can become the strongest constraint. One general consideration from figure 15 is that the available region implies:

- That VLL are localized toward the IR brane. In the dual theory it means that VLL have a high degree of compositeness. In particular $c \lesssim 0.37$.

- There is a lower bound on the mass of VLL. In particular the lightest VLL mass is $M_{\widetilde{\mathcal{L}}} \gtrsim 270\,\text{GeV}$.

A smoking gun for this theory would be, apart from the direct detection of a KK mode at $\sim 2\,\text{TeV}$, the direct detection of a charged or neutral VLL. In fact VLL are produced at the LHC by Drell-Yan production and their present bound at 95% CL, based on the ATLAS analysis at $\sqrt{s} = 8\,\text{TeV}$ and an integrated luminosity of $20.3\,\text{fb}^{-1}$, is the mild one $M_{\widetilde{\mathcal{L}}} \gtrsim 168\,\text{GeV}$. However with increasing luminosity and center of mass energy $\sqrt{s} = 13\,\text{TeV}$ we expect the bounds will rapidly improve.

The last point we want to comment is the capability of this theory to encompass dark matter (DM) with the cosmological abundance consistent by WMAP results $h^2\Omega \simeq 0.12$ [16]. In our theory (with 5D SM plus VLL) there is no candidate to DM as the lightest VLL,

JHEP05(2017)016

$\widetilde{\mathcal{L}}$, decays with a width $\propto (U_L^{31}U_R^{21}, |U_L^{31}|^2 + |U_R^{21}|^2)$. One could then enlarge the theory with a new VLL$'$ sector (where a discrete symmetry prevents the mixing with the SM leptons) which includes a (sterile) singlet $S'(x,y) \propto \mathcal{S}'(x)$ (the 5D counter-part of the 4D right-handed neutrino field), as in refs. [49, 50], mixed with the VLL$'$ active neutrino N' by the 5D Lagrangian

$$\mathcal{L}_5 = \widehat{Y}_S \overline{D}'(x,y)\sigma H^\dagger(x,y)S'(x,y) \tag{11.1}$$

and arrange that the lightest VLL$'$ be a linear combination of the field $\mathcal{N}'$ (member of an $SU(2)_L$ doublet) and the 4D component of the sterile neutrino (along the lines of ref. [40] in 4D theories). Direct searches exclude DM which is mostly $\mathcal{N}'$, as it has unsuppressed couplings with the Z and thus large interaction rates with nucleons, but states which are mostly $\mathcal{S}'$ provide very small annihilation rates, and then lead to large relic densities which rapidly overclose the universe, unless annihilation is enhanced by resonant and/or co-annihilation effects. A thorough analysis of DM in our theory is beyond the scope of this paper and will be postponed for future investigation.

Acknowledgments

We thank M. Beneke for comments, and especially G. Panico and O. Pujolàs for many useful discussions and for having participated in the early stages of this work. L.S. is supported by a Beca Predoctoral Severo Ochoa del Ministerio de Economía y Competitividad (SVP-2014-068850), and E.M. is supported by the European Union under a Marie Curie Intra-European fellowship (FP7-PEOPLE-2013-IEF) with project number PIEF-GA-2013-623006, and by the Universidad del País Vasco UPV/EHU, Bilbao, Spain, as a Visiting Professor. The work of M.Q. and L.S. is also partly supported by Spanish MINECO under Grant CICYT-FEDER-FPA2014-55613-P, by the Severo Ochoa Excellence Program of MINECO under the grant SO-2012-0234, by Secretaria d'Universitats i Recerca del Departament d'Economia i Coneixement de la Generalitat de Catalunya under Grant 2014 SGR 1450, and by the CERCA Program/Generalitat de Catalunya. The research of E.M. is also partly supported by Spanish MINECO under Grant FPA2015-64041-C2-1-P, by the Basque Government under Grant IT979-16, and by the Spanish Consolider Ingenio 2010 Programme CPAN (CSD2007-00042).

JHEP05(2017)016

Open Access. This article is distributed under the terms of the Creative Commons Attribution License (CC-BY 4.0), which permits any use, distribution and reproduction in any medium, provided the original author(s) and source are credited.

References

[1] LHCb collaboration, *Test of lepton universality using $B^+ \to K^+\ell^+\ell^-$ decays*, *Phys. Rev. Lett.* **113** (2014) 151601 [arXiv:1406.6482] [INSPIRE].

[2] LHCb collaboration, *Angular analysis of the $B^0 \to K^{*0}\mu^+\mu^-$ decay using $3fb^{-1}$ of integrated luminosity*, *JHEP* **02** (2016) 104 [arXiv:1512.04442] [INSPIRE].

[3] Muon g-2 collaboration, G.W. Bennett et al., *Final Report of the Muon E821 Anomalous Magnetic Moment Measurement at BNL*, *Phys. Rev.* **D 73** (2006) 072003 [hep-ex/0602035] [INSPIRE].

[4] L. Randall and R. Sundrum, *A Large mass hierarchy from a small extra dimension*, *Phys. Rev. Lett.* **83** (1999) 3370 [hep-ph/9905221] [INSPIRE].

[5] J.A. Cabrer, G. von Gersdorff and M. Quirós, *Soft-Wall Stabilization*, *New J. Phys.* **12** (2010) 075012 [arXiv:0907.5361] [INSPIRE].

[6] J.A. Cabrer, G. von Gersdorff and M. Quirós, *Warped Electroweak Breaking Without Custodial Symmetry*, *Phys. Lett.* **B 697** (2011) 208 [arXiv:1011.2205] [INSPIRE].

[7] J.A. Cabrer, G. von Gersdorff and M. Quirós, *Suppressing Electroweak Precision Observables in 5D Warped Models*, *JHEP* **05** (2011) 083 [arXiv:1103.1388] [INSPIRE].

[8] J.A. Cabrer, G. von Gersdorff and M. Quirós, *Improving Naturalness in Warped Models with a Heavy Bulk Higgs Boson*, *Phys. Rev.* **D 84** (2011) 035024 [arXiv:1104.3149] [INSPIRE].

[9] J.A. Cabrer, G. von Gersdorff and M. Quirós, *Warped 5D Standard Model Consistent with EWPT*, *Fortsch. Phys.* **59** (2011) 1135 [arXiv:1104.5253] [INSPIRE].

[10] A. Carmona, E. Ponton and J. Santiago, *Phenomenology of Non-Custodial Warped Models*, *JHEP* **10** (2011) 137 [arXiv:1107.1500] [INSPIRE].

[11] J.A. Cabrer, G. von Gersdorff and M. Quirós, *Flavor Phenomenology in General 5D Warped Spaces*, *JHEP* **01** (2012) 033 [arXiv:1110.3324] [INSPIRE].

[12] J. de Blas, A. Delgado, B. Ostdiek and A. de la Puente, *LHC Signals of Non-Custodial Warped 5D Models*, *Phys. Rev.* **D 86** (2012) 015028 [arXiv:1206.0699] [INSPIRE].

[13] M. Quirós, *Higgs Bosons in Extra Dimensions*, *Mod. Phys. Lett.* **A 30** (2015) 1540012 [arXiv:1311.2824] [INSPIRE].

[14] E. Megias, O. Pujolàs and M. Quirós, *On dilatons and the LHC diphoton excess*, *JHEP* **05** (2016) 137 [arXiv:1512.06106] [INSPIRE].

[15] E. Megias, G. Panico, O. Pujolàs and M. Quirós, *A Natural origin for the LHCb anomalies*, *JHEP* **09** (2016) 118 [arXiv:1608.02362] [INSPIRE].

[16] Particle Data Group collaboration, C. Patrignani et al., *Review of Particle Physics*, *Chin. Phys.* **C 40** (2016) 100001 [INSPIRE].

[17] M. Davier, *Update of the Hadronic Vacuum Polarisation Contribution to the muon g-2*, arXiv:1612.02743 [INSPIRE].

JHEP05(2017)016

[18] A. Freitas, J. Lykken, S. Kell and S. Westhoff, *Testing the Muon g-2 Anomaly at the LHC*, *JHEP* **05** (2014) 145 [*Erratum ibid.* **09** (2014) 155] [arXiv:1402.7065] [INSPIRE].

[19] W. Altmannshofer, M. Carena and A. Crivellin, $L_\mu - L_\tau$ *theory of Higgs flavor violation and* $(g-2)_\mu$, *Phys. Rev.* **D 94** (2016) 095026 [arXiv:1604.08221] [INSPIRE].

[20] B. Batell, N. Lange, D. McKeen, M. Pospelov and A. Ritz, *Muon anomalous magnetic moment through the leptonic Higgs portal*, *Phys. Rev.* **D 95** (2017) 075003 [arXiv:1606.04943] [INSPIRE].

[21] W. Altmannshofer, C.-Y. Chen, P.S. Bhupal Dev and A. Soni, *Lepton flavor violating* Z' *explanation of the muon anomalous magnetic moment*, *Phys. Lett.* **B 762** (2016) 389 [arXiv:1607.06832] [INSPIRE].

[22] C. Biggio, M. Bordone, L. Di Luzio and G. Ridolfi, *Massive vectors and loop observables: the* $g-2$ *case*, *JHEP* **10** (2016) 002 [arXiv:1607.07621] [INSPIRE].

[23] E. Coluccio Leskow, G. D'Ambrosio, A. Crivellin and D. Müller, $(g-2)\mu$*, lepton flavor violation and* Z *decays with leptoquarks: Correlations and future prospects*, *Phys. Rev.* **D 95** (2017) 055018 [arXiv:1612.06858] [INSPIRE].

[24] D. Stöckinger, *The Muon Magnetic Moment and Supersymmetry*, *J. Phys.* **G 34** (2007) R45 [hep-ph/0609168] [INSPIRE].

[25] O. DeWolfe, D.Z. Freedman, S.S. Gubser and A. Karch, *Modeling the fifth-dimension with scalars and gravity*, *Phys. Rev.* **D 62** (2000) 046008 [hep-th/9909134] [INSPIRE].

[26] E. Megias, O. Pujolàs and M. Quirós, *On light dilaton extensions of the Standard Model*, *EPJ Web Conf.* **126** (2016) 05010 [arXiv:1512.06702] [INSPIRE].

[27] M.E. Peskin and T. Takeuchi, *Estimation of oblique electroweak corrections*, *Phys. Rev.* **D 46** (1992) 381 [INSPIRE].

[28] E. Megias, G. Panico, O. Pujolàs and M. Quirós, *Light dilatons in warped space: Higgs boson and LHCb anomalies*, *Nucl. Part. Phys. Proc.* **282-284** (2017) 194 [arXiv:1609.01881] [INSPIRE].

[29] S. Descotes-Genon, L. Hofer, J. Matias and J. Virto, *Global analysis of* $b \to s\ell\ell$ *anomalies*, *JHEP* **06** (2016) 092 [arXiv:1510.04239] [INSPIRE].

[30] S. Descotes-Genon, L. Hofer, J. Matias and J. Virto, *The* $b \to s l^+ l^{-1}$ *Anomalies And Their Implications For New Physics*, arXiv:1605.06059 [INSPIRE].

[31] B. Capdevila, S. Descotes-Genon, L. Hofer, J. Matias and J. Virto, $B \to K^*(\to K\pi)\ell^+\ell^-$ *theory and the global picture: What's next?*, PoS(LHCP2016)073 [arXiv:1609.01355] [INSPIRE].

[32] M. Beneke, P. Dey and J. Rohrwild, *The muon anomalous magnetic moment in the Randall-Sundrum model*, *JHEP* **08** (2013) 010 [arXiv:1209.5897] [INSPIRE].

[33] P. Moch and J. Rohrwild, $(g-2)_\mu$ *in the custodially protected RS model*, *J. Phys.* **G 41** (2014) 105005 [arXiv:1405.5385] [INSPIRE].

[34] H.-S. Lee and A. Soni, *Fourth Generation Parity*, *Phys. Rev. Lett.* **110** (2013) 021802 [arXiv:1206.6110] [INSPIRE].

[35] F.S. Queiroz and W. Shepherd, *New Physics Contributions to the Muon Anomalous Magnetic Moment: A Numerical Code*, *Phys. Rev.* **D 89** (2014) 095024 [arXiv:1403.2309] [INSPIRE].

JHEP05(2017)016

[36] S.A.R. Ellis, R.M. Godbole, S. Gopalakrishna and J.D. Wells, *Survey of vector-like fermion extensions of the Standard Model and their phenomenological implications*, *JHEP* **09** (2014) 130 [arXiv:1404.4398] [INSPIRE].

[37] M. Carena, I. Low and C.E.M. Wagner, *Implications of a Modified Higgs to Diphoton Decay Width*, *JHEP* **08** (2012) 060 [arXiv:1206.1082] [INSPIRE].

[38] ATLAS, CMS collaborations, *Measurements of the Higgs boson production and decay rates and constraints on its couplings from a combined ATLAS and CMS analysis of the LHC pp collision data at* $\sqrt{s} = 7$ *and* 8 *TeV*, *JHEP* **08** (2016) 045 [arXiv:1606.02266] [INSPIRE].

[39] N. Arkani-Hamed, K. Blum, R.T. D'Agnolo and J. Fan, *2:1 for Naturalness at the LHC?*, *JHEP* **01** (2013) 149 [arXiv:1207.4482] [INSPIRE].

[40] A. Joglekar, P. Schwaller and C.E.M. Wagner, *Dark Matter and Enhanced Higgs to Di-photon Rate from Vector-like Leptons*, *JHEP* **12** (2012) 064 [arXiv:1207.4235] [INSPIRE].

[41] L. Randall and M.D. Schwartz, *Unification and the hierarchy from AdS5*, *Phys. Rev. Lett.* **88** (2002) 081801 [hep-th/0108115] [INSPIRE].

[42] J.A. Casas, J.R. Espinosa and M. Quirós, *Improved Higgs mass stability bound in the standard model and implications for supersymmetry*, *Phys. Lett.* **B 342** (1995) 171 [hep-ph/9409458] [INSPIRE].

[43] J.A. Casas, J.R. Espinosa and M. Quirós, *Standard model stability bounds for new physics within LHC reach*, *Phys. Lett.* **B 382** (1996) 374 [hep-ph/9603227] [INSPIRE].

[44] J.R. Espinosa and M. Quirós, *Improved metastability bounds on the standard model Higgs mass*, *Phys. Lett.* **B 353** (1995) 257 [hep-ph/9504241] [INSPIRE].

[45] G. Degrassi et al., *Higgs mass and vacuum stability in the Standard Model at NNLO*, *JHEP* **08** (2012) 098 [arXiv:1205.6497] [INSPIRE].

[46] L3 collaboration, P. Achard et al., *Search for heavy neutral and charged leptons in* e^+e^- *annihilation at LEP*, *Phys. Lett.* **B 517** (2001) 75 [hep-ex/0107015] [INSPIRE].

[47] ATLAS collaboration, *Search for heavy lepton resonances decaying to a Z boson and a lepton in pp collisions at* $\sqrt{s} = 8$ *TeV with the ATLAS detector*, *JHEP* **09** (2015) 108 [arXiv:1506.01291] [INSPIRE].

[48] CMS collaboration, *Search for long-lived charged particles in proton-proton collisions at* $\sqrt{s} = 13$ *TeV*, *Phys. Rev.* **D 94** (2016) 112004 [arXiv:1609.08382] [INSPIRE].

[49] D. Diego and M. Quirós, *Dirac Versus Majorana Neutrino Masses From a TeV Interval*, *Nucl. Phys.* **B 805** (2008) 148 [arXiv:0804.2838] [INSPIRE].

[50] G. von Gersdorff, M. Quirós and M. Wiechers, *Neutrino Mixing from Wilson Lines in Warped Space*, *JHEP* **02** (2013) 079 [arXiv:1208.4300] [INSPIRE].

JHEP05(2017)016